UNIVERSITY OF THE WITWATERSRAND

School of Civil and Environmental Engineering

"Effect of concrete quality and cover depth on the efficiency of impressed anodic current to induce corrosion of steel in concrete"

By

Abongile Aviwe Nyokana

A research report submitted to the Faculty of Engineering and the Built Environment, University of the Witwatersrand, Johannesburg, in partial fulfilment of the requirements for the degree of Master of Science in Engineering.

Johannesburg, 2018

DECLARATION

I declare that this research report is my own unaided work. It is being submitted to the Degree of Master of Science to the University of the Witwatersrand, Johannesburg. It has not been submitted before for any degree or examination to any other University.

…….. ……

Abongile Aviwe Nyokana *Date*

ABSTRACT

Accelerated corrosion tests have been used by various researchers to study the effects of corrosion of reinforcement steel embedded in concrete, within a reduced time frame. Currently there is a paucity of literature on the relationship between accelerated corrosion tests and durability parameters of concrete, even though the results from accelerated corrosion tests are used in predicting the durability and service life models of reinforced concrete.

In this study, the galvanostatic method, from the impressed anodic current technique was used to induce corrosion in eighteen 100 x 100 x 500 mm beams containing a single Y12 ribbed, high yield tensile strength bar. The study focused on chloride-induced corrosion, as such a 5% NaCl solution reservoir was placed on top of the beams so as to introduce chloride ions into the concrete. In this study, the effect of varying the concrete quality by using three different binder types, and varying the cover depth on the efficiency of impressed anodic current to induce corrosion in reinforcing steel was also be investigated.

Concrete quality was varied by using three different binder types namely, 100% PC (CEM 1), 50/50 PC/SL (CEM III A-S) and 70/30 PC/FA (CEM IV-V/W). The different concrete cover depths to reinforcing steel were 20 mm, 35 mm and 50 mm. The efficiency of the impressed anodic current technique was determined as a percentage of the theoretical mass loss, determined by using Faraday's Law over the actual mass loss. The actual mass loss was determined by conducting gravimetric tests on the steel at the end of the corrosion experiments.

The results showed a general overestimation of Faraday's mass loss for both binder types and cover depths. For the different cover depths, a closer approximation to 100% efficiency was observed in the order 20 > 35 > 50 mm. With regards to the different binder types, closer approximation to 100% efficiency was observed in the order SL > FA > PC. In general, an overestimation of theoretical mass loss was achieved due to the effect of the concrete's resistivity. A modified equation of Faraday's law was developed, taking into account the resistivity of the concrete so as to get a better estimate of theoretical mass loss.

DEDICATION

To

Mum and Dad

ACKNOWLEDGEMENTS

I would like to express my sincere gratitude towards the following people for their immense contribution towards the accomplishment of this research project:

- My supervisor, Dr Mike Otieno, for his guidance, support and attention to detail at each stage of this project which gave me encouragement and determination to pursue the realisation of the project.
- To my mum, dad and sisters for their endless love and unconditional support. Thank you for encouraging me to keep going.
- To the South African National Roads Agency SOC Ltd for funding my studies and supporting me throughout this project.
- To my fellow postgraduate colleagues in the Cement and Concrete Research Group for their support and encouragement
- To The Concrete Institute, Afrisam Pty Ltd, PPC Pty Ltd and National Research Foundation for their support in various ways.

Above all and before anything else, I thank the Almighty for making the completion of this research project possible.

NOMENCLATURE

CCI	Chloride Conductivity Index
DI	Durability Index
FA	Fly ash
GGBS/SL	Ground granulated blast furnace slag
HCP	Half-cell potential
LPR	Linear Polarisation Resistance
OPI	Oxygen Permeability Index
PC	Portland cement
RC	Reinforced concrete
w/b	Water to binder ratio
WSI	Water Sorptivity Index

Concrete beam series labels

SL – 20, SL – 35, SL – 50	Slag blended cement concrete with 20, 35 or 50 mm cover depth.
FA – 20, FA – 35, FA – 50	fly ash blended cement concrete with 20, 35 or 50 mm cover depth.
PC – 20, PC – 35, PC – 50	Portland cement concrete with 20, 35 or 50 mm cover depth

CONTENTS

LIST OF FIGURES

LIST OF TABLES

CHAPTER 1: INTRODUCTION

1.1. Background

Steel reinforced concrete is a material that is used extensively in the built environment for the construction of structures such as buildings and bridges. The extensive use of reinforced concrete (RC) is attributed to its highly versatile nature and structural performance capabilities where the concrete provides compressive strength and the steel provides tensile strength. However, reinforced concrete is not a long-lasting material as the service life of concrete structures is generally shorter than the expected design life (Tourney & Berke, 1993). The service life of RC structures is generally compromised by the ingress of deleterious substances, such as chlorides, carbon dioxide, moisture and oxygen that attack the steel and eventually cause it to corrode. If during the design stage the environmental exposure level that the concrete will be subjected to during its service life is not accurately estimated, then this will be a form of design deficiency which will reduce the service life of RC structures.

Corrosion is the destructive attack of a metal by chemical or an electrochemical reaction with its environment, and is caused by the inherent instability of metals in their metallic form. Corrosion products, such as iron oxide (rust), lead to a reduction in bond strength between the steel and concrete interface and cause cracking and spalling of the concrete (Cheng, et al., 2005). In other instances, corrosion results in the formation of pits or holes which reduce the cross-sectional area of the steel, thus reducing its strength capacity (Almusallam, et al., 1996).

Despite the detrimental effects of steel corrosion, steel is still favoured for use in reinforced concrete due to the protection offered by the concrete. The steel is physically protected by the concrete cover thickness and is chemically protected by a stable oxide passive film on its surface, which is formed by the high alkaline environment provided by the concrete (Ing, 2003). The protection afforded by the concrete is not always sufficient as aggressive environmental conditions, poor workmanship during construction and the quality of the materials used render the steel vulnerable to processes that initiate steel corrosion. Once steel corrosion is

initiated, it is followed by corrosion propagation which is a rapid progression of the corrosion process.

A damage model was developed by Tuutti (1982) which showed that the life cycle of a corrosion-affected RC structure can be split into two periods. These are the initiation period during which harmful substances penetrate through the cover but do not damage the concrete, and the propagation period during which the reinforcing steel corrodes leading to damage such as spalling and cracking. The time taken by these periods is dependent on various factors that influence corrosion, and it may take several years to several decades for the periods to manifest themselves (Tuutti, 1982). As a result of the variation in time frames, researchers use accelerated corrosion techniques to study the effects of corrosion within a realistic time-frame, under experimental laboratory environments. The techniques employed shorten the initiation period and often allow for the control of the corrosion rate depending on the type of corrosion under investigation.

Results from accelerated corrosion tests have been used to predict the ultimate load capacity as well as deflection and crack widths of corroding structures (Ballim & Reid, 2005). Subsequently, structural engineers apply the results obtained from these accelerated corrosion tests to real RC structures in the field which are subjected to natural corrosion. If the results are not applicable, there is a danger of repairs being required when it is too late and critical levels of steel corrosion have been reached and the steel has reduced tensile capacity, or when the structures are still adequate (Malumbela, et al., 2012). Hence, for realistic prediction of the durability of reinforced concrete structures, an understanding of the corrosion mechanisms of corrosion reinforcing steel is imperative.

1.2. Measuring and quantifying durability of concrete

The durability of concrete can be defined as the ability of the concrete to carry out its design service function for the duration of its design life without consequential decay (Urquhart, 2014). Researchers in South Africa have developed an approach to improving the durability of reinforced concrete. This approach is based on the philosophy that durability will be improved only when measurements of appropriate concrete cover properties can be made. The approach was formulated

by “developing suitable test methods, characterising a range of concretes, studying in-situ performance, and applying the results to practical construction” (Ballim, et al. 2009).

The approach links the durability index parameters, service life prediction models, and performance specifications with concrete quality. Durability index parameters are characterised in-situ by conducting durability index tests for oxygen permeation, water absorption and chloride conductivity on laboratory specimens. The South African Durability Index approach has adopted the strategy of providing ‘deemed to satisfy’ rules, which limit durability index values, cover depths and selected binder types with test methods that have been shown to be sensitive to material, constructional and environmental factors that influence durability (Gouws, Alexander & Maritz 2001). The tests provide reproductible engineering measures of the microstructure of the concrete as well as characterise the quality of concrete in relation to the choice of material mix proportions, compaction and curing and environment.

1.3. Research significance

Accelerated induced corrosion techniques have been used widely by researchers to study the behaviour of steel reinforcement corrosion in concrete within a reasonable time-frame. The impressed anodic current technique allows the researcher to control the corrosion rate by varying the current density or time interval of impressed current and to obtain results on the response of RC structures to different degrees of corrosion.

The degree of corrosion is one of the most important parameters in predicting the durability and service life of corroding RC structures (Yuan, et al., 2007). Over the past several years a few studies have been carried out using the impressed anodic current technique, Lee, Noguchi and Tomosawa (2002), studied the bond behaviour of corroded steel bar, El Maaddawy and Soudki (2003) studied the influence of varying the current density on the actual degree of reinforcing corrosion, and Yoon, et al., (2000 studied the interaction between loading, corrosion and serviceability of reinforced concrete

In order to correctly predict the effect of corrosion on reinforced concrete, an appropriate method must be used in the laboratory to accelerate corrosion. However, currently there is no standard procedure for accelerated steel corrosion. In order to develop a standardized procedure for accelerated corrosion tests an in-depth analysis of the important factors involved in the corrosion process is required. In an attempt to make a contribution towards a standardized procedure for accelerated corrosion tests, this study will focus on the effect of concrete quality and cover on the efficiency of impressed anodic current to induce corrosion of steel embedded in concrete. Concrete quality is influenced by the nature of raw mateials such as binder type, aggregrates used and strength required at different ages, determined using the w/b ratio (McDonald, 2009). Concrete quality can be described by the concrete's ability to resist the ingress of deleterious substances such as choride ions, water and oxygen to mention a few. The concretes ability to resist the ingress of deleterious substances can be measured as the penetrability of the concrete which in turn and can be related to the concretes durability. The durability of concrete can be quantified using the Durability Index Tests. The addition of fly ash and slag has been found to influence concrete quality by reducing its penetrability. For the purposes of this study, the concrete quality was be varied by using three different binder types, i.e. plain Portland cement concrete, fly ash and slag blended concrete.

These two parameters, namely concrete quality and cover depth, were selected because they have a physical and chemical influence on the durability of concrete. Currently, there is a paucity in literature on the efficiency of the impressed anodic current technique to accelerate corrosion, even though the results from accelerated corrosion tests are used in predicting the durability and service life models of RC.

Thus, the intention of this study is to make a meaningful contribution towards the existing literature on accelerated corrosion tests and the durability-affecting parameters that are under investigation.

1.4. Problem statement

Corrosion of reinforcing steel in concrete remains one of the major causes of deterioration and loss of durability. The service life of RC structures is governed

by several parameters such as strength, concrete quality, concrete cover, as well as age and exposure conditions. In terms of RC exposure conditions, depassivation of steel, and subsequently steel corrosion due to carbonation and chlorination is considered to be the end of the service life of RC structures (Bertolini, et al., 2004). In accelerated corrosion tests, the galvanostatic method from the impressed anodic current technique is the most commonly employed technique for inducing active corrosion. This technique uses an impressed current to drive corrosion. Faraday's law is used to model the theoretical amount of steel mass loss by relating it to the electrical energy consumed once steel passivity has been compromised. The applied current density (I_{app}) is assumed to be equal to the actual corrosion current (I_{corr}) i.e. $I_{app} = I_{corr}$.

The actual mass loss can be determined by conducting gravimetric tests on the reinforcing steel at the end of the accelerated corrosion experiment. The theoretical mass loss is related to the applied current, total time of external current applied and the area of steel over which the current is applied. Whereas, the actual mass loss is related to the actual current and the time of steel corrosion, excluding the time required to depassivate the steel and the remaining surface area of steel after depassivation. Previous research by Austin, Lyons and Ing (2004), has shown that I_{corr} is not equal to I_{app} and has been supported by Auyeung, Balaguru and Chung (2000), who found that the theoretical and actual mass loss are not the same due to various factors such as the electrical energy required to initiate corrosion, composition of the bar, electrical properties of minerals in concrete and resistivity of the concrete. The latter can be related to the concrete quality and the cover thickness.

The effect of varying concrete quality and concrete cover thickness on the efficiency of impressed anodic current to induce reinforcement steel corrosion will be investigated in this study.

1.5. Objectives and aims

The aim of this research is to study the effect of varying the concrete quality and cover on the efficiency of impressed anodic current to induce corrosion of steel embedded in concrete.

This aim will be achieved by fulfilling the following objectives:

- Compare the theoretical and gravimetric mass loss of steel in concrete made using:
    - 100% plain Portland cement (PC)
    - 50% PC replacement with ground granulated blast-furnace slag (GGBS)
    - 30% PC replacement with fly ash (FA)

  The use of GGBS and FA in concrete to reduce the effects of chloride induced corrosion has been investigated in literature by researchers such as Scott (2004). According to Grieve (2009), GGBS enhances the ability of concrete to resist chloride attack due to its ability to capture chlorides while FA content of 30% or more enhances the concretes resistance to concrete. In South Africa concrete mix proportions of 30% FA and 50% GGBS replacement are predominantly used. The three mixtures under investigation are fundamentally different and as such the purpose of this research is not to compare them as equivalent mixtures, but rather to investigate if the benefits to chloride resistance using FA and GGBS are prevalent under conditions of impressed anodic current.

- To attempt to model the effect of concrete resistivity on mass loss measurements determined using Faraday's Law.
- Compare the theoretical and gravimetric mass loss of steel in concrete with different cover depths namely, 20, 35 and 50 mm.
- Measure the chloride penetrability of concrete by conducting Durability Index tests.

1.6. Scope and limitations

The scope of this study is limited to accelerated chloride induced corrosion using the impressed anodic current will be used to induce corrosion of reinforcing steel in beams of varying concrete quality and cover depth.

Thus, the results produced from this research are limited to chloride induced corrosion, cover depths of 20, 35 and 50 mm as well as binder types of plain

Portland cement blended with 50% ground granulated blast furnace slag, 30% fly ash and 100% plain Portland cement.

1.7. Research work plan

The following working plan has been envisioned for this research report:

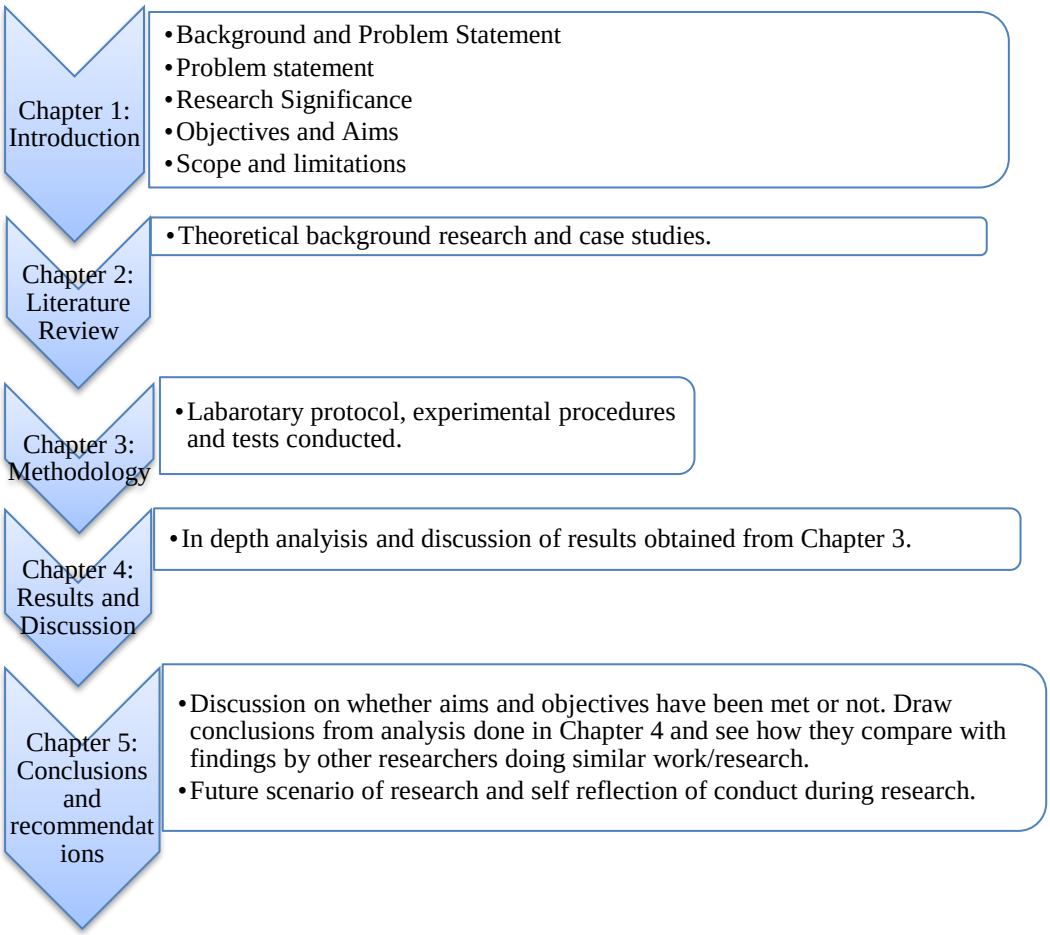

1.8. References

Almusallam, A., Al-Gahtani, A., Aziz, A. & Rasheeduzzafar, F., 1996. Effect of reinforcement corrosion on bond strength. *Construction Building & Materials,* 10(2), pp. 123-129.

Austin, S. A., Lyons, R. & Ing, M. 2., 2004. Electrochemical behaviour of steel reinforced concrete during accelerated corrosion testing. *Corrosion,* 60(2), pp. 203-212.

Auyeung, Y., Chung, L. & Balaguru, P., 2000. Bond behaviour of corroded reinforcing bars. *American Concrete Institute,* 97(2), pp. 214-220.

Ballim, Y., Alexander, M. & Beushausen, H., 2009. Durability of Concrete. In: G. Owens, ed. *Fulton's concrete technology.* ninth Edition ed. Midrand(Gauteng): Cement and Concrete Institute, pp. 155-188.

Ballim, Y. & Reid, J., 2005. Reinforcement corrosion and the deflection of RC beams - an experimental critique of current test methods. *Cement & Concrete Composites,* Volume 25, pp. 625-632.

Bertolini, L., Elsener, B., Pedeferri, P. & Polder, R., 2004. *Corrosion of steel in concrete: prevention, diagnosis, repair.* 1st ed. Weinheim: Verlag GmbH & Co.

Cheng, A., Huang, R., Wu, J.-K. & Chen, C.-H., 2005. Influence of GGBS on durability and corrosion behavior of reinforced. *Materials Chemistry and Physics,* March, 93(2), pp. 404-411.

Gouws, S., Alexander, M. & Maritz, G., 2001. Use of durability index tests for the assessment and control of concrete quality on site. *Concrete Beton,* Issue 98, pp. 5-16.

Grieve, G., 2009. Cementitious materials. In: G. Owens, ed. *Fulton's concrete technology* . Pretoria: Cement and Concrte Institute, pp. 1-16.

El Maaddawy, T. A. & Soudki, K. A., 2003. Effectiveness of impressed current technique to simulated corrosion of steel reinforcement in concrete. *Jounal pf Materials in Civil Engineering,* 15(1), pp. 41-47.

Ing, M. J., 2003. *Detection of Reinforcement Corrosion by an Acoustic Technique,* Leicestershire: Loughborough University.

Lee, H., Noguchi, T. & Tomosawa, F., 2002. Evaluation of the bond properties between concrete and reinforcement as a function of the degree of reinforcement corrosion. *Cement and Concrete Research,* 32(8), pp. 1313-1318.

Malumbela, G., Moyo, P. & Alexander, M., 2012. A step towards standardising accelerated corrosion tests on laboratory reinforced concrete specimens. *Journal of the South African Institute of Civil Engineering,* October , 54(2), pp. 78-85.

McDonald, M., 2009. Control of concrete quality . In: *Fulton's Concrete Technology.* Midrand : Cement and Concrete Institute, pp. 287-295.

Tourney, P. & Berke, N., 1993. A call for standardized tests for corrosion-inhibiting admixtures. *Concrete International,* 15 April, 15(4), pp. 57-62.

Tuutti, K., 1982. *Corrosion of steel in concrete.* 82 ed. Sweden: Swedish Cement and Concrete Research.

Urquhart, C., 2014. *Historic Concrete in Scotland Part 2: Investigation and Assessment of Defects.* 1 ed. Scotland, Edingurgh: Historic Scotland.

Yoon, S., Wang, K., Weiss, W. & Shah, S., 2000. INteraction between loading, corrosion and serviceability of reinforced concrete. *ACI Material Journal,* Nov-Dec, 97(6), pp. 637-644.

Yuan, Y., Ji, Y. & Shah, S., 2007. Comparion of Two accelerated corrosion techniques for concrete structures. *ACI structural journal,* May-June, 104(3), pp. 344-347.

CHAPTER 2: LITERATURE REVIEW

2.1. Introduction

This chapter covers the fundamentals of steel reinforcement corrosion in concrete with emphasis on accelerated corrosion using the anodic impressed current technique which is the focus of this study. Factors affecting corrosion initiation and propagation are also covered with focus on concrete quality and cover depth. Lastly factors affecting the acceleration of steel corrosion using anodic impressed current technique are discussed, with a brief discussion on typical experimental set-ups for accelerated corrosion used by researchers and a summary of research findings on existing literature.

2.2. Fundamentals of steel corrosion

2.2.1. Electrochemistry of corrosion

Iron metal that is exposed to air is covered with an oxide film. When the metal (electrode) is immersed in an aqueous solution the oxide film dissolves and a phase boundary metal/solution is formed (Thomas, 1996). The solution becomes known as an electrolyte and is electrically conductive as it contains metal ions. The electrons in the metal and the metal ions in the electrolyte form a double layer (Callister & Callister , 2000). An electric potential difference is formed across this double layer and the charge separation at the phase boundary. This electric potential measures the tendency of the metal to dissolve into the electrolyte and is dependent on the type of metal and electrolyte (Angst, 2011).

Electrochemistry is the study of reactions in which charged particles (ions or electrons) cross the interface between two phases of matter, typically a metallic phase (the electrode) and a conductive solution (the electrolyte) (Lower, 2007). This process is generally known as an electrochemical process (Lower, 2007). Corrosion is an electrochemical process that occurs on the surface of a metal in the presence of oxygen and moisture in which metals and alloys undergo transformation into oxides, hydroxides and aqueous salts. It involves two reactions, the anodic reaction and the cathodic reaction.

In the anodic reaction metal ions are inonised and go into solution leaving their electrons within the original metal. In the cathodic reaction the free electrons within the metal react with oxygen and water to form hydroxide ions. The anodic reactions is the rate limiting reaction as it determines the rate of the corrosion reaction.

Equations 2.1, 2.2 and 2.3 depict the basic processes of corrosion of a metal in aqueous solutions for the anodic reaction, cathodic reaction and overall reaction respectively (Sato, 2012):

anodic reaction: $M_M \rightarrow M_{aq}^{2+} + 2e_M^-$ (2.1)

cathodic reaction: $2Ox_{aq} + 2e_M^- \rightarrow 2Red(e_{redox}^-)aq$ (2.2)

overall reaction: $M_M + 2Ox_{aq} \rightarrow M_{aq}^{2+} + 2Red(e_{redox}^-)aq$ (2.3)

The anodic and cathodic reactions occur simultaneously and are each one half of the corrosion reaction thus they are termed 'half cell' reactions. Values of 'electrode potential' are associated with each of the half-cell reactions. There exists a potential difference between the anodic and cathodic half cell regions which generates a current flow termed corrosion current (I_{corr}) (Thomas, 1996). The sections below focus on the half-cell potential, corrosion potential and electrode potential phenomena which are fundamental concepts of electrochemistry and corrosion theory as they assist in predicting the direction and intensity of the corrosion process (Corrosion Science, 2011).

a) Half-cell potential and electrode potential

A standard electrode potential (E^0), also known as half-cell or reference electrode, can be used to measure the potential of a half-cell reaction. This is true for standard conditions where the mean temperature is 25℃, the pressure is 1.0 bar, and a concentration of 1.0 mol/l of metal ions in the electrolyte (Thomas, 1996). When a metal electrode is immersed into a solution of its own ions and at non-standard conditions, the Nernst equation can be used to calculate the electrode potential established as shown in Equation 2.4 (Krajci & Jerga, 2015):

$$E_{eq} = E^0 - \frac{RT}{zF} \ln \frac{a_{red}}{a_{ox}} \quad (2.4)$$

where E^0 is the standard half-cell (reduction or oxidation) potential; R is the universal gas constant (8.314 JK^{-1}/mol), T is the absolute temperature (K); z is the number of electrons transferred which is 2 for iron; F is Faradays constant (96487 $amp.sec$); a_{red} and a_{ox} are the reductant and oxidant activities (frequently replaced by concentrations), respectively.

The potential of an electrode is measured as a potential difference to a standard electrode with defined zero potential (usually Standard Hydrogen Electrode - E_{SHE} = 0 V), mutually connected with a salt bridge. The standard half-cell potential characterizes the nobility of the metal with the positive potential corresponding to noble metals resistant to corrosion (such as Gold where E_0 = 1.56 V) and the negative potential corresponding to base metals (such as iron where E_0= -0.44V) (Krajci & Jerga, 2015).

At equilibrium potential (E_0 *or* E_{eq}) the reduction and oxidation reactions for a half-cell reaction occur at the same time. The oxidation or reduction reaction can be expressed by the rate of transportation of electric current i.e. the net current exchange I_0 or the net exchange current density i_0, both equal to zero. The exchange current density strongly influences the corrosion rates and its magnitude depends on the type of half-cell reaction, electrode metal, electrolyte, temperature and concentrations of metal ions in the electrolyte (Küter, 2009).

Equation 2.5 shows the Butler-Volmer (Bockris, et al., 2000) equation which describes the dependence of the electric current density (i) on the potential if both a cathodic and anodic reaction occurs on the same electrode.

$$i = i_0 \{\exp\left[\frac{\alpha_a zF}{RT}\left(E - E_{eq}\right)\right] - \exp\left[-\frac{\alpha_c zF}{RT}\left(E - E_{eq}\right]\right\} \quad (2.5)$$

where i is the electrode current density (A/m^2); i_0 is the exchange current density (A/m^2) (defined as the current in the absence of net electrolysis and at zero

potential); E is the electrode potential (V); E_{eq} is the equilibrium potential (V); α_a and α_c are the anodic and cathodic charge transfer coefficients respectively.

The difference E - E_{eq} is denoted as η, the activation overpotential. Equation 2.5 represents the total current i.e. sum of cathodic and anodic currents. At potential E_{eq} the exchange current density corresponds both to the anodic and cathodic polarization curve with the respective paths of the polarization curves shown in Figure 2.1.

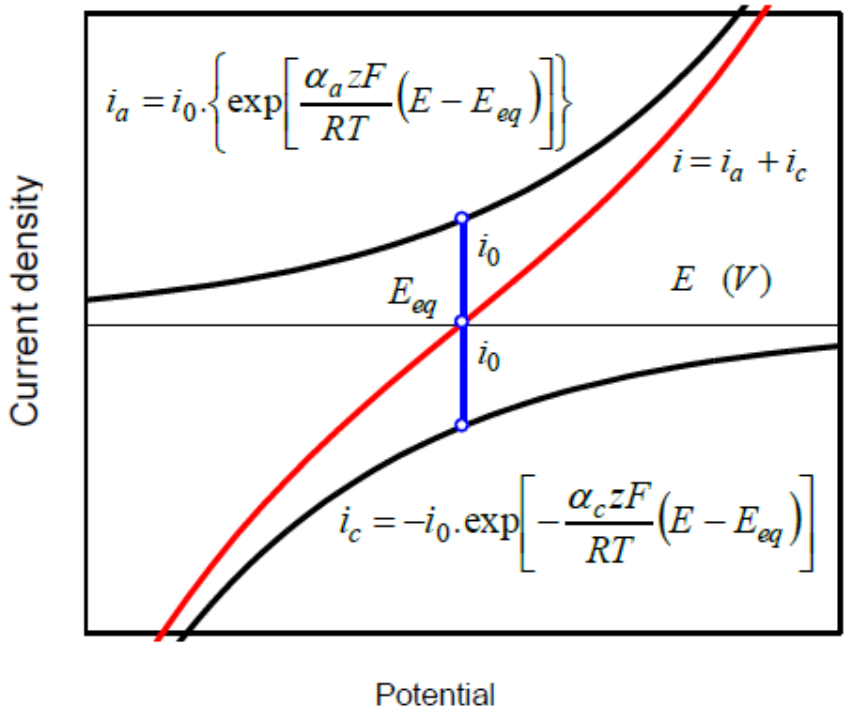

Figure 2.1: The course of polarization curve of steel in the vicinity of equilibrium potential *(Wang, 2000)*

From Figure 2.1 it can be seen that a change in the equilibrium will result in a new state and if the overpotential $\eta > 0$ the anodic reaction will predominate and the metal will dissolve (Krajci & Jerga, 2015).

The currents measured during polarization influence the shape of the polarization curve. They are a function of the transfer of the electrons at the electrolyte/electrode interface (charge transfer current), and the movement of the reactants or products at distances close to the electrode (also termed mass transfer controlled current) (Kear & Walsh, 2005).

b) Corrosion potential

When corrosion occurs on a metal surface, a corrosion potential referred to as E_{corr} is established and the actual potential adapts a mixed potential to a value between the equilibrium of the cathodic and anodic reactions (Austin, Lyons, & Ing 2004). Wagner and Traud (2006) established the mixed potential theory and the theoretical basis to these important parameters.

The anodic polarisation represents the driving force for corrosion by the anodic reaction such that the tendency for corrosion increases with the magnitude of anodic polarisation. Similarly, according to Kim and Kim (2008) anodic polarization is the only cause for steel corrosion in concrete structures.

Polarization is measured as overpotential and can be expressed as cathodic overpotential or anodic overpotential as shown in Equations 2.6 and 2.7 respectively (Bardal, 2004):

$$\eta_a = E_{corr} - E_{0,a} > 0 \quad (2.6)$$

$$\eta_c = E_{corr} - E_{0,c} < 0 \quad (2.7)$$

where η_a is the anodic overpotential, η_c is the cathodic overpotential and $E_{0,a}$ is the equilibrium potential of the anodic reaction and $E_{0,c}$ is the equilibrium potential of the cathodic reaction.

The corrosion potential (E_{corr}) is a mixed potential between the equilibrium potential of the anodic and cathodic reactions which depend mainly on the moisture content and oxygen availability (Sandberg, 1995).

2.2.2. Thermodynamics of steel corrosion

Steel that is exposed to the earth's atmosphere will always react with oxygen and moisture and revert to a lower energy state such as an oxide or hydroxide due to its thermodynamically unstable nature (Hansson, et al., 2007). Only the surface atoms of the steel are available for reaction with the atmosphere thus any coating on the steel will reduce this reaction.

Steel embedded in concrete is protected from moisture and oxygen by the concrete itself and the high alkaline solution in the concrete pores (Hansson, et al., 2007). At the normal pH levels (values between 12 to 13) of the concrete pore solution, insoluble corrosion products form on the surface of the steel creating a ferric oxide protective coating (passive film) which limits the metal loss due to corrosion to 0.1 – 1.0 µm/year (Rosenberg, Hansson, and Andrade,1989).

The ferric oxide coating forms a passive layer on the steel surface. This thermodynamic state of steel is referred to as *passivity* or *passive state* and prevents active corrosion of the steel. A metal can exist in two other thermodynamics states, the *immune state* and *active corrosion state.* According to Pourbaix (1974) *immunity* (immune state) of a metal refers to the state of a metal in which corrosion is thermodynamically impossible in a given environment. The *active corrosion state* of a metal refers to the reaction of metal with its non-metallic environment resulting in the continuing destruction of the metal. Concrete is a permeable material which makes it susceptible to the ingress of chlorides in solution as well as gases such as carbon dioxide. Contamination by chlorides and carbon dioxide as well as pH levels below 9.0 destroys the passive film resulting in active corrosion rates as high as several mm/year (Hansson, et al., 2007).

Pourbaix (1974) developed potential-pH diagrams, also referred to as Pourbaix diagrams, that depict the three different thermodynanic states of iron and iron oxides in solution. Figure 2.2 shows a simplified Pourbaix diagram for iron in water at 25℃ (iron concentration $10^{-6}\ mol/l$) with only Fe, Fe_2O_3 as solid products considered. The dashed lines in Figure 2.2 represent the equilibrium potentials below which oxygen or hydrogen reduction occurs. Water is in equilibrium with the respective hydrolysis ions (H^+ and OH^-) between these dashed lines. At low potentials iron is immune (as can be seen in the diagram) and is in a non-reactive state where it does not dissolve into solution nor react with water to form passive oxides. At low potentials and high pH values *low potential corrosion* may occur when the oxygen content is extremely low (Silva, 2013).

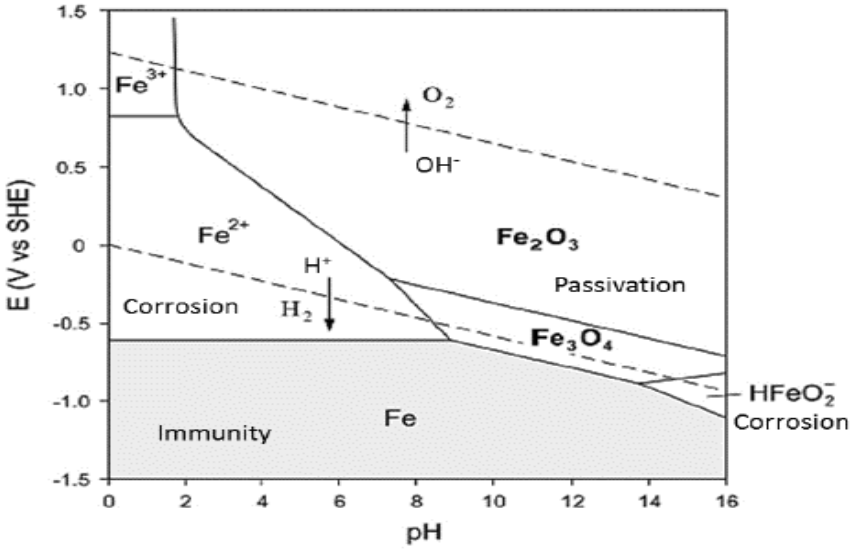

Figure 2.2: Simplified Pourbaix diagram for iron in water (for iron concentration 10^{-6} mol/l and 25℃) *(Pourbaix, 1974)*

Pourbaix diagrams consist of stability domains and equilibrium lines. The former describes the domains of favoured thermodynamic stability of the different metal species. The latter describes the lines representing the various possible reactions of the aqueous chemical system.

The pH dependency of an equilibrium line is determined from the anticipated H^+or OH^- ions in the reaction leading to the following types of equilibriums lines in the Pourbaix diagram (Küter, 2009):

i. Equilibrium lines of *half-cell reactions with participation of* H^+*or* OH^-ions which correspond to inclined lines in the Pourbaix diagram.
ii. Equilibrium lines of *half-cell reactions without participation of* H^+*or* OH^- ion which correspond to horizontal lines in the Pourbaix diagram.
iii. Equilibrium lines of *acid-base reactions with participation of* H^+*or* OH^-ions which correspond to vertical lines in the Pourbaix diagram.

From the equilibrium lines, presented in combination with the associated stability domains in the Pourbaix diagram in Figure 2.2, preliminary conclusions on the thermodynamics of iron have been made by Pourbaix (1974a). These conclusions are extended and correlated with other aspects of $Fe - H_2O$ systems as well as

Pourbaix diagrams for other metals and elements transferred to the concrete environment. Pourbaix (1973) stated that the distance between the equilibrium lines which limits the immune area, and the equilibrium line which limits the stability domain of water, decreases with increasing pH. This indicates that the corrosion rate of iron decreases with increasing solution pH, furthermore, it was observed that the potential is lifted into the passive region in alkaline to neutral solutions with dissolved oxygen. Below neutrality the passive layer is not stable and dissolved oxygen increases the corrosion rate. Subsequently, acid environments lead to high corrosion rates not only by providing more oxidising power but by not allow for passivation of iron (Pourbaix, 1973).

The applicability of the Pourbaix diagram to steel corrosion in concrete is limited as Pourbaix diagrams are limited to one metal in pure solution and do not take into account the influence of other substances which affect the thermodynamics of the system to a large extent (Küter, 2009). Pourbaix diagrams only reflect the thermodynamic state of the selected environment for a certain situation i.e. metal ion concentration, temperature, pressure and the effects that influence the actual conditions such as the surface of a metal. Furthermore, although the theory behind the Pourbaix diagram is rather simple, its establishment is calculation intensive (Silva, 2013).

2.3. Corrosion of steel in concrete

Corrosion of steel in concrete can be described as the destructive attack of a metal by chemical or electrochemical reaction with its environment (Bell, 2017). According to Ing (2003) the requirements for steel corrosion in concrete are as follows:

Anode: this is where metal ions go into solution as positively charged ferrous ions (Fe^{2+}), liberating electrons that travel through the steel to the cathode. The anode is the site for corrosion which undergoes the oxidation reaction as shown:

Oxidation reaction: $$Fe \rightarrow Fe^{2+} + 2e^{-} \quad (2.8)$$

Cathode: no corrosion occurs here, instead oxygen (O_2) and water (H_2O) present in the concrete matrix react with the free electrons from the anode to form

hydroxyl ions (HO^-) which in turn migrate to the anode and react with the (Fe^{2+}), to form ferrous hydroxide ($(FeOH)_2$). This is an electrically neutral ferrous hydroxide that can react further with O_2 and H_2O to form hydrous ferric oxide $Fe_2O_3 3H_2O$, which is a red brown dust.

Reduction reaction: $$H_2O + \frac{1}{2}O_2 + 2e^- \rightarrow 2OH^- \quad (2.9)$$

Metallic path: the steel embedded in the concrete that electrically connects the anode and cathode completing the corrosion circuit.

Electrolyte: the alkaline pore solution (salts and moisture) in concrete that conduct electric current by ionic flow.

The two half-cell reactions (oxidation and reduction) described above occur simultaneously and produce the overall reaction below (Pourbaix, 1973):

$$Fe + H_2O + \frac{1}{2}O_2 \rightarrow Fe(OH)_2 \quad (2.10)$$

The overall reaction results in several corrosion products, such as $Fe(OH)_2$ as shown in Equation 2.10. The factors that will speed up the corrosion rate are an increase in the amount of oxygen, moisture, pH, temperature, chlorides and carbon dioxide (Marcotte, 2001). According to (Hansson, et al., 2007) the most detrimental consequence of reinforcement corrosion is the accumulation of expansive and insoluble corrosion products in the concrete. These corrosion products result in the increase of internal pressure leading to cracking and spalling of the concrete cover. Figure 2.3 shows the different densities and volume expansion products of the various corrosion products detected by several researchers (Liu and Weyers, 1998; Roberge, 1999; Jaffer and Hansson, 2009). As can be seen in Figure 2.3, the relative unit volume of corrosion products can be as much as five-unit volumes more ($Fe_2O_3 3H_2O$) than the unit volume of pure iron. Several researchers (Roberge, 1999; Broomfield, 1997; Jaffer and Hansson, 2009) found that the type of corrosion product is mainly dependant on two factors, the pH of the pore solution and the availability of oxygen.

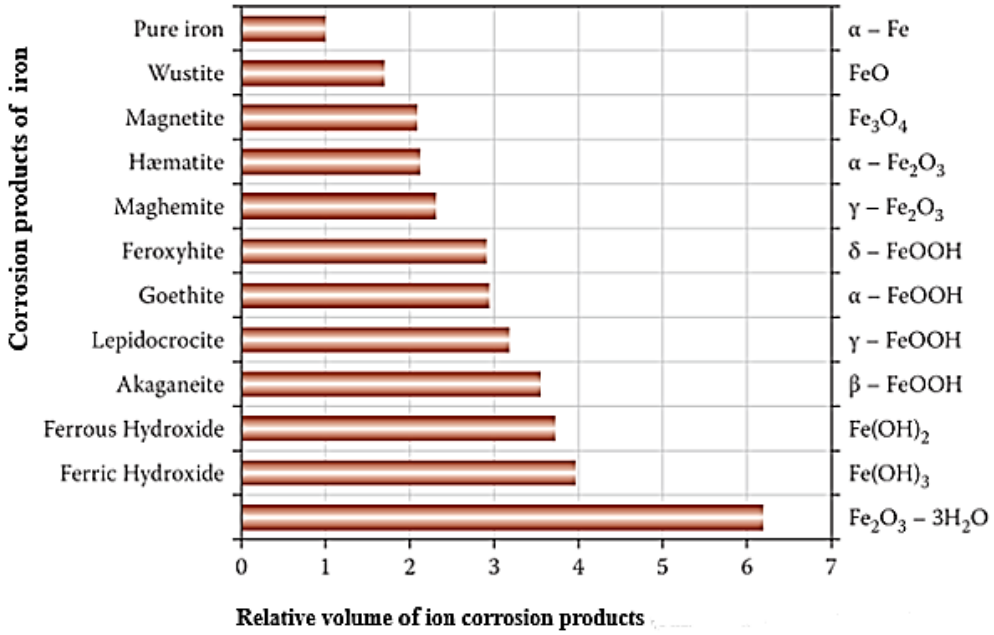

Figure 2.3: Corrosion products of iron (volume in cm^3) (Jaffer and Hansson, 2009)

According to Liu and Weyers, (1998); Bhargava, et al., (2006); El Maaddawy and Soudki, (2007), ferrous hydroxide is the main corrosion product of steel embedded in concrete. After cracking of the concrete cover more stable products such as hematite and magnetite are formed due the increase in oxygen supply.

Researchers conducting accelerated corrosion test by immersing the concrete specimens in salt solution have observed greenish-black corrosion products exuding the concrete indicating a large presence of ferrous hydroxide (Malumbela, et al., 2010a; Lewis, 2012;). Upon reaching the surface, the corrosion products turned reddish-brown indicating a conversion to the more stable compounds such as haemetite and magnetite.

In drier conditions and slower corrosion rates oxygen is expected to be in abudance resulting in the formation of already stable reddish-brown corrosion products (Francois and Arliguie, 1998; Castel, et al., 2003; Zhang, et al., 2010).

2.4. Corrosion initiation of steel in concrete

The high alkaline environment provided by the pore solution in the concrete creates a passive film around the reinforcing steel that arrests corrosion to negligible values i.e. (<0.1 µA/cm^2) throughout the life of the structure (Ing,

2003). There are two main aggressive substances that cause corrosion of reinforced concrete structures, these are carbon and chlorides. The following sections will discuss the causes of corrosion onset of the two aggressive agents which are termed carbonation-induced corrosion and chloride-induced corrosion for the ingress of carbon and chlorides respectively. Special emphasis will be placed on chloride-induced corrosion initiation as it is the main focus of this study.

2.4.1. Carbonation-induced corrosion of steel in concrete

Carbonation is a slow process where atmospheric carbon dioxide ingresses the pore structure of the hardened cement paste and reacts with the calcium hydroxide ($Ca(OH)_2$) to form calcium carbonate ($CaCO_3$) as shown in Equation 2.11:

$$CO_2 + Ca(OH)_2 \rightarrow CaCO_3 + H_2O \quad (2.11)$$

This process leads to a reduction in the pH of the pore solution in concrete from around 12.5 to around 8.5 at complete carbonation. This renders the passive film on the steel surface unstable and the metal susceptible to corrosion (Ballim, et al., 2009). Carbonation progresses into the concrete as a 'front' and is a slow process with the rate dependent on the porosity and permeability of the concrete cover and estimated at up to 0.1 mm per year in high-quality concrete (Zhou, et al., 2014).

There are several models available in literature that describe the rate of advancement of carbonation. The most commonly used one is given in Equation 2.12 (Parra & Valcuende, 2010):

$$x = K\ (t^{0.5}) \quad (2.12)$$

where x is the carbonation depth (mm), t is the concrete exposure time (months) and K is the carbonation coefficient ($mm/\sqrt{month}$).

Carbonation is rarely a problem in structures with good concrete quality and adequate cover and does not occur if the concrete is water-saturated or in very dry conditions. This type of corrosion is prevalent in structures in industrial areas and car parks and is characterised by microcell/homogenous corrosion (Boddy, et al.,

1999). The favourable conditions for increased carbonation rate are temperature around 20˚C, relative humidity in the range of 50-70 %, increased CO_2 concentrations, water/binder (w/b) ratios equal to or greater than 0.6 and the use of cement extenders such as fly ash (FA) and ground granulated blast-furnace slag (GGBS) (Silva, et al., 2014).

2.4.2. Chloride-induced corrosion of steel in concrete

This type of corrosion occurs in RC structures that are exposed to chloride ions. The main sources of chlorides in RC structures are sea-water i.e. a marine environment, de-icing salts and salt contaminated soil. Chloride ions can penetrate through the concrete cover or reach the steel through cracks. Corrosion of RC structures due to contamination by chloride ions is the most extensively researched and documented type of corrosion in literature as the mechanisms by which chlorides promote corrosion are not entirely known. The consensus in literature is that corrosion is initiated when the chloride content at the steel level reaches (and exceeds) a critical value called the *chloride threshold or critical chloride content* and in the presence of oxygen and moisture (Page & Treadaway, 1982). The chlorides then attack the passive oxide film protecting the steel surface and lead to *localised corrosion* or *pitting corrosion* (where pits/small cavities develop on the steel) as shown in Figure 2.4 (Le, 2010).

The following sections will disscus chloride-induced corrosion initiation in more detail such as chloride threshold value, free chlorides vs. bound chlorides and lastly factors affecting chloride induced corrosion.

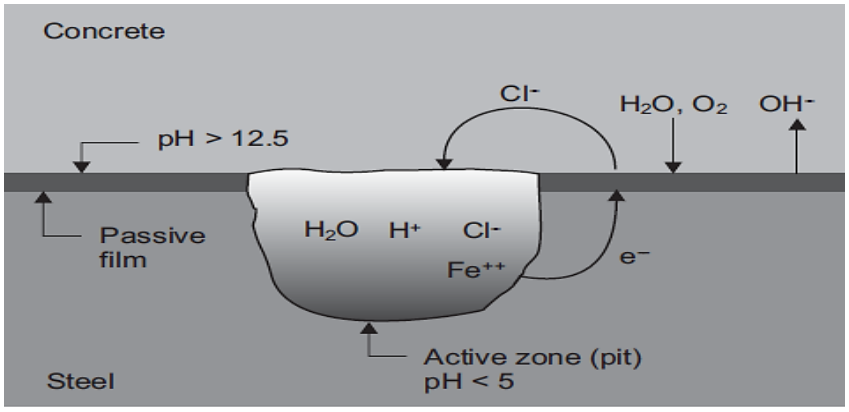

Figure 2.4: Pitting corrosion of steel bar in RC exposed to Cl^- ions *(Le, 2010)*

2.4.3. Chloride threshold value/critical chloride content

The chloride threshold value or the critical chloride content (C_{crit}) is commonly defined in literature as the chloride content required for depassivation of the steel. In in other words it is the amount of chloride content accumulation at the steel level required to initiate corrosion (Schiessl and Raupach, 1990; Schiessl and Lay, 2005). C_{crit} values are commonly expressed in literature in two ways; (1) as a percentage weight of concrete and (2) as a percentage weight of the cement.

The knowledge of reliable C_{crit} values is crucial and has been identified to be one of the most decisive input parameters in probabilistic service life modelling (Gulikers, 2006). Presently there is no general agreement on a C_{crit} value with results reported in literature scattering over a large range (Glass and Buenfield, 1997; Ann and Song, 2007). This is due to the difference in expressions; measuring techniques; testing conditions as well as the complexity of initiation of pitting corrosion (Angst, et al., 2009). Consequently, conservative values are used for critical chloride content with the common practice being to limit the tolerable total chloride content to or around 0.4% by weight of cement in European and North American countries (RILEM, 1994). In the 'fib model code for service life design' the critical chloride content is a stochastic variable where C_{crit} is defined by a beta-distribution with a lower boundary and mean value of 0.2% and 0.6% total chloride content by weight of cement respectively (FIB, 2006).

The value of C_{crit} can also be expressed as the free chloride content relative to the weight of the concrete or as the free chloride ion concentration expressed as $(Cl^-)/\ (OH^-)$ mole ratio. The latter expression of critical chloride content considers the influence of the pH value of the pore solution on the chloride ion activity as reported by Bertolini, et al., (2004) and has been cited in earlier works by Venu, et al. (1965); Hausmann (1967); Gouda (1970). Later works by Shi, et al. (2009) reported that the pitting corrosion of steel is governed by the competition between aggressive Cl^- and inhibitive OH^-, thus making the $(Cl^-)/\ (OH^-)$ ratio a more reliable indicator than the chloride concentration. In practice though, it is much easier to express C_{crit} as the total chloride content

relative to the weight of cement or concrete as it is near impossible to measure the free chloride content or the pH of the concrete pore solution. Table 2.1 shows the difference in published data of C_{crit} values for Portland cement (PC), fly ash (FA), silica fume (SF) and ground-granulated blast furnace slag (GGBS) cement blends.

The scatter in the results can be attributed to the different experimental procedures used and the numerous parameters that affect chloride induced corrosion in concrete.

Table 2.1: Total chloride content values under outdoor exposure conditions

Binder Type	C_{crit} (% by mass of concrete)	Reference
FA, SF, GGBS	*0.3 – 0.75*	*Sandberg, 1998*
PC, GGBS, FA	*0.25 – 0.75*	*Breit, 1998*
PC	*0.4 – 1.3*	*Morris, et al., 2004*

2.4.4. Free vs. bound chlorides

Chloride ions exist in concrete matrix as free and bound chlorides. Free chlorides are water-soluble chlorides dissolved in the concrete pore solution and bound chlorides are bound to the binder matrix (Glass, et al., 1996).

a) Bound chlorides

All mineral cements bind chlorides to a certain degree thus strongly influencing the rate at which chlorides from an external source penetrate the concrete (Scott, 2004). Bound chlorides are effectively removed from the transport system within the pore solution, resulting in changes to the pore solution concentration (Glass, et al., 1997). Subsequently, it is not the total chloride content that is involved in corrosion.

Chlorides are removed from the pore solution through physical binding, as a result of adsorption to the hydration products (calcium silicate hydrate) (Lambert, et al., 1991; Oh, et al., 2003). Chlorides are further removed from the pore solution through chemical binding with concretes tricalcium aluminate (C_3A) or tetracalcium aluminoferrite (C_4AF) phases (Shi, et al., 2009). The amount of

chlorides available in the pore solution as a result of chloride binding and the pH of the pore solution are also determined by the type of binder which in turn influences corrosion initiation (Angst, et al., 2009). Zhang, et al. (2011) reported a reduction in chloride diffusion coefficent of blended cement over plain Portland cement concrete such that 10 to 20% replacement of microsilica in cements resulted in a reduction of 2 to 11 times in chloride diffusion coeffiecent than that of plain Portland cement concrete. This may be attributed to the densification of the blended cement cocncretes microstructure due to the development of secondary calcium silica hydrate.

Bound chlorides were generally assumed to not pose a corrosion risk. However works by Glass, et al. (2000) and Bertolini, et al. (2004) showed that bound chlorides may be released to participate in the corrosion process and can pose the same risk as free chlorides.

b) Free chlorides

Free chlorides are those dissolved in the concrete pore solution. The expression of the chloride threshold values in terms of the *free chloride content* assumes that the bound chlorides are completely removed from the pore solution and pose no risk for pitting corrosion initiation (Angst, et al., 2009). It is a generally believed that only free chlorides can promote pitting corrosion and not those bound. Contrary to the general belief, Glass, et al. (2000) and Bertolini, et al. (2004) reported that bound chlorides do play a role in corrosion initiation because they are released when the pH value of the pore solution drops to values below 11.5, with chloride concentrations of 0.6 kg/m^3 (Hartt, et al., 2004) and 0.20% by weight of cement being able to initiate rebar corrosion.

2.4.5. Factors affecting chloride-induced corrosion corrosion iniation of steel in concrete

The initiation of chloride induced corrosion is affected by various factors. These factors are dependedent on concrete cover quality (binder type, w/b ratio, curing), concrete cover thickness, chloride content and chloride binding capacity of the binder. These factors are discussed in the sub-sections that follow.

a) Effect of critical chloride content on corrosion initiation

As mentioned in the previous Section 2.4.2, there is no general consesus on the single value for the critical chloride content, (also referred to as the critical threshlod level), valid for all different binder types and exposure environments. The value of C_{crit} is affected by numerous interrelated parameters, some of which are Steel-concrete interface; Concentration of hydroxide ions in the pore solution (pH); Electrochemical potential of the steel; Binder type and w/b ratio; Degree of hydration (Cigna, et al., 2002):

Glass and Buenfeld (1997) suggested that the condition of the steel-concrete interface, the pH of the concrete pore solution and the steel potential be considered as the most dominating influencing factors. The variety of factors influencing the C_{crit} value is a clear indicator of the complexity of developing a unique C_{crit} value applicable to a wide range of structures in various exposure conditions. As a result of the lack of a clear defined value of C_{crit}, designers use conservative values for the maximum allowable chloride ion content in concrete.

Table 2.2 shows the maximum allowable free chloride content for different types of concrete members, prescribed by the American Concrete Institute (ACI 318, 2000). The critical chloride content value can be reduced by lowering the w/b ratio or by the addition of cement extenders. The effects of w/b ratio on the chloride concentration were investigated by Petterson and Sandberg (1997), the researchers found that an increase in w/b ratio from 0.4 to 0.6 resulted in approximately a 40% reduction in the critical chloride concentration.

Table 2.2: Maximum chloride ion content of concrete (ACI 318, 2000)

Type of Member	**Maximum Cl^- (% by weight of cement)**
Prestressed concrete	*0.06*
Reinforced concrete exposed t chloride in service	*0.15*
Reinforced concrete protected from moisture in service	*1.00*
Other reinforced concrete structures	*0.3*

For blended cements, their slow early hydration processes lead to higher short-term concrete permeability which may be attributed to the lower threshold values (Scott, 2004). Table 2.3 shows the various chloride threshold values for concretes with different binders.

The results presented by Scott (2004) show varying values for the threshold values for different binder types. Other researchers have achieved different chloride threshold values for the same binder types. Ultimately a reduction in the critical chloride content leads to a decrease in the time to corrosion initiation.

Table 2.3: Chloride threshold for different binder types (Scott, 2004)

Binder Type	Chloride threshold (% conc. by mass of binder)
Plain Portland Cement (PC)	*0.53*
75/25 PC/GGBS	*0.41*
50/50 PC/GGBS	*0.08*
25/75 PC/GGBS	*0.02*
70/30 PC/Fly ash	*0.36*
50/43/7 PC/GGBS/silica fume	*0.08*

b) Effect of chloride binding capacity on corrosion initiation

Chloride binding is the removal of chloride ions from the pore solution through interaction with the concrete matrix such as chemical reaction with C_3A to form calcium chloroaliminates (Boddy, et al., 1999). Chloride binding affects the level of free chlorides in solution and influences chloride transport through partial blocking of pores due to the formation of the calcium chloro-aliminates (Scott, 2004).

The degree of chloride binding related to the binder type is dependent on the content of C_3A and C_4AF phases in the cement, the main parameters in the formation of Friedel's salt between chlorides and the AFm phases that remove substantial amounts of chloride from the pore solution. The amount of Calcium-Silicate-Hydrate (C-S-H) gel in the concrete was also reported by Tang and

Nilsson (1993) to be a strong influencer of the chloride binding capacity of the concrete such that binders containing admixtures like silica fume (SF), pulverised fly ash (FA) or ground granulated blast furnace slag (GGBS) offer larger surface areas for chloride adsorption due to enhanced formation of more C-S-H gel. However, whilst the improved chloride binding capacity may incease C_{crit}, a review by Angst, et al. (2009) reported that there is an expected decrease in the pH of the pore solution contributing to the instability of the passive film. Despite this, the benefits of binders containing admixtures out weighs the consequence of the reduced pH value of the pore solution. Work by Arya, et al. (1990) showed increased binding capacity of slag cements compared to PC for admixed chlorides, the results from their work are summarized in Table 2.4.

Table 2.4: Effect of binder type on chloride binding (Arya et al., 1990)

Binder Type	Total Cl^-	Free Cl^-	Bound Cl^-	% Bound
PC	*1.635*	*0.831*	*0.804*	*50*
30% FA	*1.887*	*0.818*	*1.069*	*57*
70% slag	*1.750*	*0.830*	*0.920*	*53*
10% SF	*1.265*	*0.684*	*0.581*	*46*

From the work of Arya et al. (1990) shown in Table 2.4, it can be seen that 30% FA had a greater binding capacity (57%) compared with 70% slag (53%). Contrary to these findings, Glas, et al. (1997) noted a variation in the order of binding capacity with 65% slag resulting in the greatest percentage of chloride binding capacity.

The binding of chlorides leads to an increase in the time to corrosion initiation. Tarek, et al. (2002) examined concrete after 15 years of exposure in tidal zones in their study on the effects of cement extenders on chloride binding and limiting the ingress of chlorides. The study showed that for an assumed cover depth of 70 mm and a C_{crit} value of 0.4% free chlorides by mass of cement, the time to corrosion initiation is 22, 65 and 150 years for PC, FA (10 – 20%), slag (60 - 70%) respectively. The effects of binder type and chloride binding are clearly shown to

influence the time required for chlorides to attain sufficient concentration to inititate corrosion.

c) Effect of binder type on corrosion initiation

The effect of binder type on corrosion initiation is based on the critical threshold level of the different binder types. Conflicting results are presented in literature by the different researchers on the effects of GGBS, FA and SF cement replacement on the critical threshold level.

Thomas, Mathews and Haynes (1990), Bramford and Chapman-Andrews (1994) reported that cement replacement with GGBS and FA had no effect on the chloride threshold level. Whereas Thomas (1995) reported that cement replacement with FA showed a significant reduction in chloride threshold level due to its effect of reducing the hydroxide concentration of the pore solution. According to Thomas (1995) even though FA has a lower chloride threshold value, the overall effects of FA are beneficial due to increased resistance to chloride penetration. A reduction in the critical chloride threshold level was also reported for cement replacement with GGBS and SF by MacPhee and Cao (1993), and Hansson and Sorensen (1990).

d) Effect of w/b ratio on corrosion initiation

The capillary porosity of the cement matrix is a function of the w/b ratio (for a specified curing conditions) such that a lower w/b ratio helps to stabilise the micro environment at the depth of the steel. A lower w/b ratio results in a denser pore structure of the concrete, increasing the resistivity of the concrete and limiting the ingress of oxygen (Scott, 2004). The effect of the w/b ratio on corrosion initiation is governed by its influence on the chloride diffusion coefficient and chloride threshold level. According to Byfors (1990), a lower w/b ratio results in a higher threshold level through a reduced leaching rate for alkalis and a buffer for unreacted cement which helps to maintain a high concrete alkalinity. Experimental results by Pettersson (1993) shown in Figure 2.5, support Byfors (1990) as they indicate a higher chloride threshold level for concrete with a lower

w/b ratio such that an increase in w/b from 0.4 to 0.6 resulted in approximately a 40% reduction in the critical chloride content.

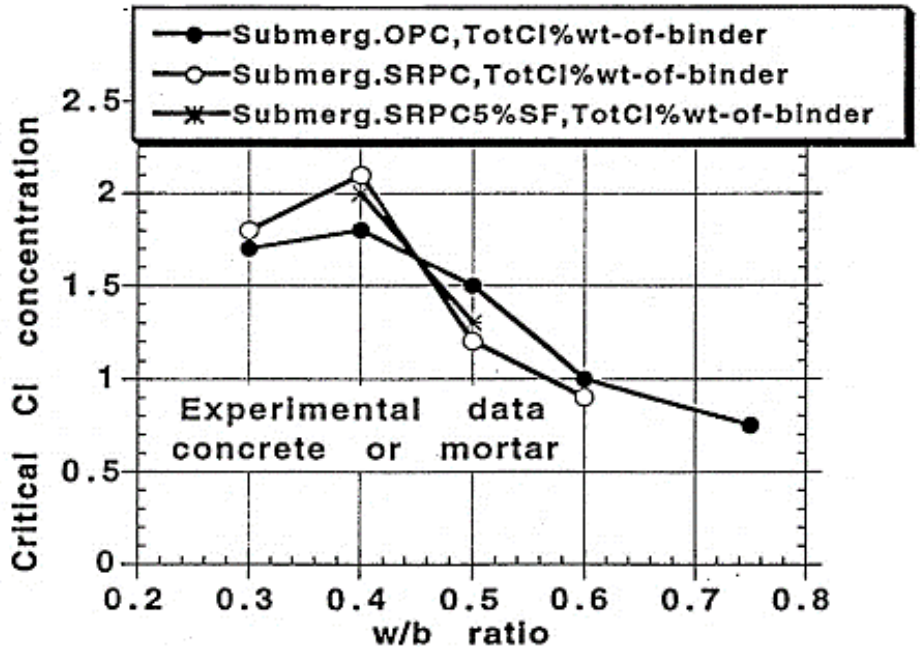

Figure 2.5: Experimental data for the chloride threshold levels for corrosion initiation in submerged concrete. (*Pettersson, 1993).*

e) Effect of curing on corrosion initiation

Curing is the process of allowing the concretes microstructure to mature with time. This process should be conducted in a manner that allows the cement, during the hydration process, to develop a cement matrix with as little capillary porosity as possible at the time of initial environmental exposure (Nilsson, et al., 1996). The curing time is often determined by the strength requirements of the concrete, for example, if concrete strength is specified at the age of 28 days, then the concrete is cured for 28 days.

However, concrete that will be exposed to chlorides may require additional curing time to provide the concrete with an advantage of developing a denser microstructure. The Danish Code of Practice (1926) for marine RC structures specifies a minimum of six weeks of curing time before concrete made with Portland cement is exposed to sea water which contains approximately 3.5% chlorides. Insufficient curing time increases the capillary porosity and microstructural defects; increases cracks and gross porosities of the cement

matrix. Subsequently this increases the concretes permeability to deleterious substances such as chloride ions which have dimensions in the order of 2 Å (Nilsson, et al., 1996). Whereas the capillary pores have dimensions in the order of 0.02 – 50 Å and can thus easily transport ions when filled with pore fluid, or transport gases when filled with air (Nilsson, et al., 1996).

f) Effect of concrete cover depth on corrosion initiation

The concrete cover *(covercrete)* provides a physical protective barrier between the reinforcing steel in the concrete and the deleterious substances, such as chloride ions, in the external environment. The time taken for deleterious substances to penetrate the concrete cover depth is dependent on quality and thickness of the covercrete. The protective abilities of the covercrete are hindered by imperfections such as cracks and honeycombing on the covercrete surface.

An increase in the concrete cover thickness and concrete cover quality results in an increase of the service life of a structure due to an increase in corrosion initiation (Torrent, et al., 2007). However, the thickness of the concrete cover can only be increased to a maximum of 80 – 90 mm as any further increase in the thickness results in wide flexural cracks which counteract the function of the concrete cover (Neville, 1998).

g) Effect of cover cracking on corrosion initiation

The concrete cover provides a physical barrier that limits the ingress of moisture, oxygen and corrosion inducing species such as chloride ions. The presence of macro-cracks and cavities on the concrete cover significantly increases the chloride penetrability of the concrete. The cracks in the concrete cover reduce the travel path of corrosion inducing species and alters their transport mechanisms. Macro-cracks in the concrete cover that do not reach the concrete surface are often not filled with water which is required for movement of chloride ions within the concrete. Under these circumstances the macro-cracks become barriers against chloride ingress. On the other hand, macro-cracks in submerged structures are permanently filled with water and thus act as a high velocity diffusion path for chloride ions. Under these conditions the cracks tend to be sealed by reaction

products such as manganese hydroxide and calcium carbonate from the concrete and the seawater compounds reactions. Thus, the sealed cracks hinder the movement of chloride ions within the concrete (Stillwell, 1983).

The most aggressive exposure condition for cracked concrete is a combination of wet and dry exposure such as tidal spray zones and de-icing salt application. Under these conditions the cracks will be filled with saline water during the wet period and a concentrated chloride content during the drying period. Mangat and Gurusamy (1987) conducted a study on chloride ion concentrations close to cracks and found that the concentration in the vicinity of cracks increases with increasing crack width.

Cracks wide and deep enough to reach the steel surface provide direct access to the steel surface effectively eliminating the corrosion initiation phase. Whereas the effect of fine cracks (width less than 0.1 mm) on concrete permeability is highly dependent on the crack intensity. Studies by Samaha, et al., (1992) found that load-induced fine cracks will not increase the permeability until the load exceeds 75% of maximum strength. Based on these findings, the crack intensity must exceed a certain level before the cracks systems becomes connective and able to influence permeability.

Similar findings have been reported by Fagerlund (1993) who modelled chloride penetration into concrete with and without cracks and showed that isolated fine cracks have only a marginal effect on the diffusivity of concrete unless the frequency and crack width are exceptionally large. Currently, there is limited information in literature with regards to ingress of aggressive agents into cracked concrete as the transport properties of cracked concrete are more complex and not clearly understood and cannot be correlated with those measured on uncracked concrete (Nilsson, et al., 1996).

2.4.6. Chloride-induced corrosion initiation as a function of time

The mechanism of ingress is an important factor in determining the time taken for the chloride ions to reach the reinforcing steel level as it varies in different environmental exposure conditions. In partially saturated concrete, chlorides enter

by adsorption and capillary forces (Grantham, et al., 1997). In water-saturated concrete, clorides are considered to penetrate the cover by a diffusion mechanism, with the driving force being differential gradients (Andrade, 1993). In this scenario, Ficks's second law of diffusion can be applied to model the rate of chloride penetration.

The probability for corrosion initiation as a function of time can be calculated by means of a full-probabilistic or semi-probabilistic approach. This is similar to that used in the structural design limit states that indicates the boundary between the desired and the adverse behaviour of the structure (Bertolini, et al., 2016). In this approach, all the variables are described in a statistical manner, namely by means of probability distribution and the related parameters (mean value and variance) (Angst, 2011).

Several researchers (Maage, et al, 1995; Sangues and Kranc,1997; and Weyers,1998) have developed models based on Fick's second law of diffusion, to predict the length of the corrosion initiation period under various circumstances as shown in Equation 2.13:

$$\frac{\partial C}{dt} = D\frac{\partial^2 C}{\partial x^2} \tag{2.13}$$

where, *C* is the concentration of chloride ions, *t* is the time, *x* is the distance, and *D* is the diffusion coefficient which depends on the diffusing species and the concrete microstructure with boundary conditions of:

$C_x = 0$ at $t = 0$ *and* $0 < x < \infty$

$C_x = C_s$ at $x = 0$ *and* $0 < t < \infty$

where C_x is the chloride concentration at depth *x* at time *t* and C_s is the surface chloride concentration.

Fick's second law of diffusion is used to mathematically describe the penetration of chlorides through the cover zone whilst at the same time recognising that the actual transport mechanisms are far more complicated than the pure diffusion

mechanisms assumed for the model (Angst, 2011). Many of the chloride-induced corrosion initiation prediction models are based on Fick's second law of diffusion, for example the South Africa chloride prediction model (Mackenzie, 2001). Nilsson, et al. (1996) and Nilsson (2009) found that the empirical assumptions of diffusion allows modelling chloride ingress into concrete with reasonable accuracy, even for concrete exposed to continuous wetting and drying cycles. Subsequently many models based on Fick's second law of diffusion make use of the "error-function solution", expressed in Equation 2.14 (for 1-dimensional ingress):

$$C(x,t) = C_0 + (C_s - C_0)\left[1 - erf\left(\frac{x}{\sqrt[2]{D_a(t) \cdot t}}\right)\right] \qquad (2.14)$$

where: $C(x,t)$ = chloride content at depth *x* and time *t*

C_0 = initial, uniformly distributed chloride content in the concrete

C_s = chloride content at the exposed concrete surface

t = concrete age

D_a = apparent chloride diffusion coefficient.

D_a is considered to be a time-dependent variable due to the proceeding cement hydration which results in the continuously changing nature of the concrete microstructure (Mangat & Molloy, 1994).

Results from field and laboratory data have shown that the time-dependency of D_a can be empirically described by the relationship shown in Equation 2.15 which takes into account the decrease in chloride diffusivity with time due to the effects of continued hydration and chloride binding (Mangat & Molloy, 1994):

$$D_a(t) = D_0 \cdot (\frac{t_0}{t})^n \qquad (2.15)$$

where D_0 is a reference apparent diffusion coefficient, t_0 is the reference age and *n* is the age factor, which is a constant depending on concrete quality (binder type and w/b ratio).

The equation described above has been discussed extensively in literature and it has been well accepted that the diffusivity of concrete changes with time (Nokken,

et al., 2006). In the equation above D_a is referred to as "diffusion coefficient" only because it is a variable in Fick's second law of diffusion. It is not a true diffusion coefficient but rather an empirical parameter determined as the concretes resistance to chloride penetration and evaluated by means of an accelerated test (Nokken, et al., 2006). The test results are corrected using coefficients that consider the the real environmental exposure conditions as they cannot be direcly used to predict the chloride penetration in a structure. The acceptable failure probability, of pre-set performances of the structure as a function of time, should be selected on the basis of the severity of the adverse event ocurring (limit state) (Bertolini, et al., 2016). Figure 2.6 shows the use of these performance-based models using an example of calculation of the probabiliy of failure for the splash zone of a marine structure requiring a design service life of 100 years.

In Figure 2.6 P_f is assumed as the probability of initiation of chloride-induced corrosion and is plotted as a function of the mean value of concrete cover thickness.

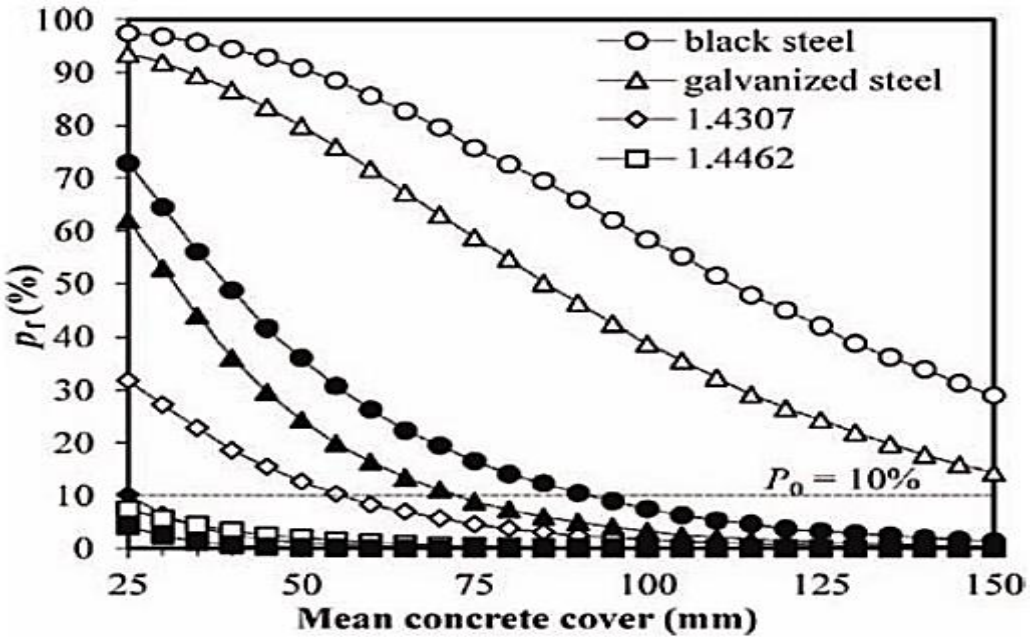

Figure 2.6: Probability of failure, P_f, as a function of mean concrete cover thickness, the type of reinforcement, and the type of binder (OPC = clear symbols and BF = shaded symbols), calculated for w/b = 0.45 (*Lollini, et al., 2015*).

The effect of different binders (Portland cement – OPC and blended cement with 70% of ground granulated blast furnace slag – BF), different types of reinforcing

bars (black steel, galvanised steel, and type 1.4307 and 1.4462 EN standard stainless steels) and a water/binder ratio of 0.45 is shown in the graph.

This graph can be used to determine the concrete binder type and type of reinforcement which will estimate the service life based on the combinations of minimum cover thickness, type of concrete and type of reinforcement. For example, when considering a target probability, P_0 of 10% for conventional black steel rebars and OPC concrete, a concrete cover higher than 150 mm would be required, making it unfeasible to guarantee the service life (Bertolini, et al., 2016). Furthermore, even in concrete made with ground-granulated blast furnace slag cement (BF) and a water/binder ratio of 0.45 a concrete cover thickness of 90 mm would be required. The graph shows that much more reasonable values of concrete cover thickness can be achieved with the use of corrosion resistant reinforcing bars (stainless steel bar) are used even when using ordinary Portland cement.

2.5. Corrosion propagation of steel in concrete

Corrosion propagation is the progresson of corrosion after the corrosion initiaiton period, if there is sustained availability of deleterious substances such as chlorides as well as moistures and oxygen. At this stage the steel is said to be in an active corrosion state which has the following detrimental effects (Jeffer & Hansson, 2009):

i. Formation of expansive corrosion products that exert pressure on the concrete resulting in cracking, delamination and spalling of the concrete cover,
ii. Reduction in steel mass and cross-sectional area which renders the concrete susceptible to structural failure.

Generally it is accepted that corrosion rates of less than 0.1 $\mu A/cm^2$ indicate passive corrosion and corrosion rates higer than 0.1 $\mu A/cm^2$ indicate active corrosion (Alonso et al., 2002).

At low corrosion rates, in the order of 1 $\mu A/cm^2$, it is estimated that the propagation may continue for 20 years before cracking of the concrete covers occurs (Andrade, et al., 1993). Active corrosion presents itself on the surface of the steel in various forms and characteristics and is described by the term morphology of steel. For the purposes of this study focus will be placed on the morphology of chloride induced corrosion discussed in the section below.

2.5.1. Forms of steel morphology for chloride induced corrosion

There are two main forms of steel morphology due to chloride induced corrosion, general/uniform corrosion and pitting/localised corrosion.

a) General/uniform corrosion

This form of steel morphology presents itself as uniform and general corrosion attack on the entire surface of the steel without any localised attack. This is due to anodic and cathodic reactions constantly exchanging places on the steel surface. (Küter, 2009).

General corrosion does not penetrate deep into the steel but is rather relatively evenly distributed over the majority of the surface thus resulting in uniform thickness reduction. This type of corrosion is not regarded as particularly dangerous as it occurs at a steady and often predictable rate thus facilitating easy control. One of the methods of controlling or mitigating the effects of this morphology of corrosion is making the steel thick enough to function for the service life of the component (Nimmo & Hinds, 2003). The corrosion rate can be expressed as mean loss of metal per unit over time, thus in order to facilitate corrosion for the service life of the steel, thicker steel sections can be used.

b) Pitting corrosion

Pitting corrosion occurs when the corrosion potential (E_{corr}) exceeds the critical potential, which is also termed, the pitting potential (E_{pit}), value in the pitting range of the polarization curve as illustrated in Figure 2.7:

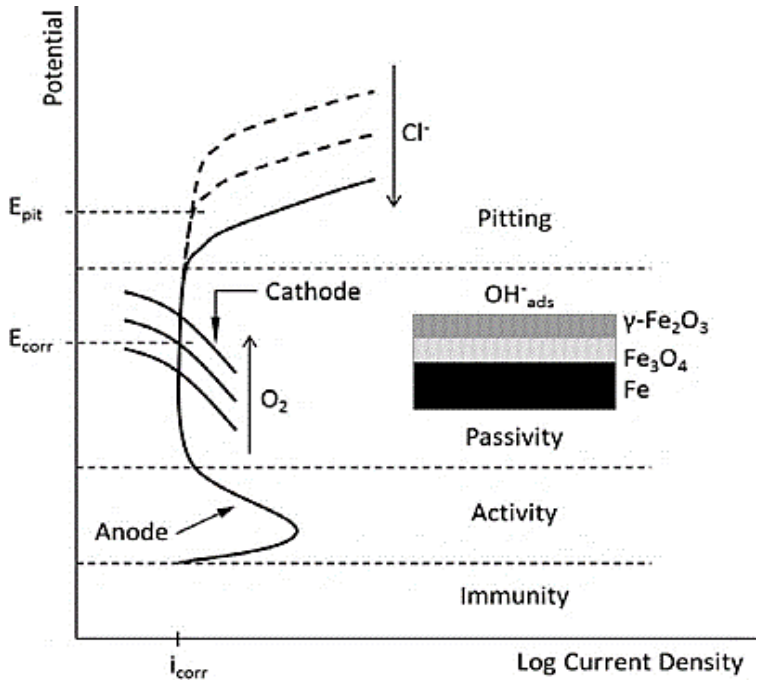

Figure 2.7: Polarization curve for steel exhibiting passivity. Influence of oxygen and chloride ions in corrosion potential and pitting potential. (*MacDougall and Graham, 2003 and Sandberg, 1995).*

As shown in Figure 2.7, E_{pit} decreases with deceasing concentration of the aggressive species (such as chlorides). E_{pit} is also dependent on other factors such as the pH of the pore solution, temperature, microstructure and composition of the concrete-steel interface or composition and finish of the steel surface (Bertolini & Redaelli, 2009).

Pitting corrosion presents itself as localised damage (localised corrosion) of the reinforcing steel, forming a pit (small) or cavity. As a result of deoxygenation-acidification mechanisms occurring within the corrosion pit, *a macro-cell* is established (Shreir, et al., 1994). Macro-cell corrosion normally occurs when the actively corroding bar is coupled to a passive bar either because of its different composition or because of different environment (Hansson, et al., 2006). Chloride-induced corrosion is characterised by the formation of relatively small pitting sites that act as the anode while the large passive steel areas act as the cathode (Gulikers, 1996). Thus, a macro-cell is the spatial separation of the anodic and cathodic half-cell reactions.

Figure 2.8 shows a schematic representation of the localised character of pitting corrosion with the involved charge transfer reactions, mass transport processes and the macro-cell (Angst, 2011).

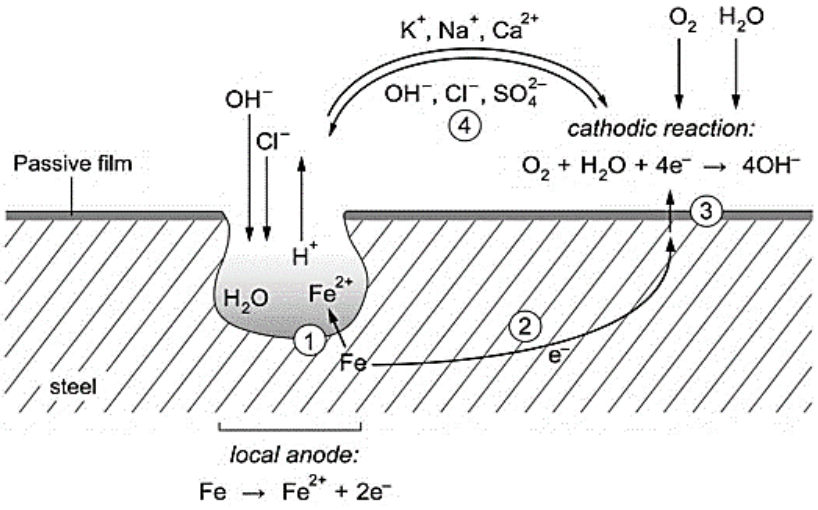

Figure 2.8: Schematic illustration of chloride induced pitting corrosion and corrosion steps 1 to 4. *(Angst, 2011).*

Figure 2.8 shows the corrosion steps in a pitting corrosion cell. Step 1 describes anodic dissolution after pit formation due to passivity breakdown, step 2 describes flow of electrons through the metal, step 3 describes the reduction reaction and step 4 describes the ionic current flow through the electrolyte where cations (Na^+, Ca^{2+}, K^+), move towards the cathode whilst anions (OH^-, Cl^-) move towards the corrosion pit. In a macro-cell there is a current passing through the circuit and according to Kirchhoff's law there must be continuity in the currents (Ries, 1983), thus the four steps occur simultaneously (Angst, 2011):

i. Anodic dissolution of iron and release of electrons according to Equation 2.13:

$$Fe \rightarrow Fe^{2+} + 2e^- \quad (2.13)$$

ii. Transport of electrons through the metal from the anodic sites

iii. Cathodic reactions to consume the electrons; for steel corrosion in concrete mainly oxygen reduction according to Equation 2.14:

$$H_2O + \frac{1}{2}O_2 + 2e^- \rightarrow 2OH^- \quad (2.14)$$

iv. Flow of electric current through the electrolyte between anodic cathodic sites carried by flux ions.

The slowest of these steps will be the limiting rate step and will therefore determine the rate of corrosion.

Since steel is highly conductive the current flow through the metal is never rate limiting thus the rate limiting step will either be the anodic reaction, cathodic reaction or the ionic current flow through the electrolyte. The limiting rate is not easily identifiable as the rates of the individual steps are not independent on each other.

The corrosion rate can be measured as the flux of electrons in the macro-cell. When the cathodic reaction is the rate limiting step, the process is said to be under *cathodic control.* This may be due to oxygen starvation in submerged structures and thus mass transfer limits the cathodic reaction. When the flow of the ionic current through the electrolyte (from the anodic to the cathodic site) is the rate limiting step, the process is said to be under *ohmic control*. This may be due to a high ohmic resistance or possibly the geometrical configuration. When the anodic reaction is the rate limiting step, the process is said to be under *anodic control.* In the active state, this may be due to the pit geometry restricting mass transport thus the mechanism is more aptly termed *anodic diffusion control* (Angst, et al., 2011). Mass transport is a term used to describe the movement of charged ions or neutral species that allows the flow of electricity through an electrolyte solution (Bird, et al., 2007).

Pitting corrosion has been described as the most destructive and vicious form of corrosion that is difficult to measure quantitatively due to the difficulty in detecting the number, size and distribution of corrosion pits which are often covered in corrosion products (Bird, et al., 2007). The consequence of this form of corrosion is a concentrated loss of steel in a localised area making the structure susceptible to sudden failure which is the most insidious type of failure as it occurs without warning.

2.5.2. Factors affecting corrosion propagation of steel in concrete

The rate of corrosion propagation is governed by factors such as temperature, w/b ratio, oxygen concentration, moisture content, binder type, concrete cover, resistivity of the concrete and the environmental exposure conditions. This section will focus on factors affecting chloride-induced corrosion rate with emphasis on concrete quality (binder type and w/b ratio) and concrete cover.

a) Effect of temperature on corrosion propagation

The corrosion reaction rate follows the universal dependence of chemical reactions on the surrounding temperature where the rate of the chemical reaction increases with an increase in the surrounding temperature CScott, 2004). However, experimentally, the relationship between temperature and corrosion rate is found to be more complex than this as it is influenced by factors such as the reduction in the solubility of the dissolved oxygen, and accelerated drying of the concrete (Scott, 2004).

Virmani and Clear (1983) proposed the following equation for the relationship between temperature and corrosion current:

$$i_1 = i_2 e^{2283\left(\frac{1}{T_2}-\frac{1}{T_2}\right)} \quad (2.15)$$

where: i_1 = corrosion current density at at temperature T_1

i_2 = corrosion current density at temperature T_2

T_1 = temperature of concrete at measurement (in degree K)

T_2 = temperature that one desires to know the corrossion current density (in degree K)

There is a discrepency in literature on the effect of temperature on the corrosion rate where Virmani and Clear (1983) reported a 1.3 factor increase in the corrosion rate for a 10 K increase in temperature, whilst Schiessl and Raupach (2009) report and a 2 factor increase in the corrosion rate for a 10 ℃ increase in temperature. Lopez et al., (1993) proposed a different approach and suggested that the effects of temperature should be considered in conjuction with the available electrolyte. For a constant supply of electrolytes as in the case of saturated

conditions, the temperature effects will be more pronounced and will follow the estimates reported by Schiessl and Raupach (2009). In the case of cyclic wetting and drying the comparison of corrosion rates across various temperatures will follow Equation 2.15 proposed by Virmani and Clear (1983).

b) Effect of w/b ratio and binder content on corrosion propagation

The w/b ratio and binder content influence the quality of concrete by influencing its permeability. Thus the w/b ratio does not control the rate of corrosion but rather 'permeability' which is a function that affects the corrosion of reinforcing steel (Kumar, et al., 2013).

An increase in the w/b ratio increases the oxygen diffusion coefficient (Kumar, et al., 2013). The availibility of oxygen governs the cathodic reaction rate for concrete in moist environment, thus decreasing the w/b ratio decreases the quantity of oxygen available and subsequently suppresses the cathodic rate leading to a decrease in the corrosion rate.

Mangat and Molloy (1992) conducted a study to investigate the corrosion rates for 12 mm diameter reinforcing steel bars cast in concrete with five different w/b ratios and binder contents. They found that the w/b ratio had a significant impact on the corrosion rate of steel, with the total binder content being less significant. Their results are reported in Table 2.5 and were supported by Rasheeduzzafar et al. (1990), who obtained similar results.

Table 2.5: Influence of w/b ratio and binder content on corrosion rates (Mangat and Molloy, 1992)

w/b	Binder *(kg/m^3)*	i_{corr} *($\mu A/cm^2$)*	Cl^- (% mass cement)
0.45	*430*	*0.13*	*1.4*
0.58	*430*	*0.65*	*2.0*
0.76	*430*	*2.16*	*2.3*
0.58	*330*	*0.62*	*1.73*
0.58	*530*	*0.52*	*1.21*

From Table 2.5 it can be seen that the highest corrosion rate was obtained in concrete with the highest w/b ratio of 0.76 and the highest chloride concentration. The lowest corrosion rate was obtained in concrete with the lowest w/b ratio.

The binder content is shown to not significantly affect the corrosion rate as it varied from 0.52 to 0.65 $\mu A/cm^2$ for binder contents of 530 and 330 kg/m^3 respectively. Thus the effect of the w/b was found to be more considerable such that lowering the w/b ratio resulted in lower corrosion rates

Schiessl and Raupach (1990) noted a similar reduction in corrosion current form 59 μA to 25 μA for w/b ratios of 0.6 and 0.5 respectively. They attributed this phenomenon to the lower permeability of the concrete with 0.5 w/b ratio. It is therefore surmised that the w/b ratio affects the corrosion characteristics of concrete through the densification of the pore structure, limiting the ingress of oxygen and increasing concrete resistivity.

c) Effect of addition of cement extenders on corrosion propagation

Cement extenders are mineral additives which can be incorporated into concrete to improve the physical and chemical properties of concrete such as reducing the permeability and increasing the resistivity of concrete. According to Bentur (1991) this is due to a more refined pore structure and improved characteristics of the interfacial transition zone (ITZ), than in ordinary Portland cement. Mineral additives such as condensed silica fume (CSF), ground granulated blastfurnace slag (Slag) and pulverised fly ash (FA), are added to ordinary Portland cement in various constituent amounts governed by several standards; (BS/EN 934-2, 2003; ASTM C989, 2006; ASTM C1157, 2003) to name a few. Sirivivatnanom, et al. (1994) conducted a study to investigate the impact of three cement extenders, at various replacement levels, on the corrosion rate of steel. The diffusion characteristics of blended cement differ substantially from those of plain Portland cement with corrosion rates affected by variations in the chloride content at the steel level. However the chloride concentrations in the first 10 mm are generally not significantly different (Scott, 2004), thus in their investigation, Sirivivatnamon et al. (1994) provided a 10 mm cover to the steel so that corrosion rates could be

reasonably compared. Figure 2.9 shows the effects of cement extenders on macrocell corrosion rate. The results from the macrocell corrosion test show the effectiveness of cement extenders in reducing the corrosion rate.

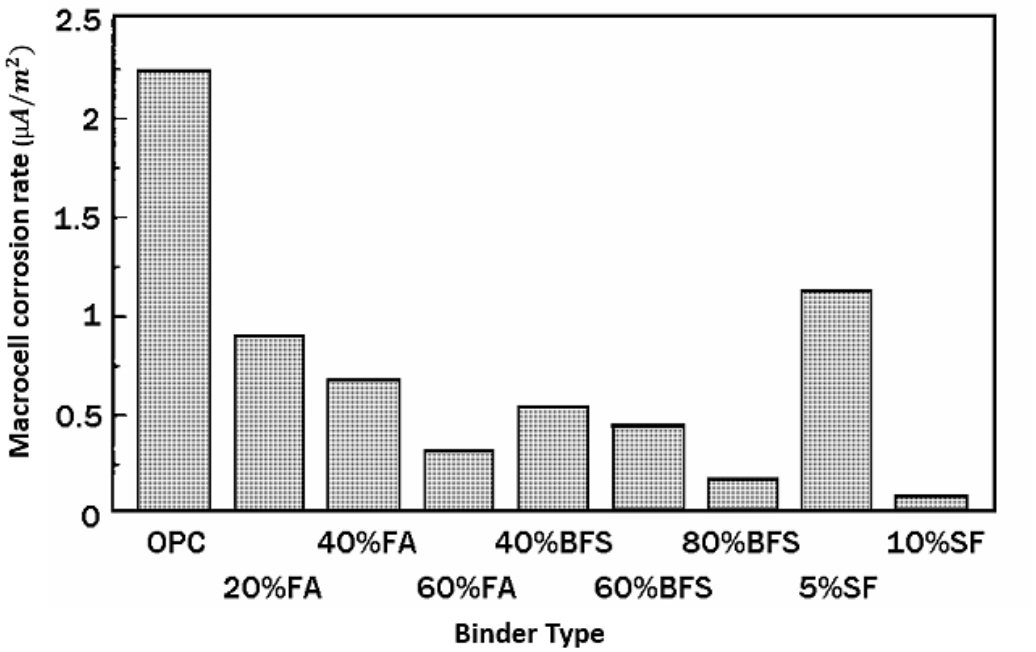

Figure 2.9: Effect of cement extenders on macro-cell corrosion of steel (Sirivivatnamon et al., 1994)

From Figure 2.9 it can be seen that concrete from ordinary Portland cement has the highest corrosion rate when compared to concrete made from fly ash (FA), blast-furnace slag (BFS) and silica fume (SF) blends. When considering the blended cements it can be seen that the general trend is a decrease in corrosion rates with increasing replacment values of cement extenders.

The results show that the most effective cement extender replacement value in reducing the corrosion rate is 10% SF, followed by 80% BSF and lastly 60% FA. Although the 80% BSF cement extender replacement value might be considered quite high, similar results were reported by Scott (2004) who conducted a study comparing the corrosion rates of different replacement values of blast furnace slag. The study found that the blast-furnace slag replacement values of 25%, 50% and 75% had corresponding average corrosion rates of 0.086, 0.086 and 0.063 $\mu A/cm^2$ respectively. As can be seen, increasing the concentrations of any of the cement extenders consistently reduces the corrosion rate, with similar results

obtained by Page, et al. (1986); Petterson (1992); Thomas (1996); Scott (2004), but with some variability in the cement extender replacement value and type for the lowest corrosion rate.

Contrary results were reported by Mangat et al. (1994) and Arya and Xu (1995) who showed that at cover a depth of 10 mm, FA had a higher corrosion current density than ordinary Portland cement. This contradictory nature of information reported by researchers on the influence of cement extentenders is an indication that the chemical and physical processes at work are not entirely understood and thus require further investigation.

d) Effect of moisture content and oxygen availability on corrosion rate

Oxygen and moisture are required at the steel level for the cathodic reaction of the corrosion process to occur. In dry conditions, there is a lack of moisture and in saturated conditions there is a lack of oxygen as it does not readily dissolve in water, making the cathodic reaction the rate limiting reaction which ultimately slows down the corrosion reaction.

The movement of O_2 from the atmosphere to the steel level is impaired by high moisture contents and is determined by the concrete cover depth and diffusion coefficient for O_2. Whereas in the case of concrete exposed to seasonal fluctuations or periods of cyclic wetting and drying the seasonal moisture acts as an electrolyte and allows for the ingress of O_2 into the concrete. Thus, the moisture content and the availability of oxygen strongly influence the corrosion reaction and are dependent on the internal relative humidity (RH) of the concrete which is in turn profoundly affected by the w/b ratio and concrete cover depth (Tuutti, 1982).

Increasing the RH of concrete results in an increase in the corrosion rate with a RH ‘threshold’ of 85% suggested by Enevoldsen et al. (1993) for the promotion of corrosion. According to Tuutti (1982) cathodic control becomes effective at RH above 90%. Thus, the maximum expected corrosion would occur where the RH of the concrete is between 85% and 90%.

e) Inflence of concrete resistivity on corrosion rate

For corrosion to occur the concrete surrounding the steel needs to provide a path for the ionic current to flow between the anodic and cathodic sites on the steel surface (Polder, 2001).

The resistivity of the concrete is an expression of the transport rate of ionic currents and is affected by the w/b ratio and binder type (Küter, 2009). Concretes with low resistivity offer less resistance to ionic movement which results in higher corrosion rates.

Table 2.6 summarises the relationship between the resistivity of concrete based on an evaluation of real structures, by Andrade and Alonso (1996), where concrete resistivity values between 10 and 100 $k\Omega.cm$ pose a low to high risk level of corrosion. In Table 2.6 it can see that an increase in resistivity of concrete results in low corrosion rates. The resistivity of the concrete can be increased by reducing the w/b ratio or incorporating cement extenders thus lowering the pore volume which results in fewer channels available for ion transport.

Table 2.6: Relationship between resistivity and corrosion risk (Andrade and Alonso, 1996)

Resistivity $k\Omega.cm$	**Risk Level**
>100 – 200	*Corrosion values will be very low even if chloride contaminated*
10 – 100	*Low to high corrosion rate*
<10	*Resistivity is not the controlling parameter*

f) Effect of concrete cover depth on corrosion propagation

The previous sections have shown in various ways what the effect of the concrete cover depth on the corrosion rate is and have been demostrated effectively in works by Ing, (2003), Bertolini, et al. (2016), Torrent, et al. (2007) and Raupach (1996) to name a few. Lambert, et al., (1991), conducted a study to investigate the corrosion rate of a 3 mm diameter rod at cover depths of 10, 20, 30 and 40 mm. The researchers observed an effective corrosion rate of 20, 0.2, 0.04 and 0.04 $\mu A/cm^2$ at 10, 20, 30 and 40 mm respectively.

This decrease in corrosion current with increase in cover may be explained by the decreasing availability of oxygen at greater cover depths as illustrated in Figure 2.10.

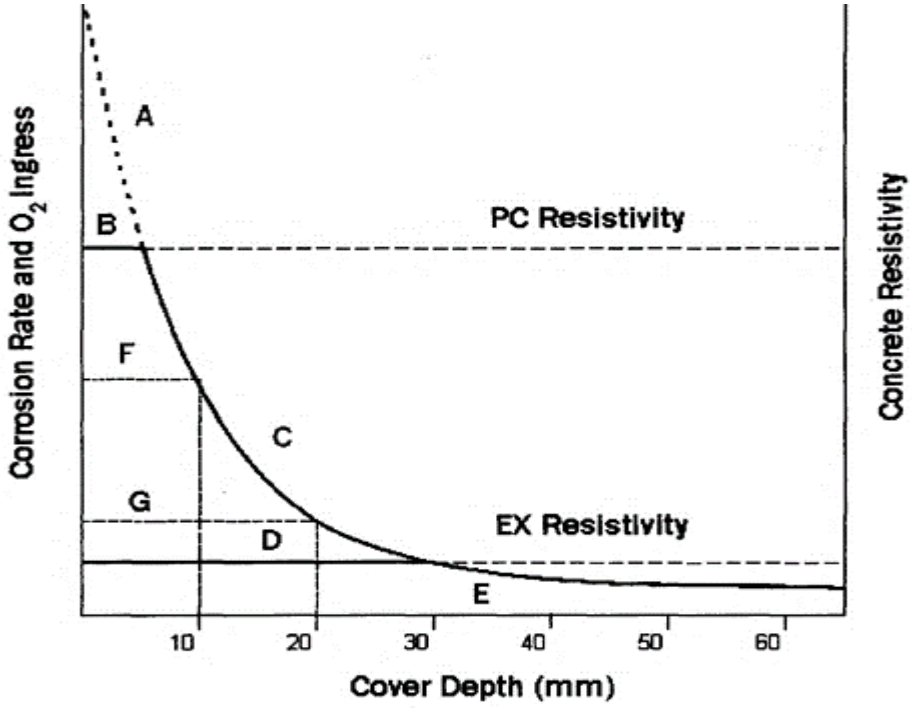

Figure 2.10: Relationship between oxygen, resistivity, corrosion rate and cover depth (Scott, 2004)

Figure 2.10 depicts the general relationship between the availability of oxygen, corrosion rate and resistivity. The availability of oxygen at a given cover depth is defined by curve ACE, the resistivity controls are shown in horizontal lines PC and EX for ordinary PC concrete and concrete made with cements extenders respectively. The combined line BCE defines the maximum possible corrosion rate. At cover depths 10 to 30 mm the corrosion rate is shown to be controlled by the resistivity of the concrete whereas at cover depths greater than 30 mm the corrosion rate is oxygen controlled. As can be seen on the graph, the increase of cover reduces the corrosion rate but is not as effective as the inclusion of cement extenders.

Other researchers (Andrade, et al. 1993; Francois and Arliguie, 1999) have attempted to model the propagation phase of the deterioration processes as well as the cracking of the concrete cover. However, this was complicated a certain

combination of crack characteristics such as width, orientation with regard to steel and frequency, can effectively eliminate the initiation phase altogether and commence the propagation phase (Ing, 2003). Cracking of the concrete cover significantly increasing the penetrability of the concrete by shortening the travel path and exposing the steel for corrosion inducing species (Andrade, et al., 1993) as the transport mechanisms of cracked concrete are more complex than those of uncracked concrete.

2.6. Electrical resistivity of concrete

The electrical resistvity of concrete is an important parameter for a meaningful study of reinforcement corrosion and can be described as the concrete's ability to withstand transfer of charged ions which is highly dependent on its electrical resistivity expressed as ohm-m (polder, 2001). The conductivity, (which is the inverse of resistivity), of a saturated specimen provides information on the resistance of the concrete to penetration of ionic species, such as chlorides, by the diffusion mechanism (Ghosh & Tran, 2015). Subsequently the electrical resistivity can be used to predict the diffusion coefficients of chloride ions and water permeability (Christensen, et al., 1994). Resistivity measurements are based on the assumption that the majority of conduction occurs through the fluid phase (pore solution) whilst concrete is a composite consisting of two other phases, a vapour phase (air) and a solid phase (aggregate and cementitious solids). This assumption is motivated by the conductivity of the liquid phase, with resistivity values which ranges from 0.01 to 0.05 Ohm-m, being several orders of magnitude higher than the conductivity of the solid and vapour phases, with resistivity values which are approximately 10^9 Ohm-m and 10^{15} Ohm-m respectively (Rajabipour & Weiss, 2006). Spragg, et al. (2011) describes the overal electrical resisitivity of concrete as a function of the resistivity of the fluid in the pores, the degree of saturation, and the volume and connectivity of the pore network as shown in Equation 2.16:

$$\rho = \rho_o \cdot F \cdot f(s) \tag{2.16}$$

where ρ is the bulk resistivity, ρ_o is the resisistivity of the fluid phase, F is the formation factor which is the inverse porosity (volume of pores) and connectivity

of pores, and $f(s)$ is a function that describes the degree of saturation which is 1.0 for a saturated system. Based on Equation 2.16, resistivity decreases with a higher water content (pore volume) and a more open pore network.

The development of electrical resistvity measurement techniques as a non-invasive and non-destructive (NDT) technique for evaluating the durability of concrete structures has acquired the interest of various researchers such as Gowers and Millard (1999); Polder (2001); Goueygou, et al. (2008); and Sengul (2014) to name a few.

Initially the Rapid Chloride Permeability Test or RCP test was a widely used test method used to eveluate concrete durability based on electrical concepts. The test method involves placing a test specimen, approximately 100 mm diameter and 50 mm thick, between electrodes in different solutions and integrating the charge that is passed over a six hour testing period (ASTM C1202, 2010). Despite its popularity this test method has a few draw backs which were highlighted by Shane, et al. (1999) and Riding, et al. (2008). Firstly the test is performed using high voltage and direct current which limits each sample to providing a single measurement, secondly saturating the specimen can take a relatively long preparation time and thirdly the potential for heating effects due to the large voltage and modification of the microstructure (Shane, et al., 1999). In response to these drawbacks alternative testing methods have been proposed which are based on the concept that electrical resistivity is the ratio between applied volate *(V)* and resulting current *(I)* (which is carried by the ions dissolved in the pore liquid) multipled by a cell constant (Polder, 2001). Thus, electrical resisivity is dependent on the materials capability to withstand the transfer of ions subject to an electric field, and is an inherent characteristic of the material that is geometry independent as described in Equation 2.17 (Layssi, et al., 2015):

$$\rho = k \cdot R = k\,(VI) \qquad (2.17)$$

where R is the resistance, k is a geometric factor (cell constant) which depends on the size and shape of the sample as well as the distance betwen the probes on the testing device (Layssi, et al., 2015).

Electrical resistivity measurements can be performed non-destructively by using surface electrical resisitivity (SR) measurements techniques and bulk electrical resisitivity (BR) measurements techniques. Surface electrical resistivity can be measured using the following device techniques (1) Wenner four-point line array test, (2) surface disc test.

2.6.1. 4-point Wenner probe resistivity test

The surface electrical resistivity of concrete may be measured using the Wenner probe technique which was first introduced by Wenner for geologist's for determining soil strata and then modified through time for application in concrete (Wenner, 1916). The Wenner four-point line array test consists of four equally spaced linear electrodes where the two exterior probes apply an alternatng current (AC) to the concrete surface whilst the two interior probes measure the electrical potential. The test is non-destructive and is relatively fast to perform as it requires little to no sample preparation and is suitable for on-site measurement. This test method has been standardadised by AASHTO TP 95-11 (2011) which specifies an electrode (probe) spacing of 38mm (1.5 inch) and an AC frequency of 13Hz. The set-up of the of the four-point electrode measurement is shown in Figure 2.11.

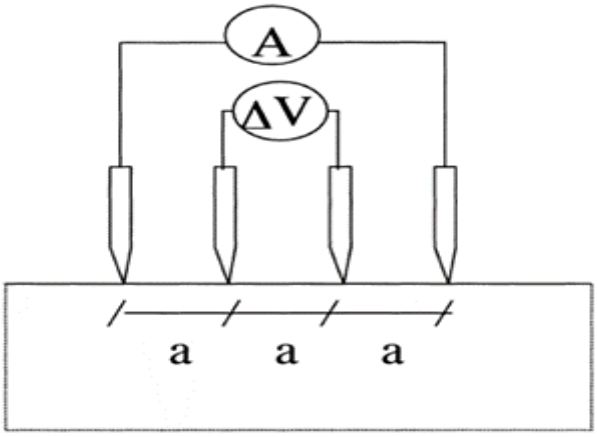

Figure 2.11: Set-up of four electrode measurement of concrete resistivity where 'A'is the ammeter reading, '$\Delta V'$ is the change in voltage and 'a' is the probe spacing (Polder, 2001)

For this test technique the cell constant is defined as in Equation 2.18 for a semi-infinite homogenous material (Polder, 2001):

$$K = \gamma \cdot a \tag{2.18}$$

where a is the probe spacing (equally spaced) and γ is the dimensionless geometry factor, 2π for semi-infinite concrete elements such as slabs (Polder, 2001). Concrete elements with smaller dimensions such as cylinders and cubic specimens prepared in the laboratory for experiments will have a different geometry factor.

2.6.2. Surface disc resistivity test

This electrical resistivity measurement technique consists of an electrode (disc) placed over steel reinforcing bar and measuring the distance between the disc and reinforcing bar (cover). This technique requires a connection to the steel rebar and full rebar continuity, which may not always be possible on site. The cell constant is dependent on the cover depth and the rebar diameter. For cover depth, disc and bar diameter being 10 – 50 mm the cell cell constant is approximately 0.1 m ($k = 0.1$) (Polder, 2001). The surface disc test measurement is shown in Figure 2.12:

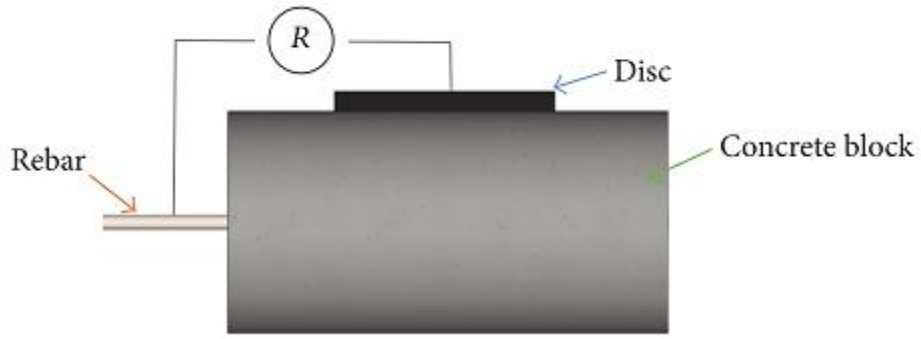

Figure 2.12: Set-up of surface disc test for measurement of concrete resistivity (Polder, 2001)

2.6.3. Bulk electrical resistivity test

This test technique consists of placing two electrodes (parallel metal plates) on opposite concrete surfaces. A moist sponge is placed in between the plates and the concrete specimen which are generally standard cylinders, cubes or cores from existing structures (Azarsa & Gupta, 2017). The sponge is required to ensure good eletrical contact between the plates and the specimen and the moisture facilitates as a conductive medium. This test method has been standardised by ASTM C1760-12 in 2012. The electrical resistivity is determined by measuring the current passing through all the phases of the specimen (cement paste, aggregates)

thus the term “bulk” AASHTO TP 95-11 (2011). The test method set-up is shown in Figure 2.13.

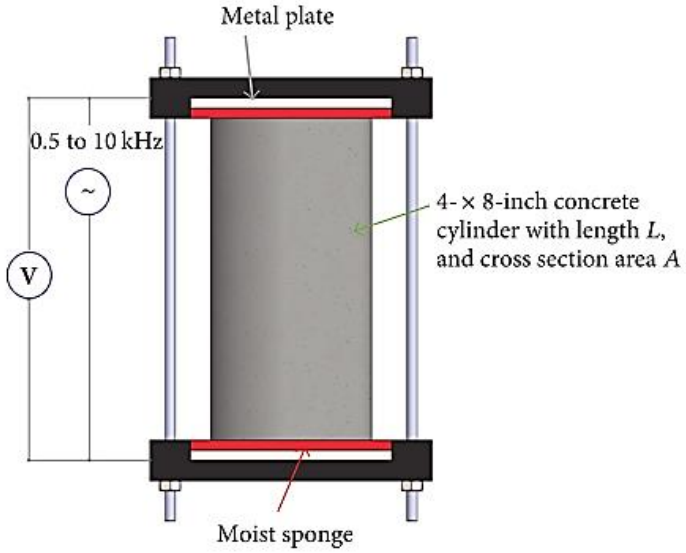

Figure 2.13: Set-up for bulk electrical resistivity measurement technique (Polder, 2001)

The cell constant in this technique is obtained by Equation 2.19:

$$K = (A/L), \tag{2.19}$$

where A is the cross-sectional area perpendicular to the current and L is the height of the specimen. This test is non-destructive and relatively quick to perform but is limited for on-site field measurements as access to opposite sides of the concrete element may not always be possible (Azarsa & Gupta, 2017).

2.6.4. Factors affecting electrical resistivity measurements

As with any test there are certain factors that need to be taken into consideration that can influence the measured results. The factors investigated in published literature that influence electrical resistivity measurements have been divided into two groups (1) intrinsic factors affecting the electrical resistivity of concrete and (2) factors affecting the electrical resistivity measurements. For electrical resistivity measurements, the major factors that need consideration are specimen geometry, moisture content, temperature, electrode spacing, presence of rebar and presence of cracks as they may influence the measured electrical response (Azarsa & Gupta, 2017). For the test techniques discussed in the previous section, the geometry of the test specimen is considered by applying a geometry factor (cell

constant) to the resistance measured. Geometry factors for different specimen sizes can be determined experimentally as described by Rajabipour (2006) or numerically as described by Morris, et al. (1996).

2.6.5. Intrinsic factors affecting the electrical resistivity of concrete

a) Effect of curing conditions

Curing occurs after the concrete has been poured and involves the maintenance of desired moisture and temperatures conditions for extended periods of time which largely depend on the specified strength, ambient weather condition and size and shape of member. Proper curing results in continued strength development and adequate moisture for continued hydration which can only take place when the vapour pressure in the capillaries is sufficiently high, about 80 % of saturation pressure (Neville, 1973). Hydration products in the cement matrix block pores thus reducing their size and connectivity (Tan & Gjorv, 1996). The cover concrete is more sensitive to drying and curing may be adequately provided through various techniques such as ponding and immersion; saturated wet coverings; left in place formwork; and spraying and fogging (Zemajtis, 2002). The selected technique depends on the size of the member and environment for example small laboratory specimens may be cured by immersion whilst members on site may be cured by left in place formwork. However different curing techniques result in different degrees of hydration and resistivity values of the concrete. A study performed by Weiss et al. (2013) simulated a mortar with a cement to water ratio of 0.42 with three curing conditions: (1) sealed during curing and testing, (2) sealed during curing and saturated during testing, and (3) saturated during curing and testing.

The researchers concluded that the sample that was sealed during both testing and curing had the highest resistivity whereas the sample that was sealed during curing and saturated at time of testing had the lowest resistivity. The samples that were sealed and saturated at time of testing had a similar resistivity with those that that were continually saturated for the same degree of hydration. Guneyisi et al. (2005) observed that for a given water-cement ratio a better curing procedure

yielded higher electrical resistivity, where immersion of the sample in a water bath of fixed temperature is considered a more efficient curing technique than ponding and spraying. This is because immersion of the sample results in a higher degree of saturation in comparison to ponding. Studies have shown that differences in resistivity can develop as a result of sample storage and curing conditions as they influence the degree of hydration, the degree of saturation, and the pore structure (Spragg, et al., 2013).

b) Effect of water/cement (w/c) ratio

The water-cement ratio is generally one of the main factors that contribute to the permeability of the concrete. A study by Rupnow and Icenogle (2012) showed that a higher w/c ratio results in a higher percentage of porosity leading to a lower electrical resistivity value, indicating a more permeable concrete. Similar results were reported by Van Noort, et al. (2016) who conducted experiments on different concrete compositions with various w/c ratios. On the contrary, studies on concrete containing supplementary cementitious materials such as slag, showed an increase in electrical resistivity for an increase in w/c ration from 0.35 to 0.65, indicating a less permeable concrete (Rupnow & Icenogle, 2012). This may be attributed to the differing hydration processes of concrete containing various cementitious materials as electrical resistivity measurements are affected by the degree of hydration (Presuel-Moreno & Liu, 2012). At a fixed cement content, increasing the w/c ratio leads to a higher volume fraction of hydrated cement paste in the concrete mix and results in lower concrete electrical resistivity. On the other hand, reducing the w/c led to a decrease in the resistivity of the pore solution due to the greater ionic concentration of the solution (Azarsa & Gupta, 2017).

c) Effect of aggregate size and type

In the hardened cement paste of concrete the electrical current can easily flow through the pore system of the paste as the aggregates generally have a higher electrical resistivity, depending on their size and type (Azarsa & Gupta, 2017). An experimental study conducted by Sengul (2014) indicated that increasing the aggregate content resulted in higher electrical resistivity whilst increasing the aggregate content and reducing the cement paste for a given volume resulted in

higher resistivity values as the porous hardened cement paste is replaced by denser aggregate. He also reported that the resistivity of the mixture containing 60% aggregate with size 16-32 mm was approximately 3 times higher than that of the hardened cement paste. The effect of aggregate size is such that larger aggregates (16-32 mm) result in higher electrical resistivity when compared to smaller sized aggregates (0-4 mm).

Sengul (2014) also studied the effect of aggregate type on electrical resistivity measurements by comparing concrete containing crushed limestone and with concrete containing gravel. He reported that crushed limestone showed higher electrical resistivity values and attributed that finding to the shape and texture of the aggregate. The crushed limestone had an irregular shape and rough texture whilst the gravel was rounded and smooth resulting in poorer bonding between the aggregate cement paste. The tortuosity of the crushed limestone may also be higher due to the irregular shape and rough surface which reduces electrical flow and in turn influences resistivity. In another study, Morris et al. (1996) used different aggregate types with the same aggregate size and achieved comparable standard deviation results. These studies by the different researchers have shown that the aggregate size and type has an effect on the measured electrical resistivity of concrete and should thus be taken into consideration when comparing electrical resistivity measurements of concrete consisting of different aggregate sizes and types.

2.6.6. Factors affecting the electrical resistivity measurements

a) Effect of temperature

Changes in temperature have been shown to have an influence on the electrical resistivity of concrete by decreasing the electrical resistivity for an increase in temperature and vice versa. This is due to the influence of temperature on the ion mobility, which increases with an increase in temperature. This in turn affects the electrical resistivity as the primary conduction path is through the ionic pore solution. In addition, an increase in temperature also has an impact on the concrete isotherm curves which also tends to reduce the moisture content of concrete which

indirectly affects the resistivity readings (Poyet, 2009). Several researchers have studied the role played by temperature on concrete electrical resistivity and have attempted to correlate its effect with true concrete resistivity values (Azarsa & Gupta, 2017). In order to compensate for the variation in temperature and its effect on resistivity, several researchers such as Gowers and Millard (1999) and Millard et al. (1991) have proposed a correction factor of 0.33 $K\Omega \cdot cm/℃$. However, their study was based on a limited range of temperatures whilst Spragg et al. (2011) have stated that for temperature variations between 10℃ and 45℃ the measured resistivity values of the same mature sample can differ by as much as 80%. For the sake a simplicity, for temperatures ranges between 0℃ and 40℃, a change in resistivity measurements between 3% and 5% per ℃ has been recommended (Polder, 2001).

b) Effect of moisture content

The moisture content of concrete has a direct relationship with the electrical conductivity due to changes in ion mobility. Thus, an increase in the moisture content results in a decrease in electrical resistivity. The range spanned by electrical resistivity measurements due to the moisture content can be as much as $10^6\ \Omega \cdot m$ for oven dried samples to as little as $10\ \Omega \cdot m$ for saturated concrete (Whitting & Nagi, 2003). Whereas in the air-dry state, electrical resistivity has been reported to be approximately 50% higher than in saturated condition (Sengul, 2014).

The effect of moisture content on resistivity was investigated by several researchers such as Smith et al. (2004); Larsen et al. (2006); Kessler et al. (2008); and Minagawa and Hisada (2013). Lim et al. (2016) reported that when moisture content decreases from 88% to 77%, the resistivity increases by an average of two times and from 88% to 66% it increases by an average of 6 times.

For quality control purposes, it is important to ensure the same degree of moisture in all concrete specimens tested for resistivity. For laboratory specimens, it is recommended that electrical resistivity be measured at surface dry, fully saturated state (which may be achieved by immersion of the specimen in water during the

curing process) whereas it was experimentally found that poor surface saturation using pressurised water and static ponding (specially used for on-site measurements) can lead to a misinterpretation of over 30% of resistivity values when compared to full laboratory saturation (Marquez, 2015). More research is required to determine other methods that can better simulate on-site saturation and the time required to obtain constant moisture level through-out the bulk of the specimen. Currently on-site measurements of resistivity are determined using surface resistivity measurement techniques where moisture is only applied on the test surface whilst the bulk resistivity is conducted on fully saturated laboratory specimens. Several researchers have investigated the correlation between surface resistivity and bulk resistivity measurements, the findings of these research undertakings are discussed in the section that follows.

c) Effect of probe spacing

Electrical resistivity measurements determined using the Wenner probe technique are based on the assumption that concrete is a heterogeneous material. However, this is not the case as the aggregates in the concrete are known to generally have higher resistivity and propagate widely in the concrete. Thus, resistivity measurements based on the Wenner probe technique may be affected by the inconsistency of the assumption that concrete is a heterogeneous material (Polder, 2001). In order to counteract this issue, several researchers have proposed using the probe spacing dimensions to mitigate the influence of the aggregates on the resistivity measurements.

In order to compensate for the local effect of aggregates, probe spacing larger than the aggregate size should be considered or as recommended by Gowers and Millard (1999), the probe spacing should be 1.5 times the maximum aggregate size. This recommendation was based on an experimentally study which also showed that as the probe spacing became smaller than the maximum aggregate size, the standard deviation in the measurements increased to around 10%.

Various probe spacing ranging from 20 to 70 mm have been recommended by Morris et al. (1996); Sengul and Gjorv (2009); Millard (1991), in order to mitigate

the influence of nonhomogeneity due to the presence of aggregates. Sengul and Gjorv (2008) varied the electrode spacing from 20 to 35 mm and found that the relative resistivity measurements of 100 mm concrete cubes increased by approximately 70%. For concrete cylinders, the effect of increasing electrode spacing had a far greater influence on resistivity values than in the cubes. Thus, the resistivity measurements observed due to wider spacing are not only due to the aggregate size but also the finite geometry. For prismatic specimens Chen et al. (2014) suggested that the effects of probe spacing can be ignored when the spacing is larger than 40 mm. However, with increasing electrode spacing the resistivity values also increased. Thus, for resistivity measurements using the Wenner probe measurement technique, when investigating the role of electrode spacing it would be better to compare resistivity values between specimens of the same size.

d) Effect of specimen geometry

For relatively small concrete elements such as cylindrical or prismatic specimens, there is interference between the course aggregates and current flow. This causes the current flow to become constricted and flow into a different field pattern. In the four-point Wenner measurement method this interference is taken into consideration by applying a correction coefficient (geometry correction factor). Morris et al. (1996) developed simulations which were established by Spragg, et al. (2013) in their work to propose the correction coefficient factor formula, as shown in Equation 2.20, which can be used when $\frac{d}{a} \leq 6$ or $\frac{L}{a} \leq 6$ (where *a* and *d* are parameters related to electrode spacing and specimen diameter respectively) (Spragg, et al., 2013).

$$k = 1.10 - \frac{0.73}{\frac{d}{a}} + \frac{7.34}{(\frac{d}{a})^2} \quad (2.20)$$

The effect of the specimen geometry has been investigated by various researchers including Bryant, et al. (2009) who found an average of 24% higher electrical resistivity values for cylindrical samples in comparison with concrete slab for various ages even when the geometry factor was used.

e) Effect of presence of rebar

In theory, electrical current fluxes take pathways having the least amount of resistivity and when there is embedded rebar in concrete, the current field is distorted (Azarsa & Gupta, 2017). The distortion in the current field is dependent on the orientation of the rebar with respect to the probe, rebar diameter and spacing and depth at which it is located (Millard, (1991); Gowers and Millard (1999); Weydert and Gehlen (1999))

Polder (2001) suggested that the electrical current may travel through the concrete volume with approximately the same depth as that of the probe spacing, thus as the probe spacing increases, the current flows deeper inside the concrete volume and when the electrical current reaches the surface of the rebar, the current is transported through the reinforcement thus resulting in lower resistivity measurements (Sengul & Gjorv, 2009). For slabs with rebar the resistivity values either increased by 33% or decreased by 25% depending on the orientation of measurements, either perpendicular or parallel.

Sengul and Gjorv (2009) studied the effect of rebar on Wenner probe resistivity measurements by taking measurements in different configurations such as placing the probe orthogonally or parallel to the rebar. They found that placing the probe orthogonally to the rebar did not influence the resistivity measurements whilst significant errors were obtained when measurements were taken directly above and parallel to the rebar. However, they suggested that measurements should be taken as far away from the rebar as possible to reduce errors and if that is not possible than electrode spacing should be kept relatively small.

Similarly, Presuel-Moreno, et al. (2009) also recommended that resistivity measurements be taken perpendicular to the rebar location. However, in real life concrete structures the rebars are placed in both the longitudinal and lateral directions and are electrically linked together thus Polder (2001) suggested that resistivity measurements with Wenner probe should be taken in diagonal alignments on the concrete surface as shown in Figure 2.14.

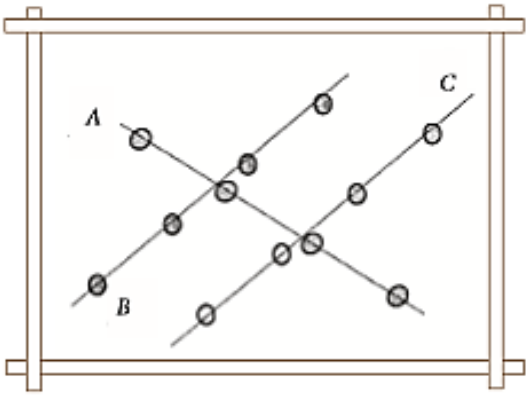

Figure 2.14: Resistivity using four electrodes at various spots in the same area to minimise influence of rebars *(Polder, 2001)*

2.6.7. Correlation between concrete resistivity and its durability characteristics

This section will discuss the two main durability characteristics of concrete that are related to electrical resistivity and their role in the two processes of reinforcement corrosion. These two processes are corrosion initiation (chloride penetration) and corrosion propagation (corrosion rate). Low resistivity is related to rapid chloride penetration and a high corrosion rate thus the risk of early corrosion damage to structures exposed to chloride can be determined by the resistivity measurement (Polder, 2001).

a) Correlation between electrical resistivity and chloride diffusion rate

Based on theoretical and experimental work there seems to be an inverse correlation between concrete resistivity and chloride diffusion (Andrade, et al. (1993); Polder (1995)). Several researchers have also reported a strong correlation between electrical resistivity and chloride diffusion rate for various concrete mixtures at different ages (Polder and Peelen (2002); Kessler, et al. (2008) Bryant, et al. (2009); Minagawa and Hisada (2013); Sengul (2014); and Lim, et al. (2016)). The chloride diffusion rate or diffusivity is the controlling parameter that determines the time required for chloride ions to diffuse into the concrete cover and reach the critical chloride threshold required to initiate corrosion (Azarsa & Gupta, 2017).The typical test methods used to determine chloride diffusivity are the Rapid Chloride Migration test (RCM), Rapid Chloride Permeability Test (RCPT), Bulk Diffusion (BD) method and Chloride Conductivity Index (CCI).

Applying the electrical resistivity to indirectly determine chloride permeability was found to be an efficient method that was less time-consuming and costly as the typical test methods (Azarsa & Gupta, 2017).

The Louisiana Transport Research Centre conducted experimental work which found good correlation between resistivity and RCP test (Rupnow & Icenogle, 2012) whilst experimental work by (Dhir, et al., 2002) and the European Union-Brite EuRam (DuraCrete R17, 2000) found a good correlation between RCM coefficients and electrical resistivity measured by two-point method. Subsequent to these experimental investigations, a provisional method for indicating the concrete's ability to resist chloride ion penetration using surface resistivity measurements was published by AASHTO TP 95 (2011).

The relationship between diffusivity of ion i and its partial conductivity can be theoretically described by the Nernst-Einstein in Equation 2.21 (McKee, 1981):

$$D_i = \frac{RT\sigma_i}{Z_i^2 F^2 C_i} \tag{2.21}$$

where D_i is the diffusivity of ion i (m^2/s); σ_i is the partial conductivity of ion i (m/s); R is the gas constant $(8{,}314\ J/mol)$; T is absolute temperature (K); Z_i is the charge of ion i; F is Faraday's constant $(96500\ Coulombs/mol)$; and C_i is the concentration of ion i (mol/m^2). Archie's law can then be applied to express the correlation between bulk resistivity, pore solution and resistivity as shown in Equation 2.22 (Sengul and Gjorv (2008); Backe, et al. (2001)):

$$F = \frac{\rho}{\rho_0} = \frac{\sigma_0}{\sigma} = a \cdot \varphi^{-m} \tag{2.22}$$

where F is the formation factor; ρ is bulk resistivity; ρ_0 is resistivity of the pore solution; a and m (dependent on tortuosity of concrete with values ranging from 1.5 to 3.2) are constants; and φ is porosity of concrete.

By combining Equations 2.21 and 2.22 the formation factor can be expressed as a function of effective chloride diffusion coefficient (D_{eff}) and chloride ion diffusion coefficient in the pore solution (D_0) as shown in Equation 2.23:

$$F = \frac{D_0}{D_{eff}} \quad (2.23)$$

For real life structures, the resistivity in the field can be measured to determine the formation factor which can then be used to determine how long it will take chloride ions to reach a critical chloride threshold at the level of the steel. Based on experimental work by Presuel-Moreno, et al. (2010) where the electrical resistivity method was used periodically during a 1000-day monitoring of reinforced concrete element exposure to marine environment, the chloride threshold (Cl_{TH}) values can also be predicted using electrical resistivity measurements. The relationship between chloride content in terms of chlorides relative to weight of cement, and resistivity (ρ) can be expressed as shown in Equation 2.24, once the geometry factor has been applied (Ramezanianpour, et al., 2011):

$$Cl_{TH}(\%) = 0.019\rho + 0.401 \quad (2.24)$$

On a more cautionary note Ramezanianpour, et al. (2011) suggested that the electrical resistivity test should be used as a quality control predictor of the chloride ingress resistance but not as a predictor of diffusion behaviour of all kinds of concretes. Long-term monitoring of various concretes by the Florida Department of Transport concluded that correlation between the RCM test and the long-term diffusion tests were equal to or slightly due to sensitivity of RCM test to the presence of supplementary cementitious materials (Vivas, et al., 2007). In general, there is consensus in literature that there is good correlation between the concrete's electrical resistivity and chloride ingress, such that lower resistivity indicates the area where chloride penetration will be faster (Polder, 2001). However, more work is required to determine if the correlation between the two parameters is the same for all kinds of concrete.

b) Correlation between electrical resistivity and reinforcement corrosion

The rate at which reinforced concrete structures deteriorate due to corrosion is primarily influenced by corrosion propagation. Corrosion propagation is influence by several factors including but not limited to oxygen availability, relative humidity and concrete electrical resistivity (Bentur, et al., 1997). Under aerated

conditions such as in the splashing area zone, there is enough oxygen available to supply the anodic current and cathodic control no longer exists. Under these conditions the corrosion rate can be limited by controlling the flow of ionic current through the concrete which is directly related to electrical resistivity of concrete. Based on these researchers such as Glass, et al. (1991); Carino (1999); Morris, et al. (2002) ASTM C876 (2015) have made attempts to correlate corrosion probability and corrosion propagation to concrete electrical resistivity.

The consensus in literature thus far is that there is an inverse relationship between reinforcement corrosion and electrical resistivity of concrete. As electrical resistivity of concrete decreases, the rate of reinforcement corrosion increases (Azarsa & Gupta, 2017). Glass, et al. (1991) proposed a theory that the corrosion rate of reinforced concrete is under anodic current reaction that is limited by the mortar resistivity. This theory is also supported by studies conducted by Bertolini and Polder (1997) and Morris, et al. (2002), who also found that concrete resistivity also affected the corrosion potential, not just the corrosion rate. The half-cell potential mapping technique has been standardized by ASTM C876 as a test method for corrosion monitoring (ASTM C876, 2015). The advantage of electrical resistivity measurements to examine corrosion probability and rate is that there is no need for electrical connection to embedded rebar which is required for half-cell potential mapping. Several researchers as well as commercial Wenner probe instrument manuals provide a general guideline interpreting electrical resistivity measurements for corrosion risk assessment as shown in Table 2.7.

The difference in the provided resistivity values stems from the various experimental set-ups used by the different researchers, concrete quality, concrete composition and initial chloride concentration. Alonso and Andrade (1996); Bertolini and Polder (1997); Carino (1999); and Gulikers (2005) proposed a linear relationship between concrete electrical conductivity and corrosion rate.

An empirical equation was proposed by Andrade and Alonso (2004) to describe the relationship between resistivity and corrosion rate as shown in Equation 2.25:

$$I_{corr} \cong \frac{3\times10^3}{\rho} \quad (2.25)$$

A different model was proposed by DuraCrete R17 (2000) and Vesikari and Soderqvist (2003) as shown in Equation 2.26:

$$I_{corr} = \frac{k_0}{\rho(t)} \times F_{cl} \times F_{Galv} \times F_{o_2} \quad (2.26)$$

where I_{corr} is corrosion rate in $\mu A/cm^2$, k_0 is constant regression parameter in $\mu m \cdot \Omega m/a$, $\rho(t)$ is actual resistivity at time t in Ωm, F_{cl} accounts for the influence of the chloride content, F_{Galv} is influence of galvanic effect, and F_{o_2} is availability of oxygen.

F_{Galv} and F_{o_2} are equal to 1.0 and F_{cl} is dependent on the chloride concentration at the location that corrosion occurs. The interpretation of electrical resistivity measurements is complicated by the many factors that influence the measured results such as moisture condition, curing conditions, w/c ratio, temperature, etc. In order to practically determine the corrosion and resistivity relationship, more field data is required as there is still a large range and scatter for correlation between the two parameters.

Table 2.7: Concrete resistivity and risk of corrosion of steel reinforcement

	Resistivity values ($k\Omega \cdot cm$		
Corrosion Risk	**Polder (2001)**	**Song and Saraswathy (2007) Elkey and Sellevold (1995)**	**Commercial Wenner probe instrument manuals (Proceq, SURF)**
High	*<10*	*<5*	*≤10*
Moderate	*10 -50*	*5 – 10*	*10 – 50*
Low	*50 – 100*	*10 – 20*	*50 - 100*
Negligible	*>100*	*> 20*	*≥ 100*

2.7. Assessment of steel corrosion in concrete

This section will give a brief description of the more commonly used corrosion assessment techniques i.e. linear polarization resistance, half-cell potential measurement, pentiostatic measurement, concrete resistivity measurement technique, et cetera. The advantages and disadvantages of each technique are discussed as well as the interpretation of the results produced by each technique.

2.7.1. Corrosion rate measurement – Linear Polarization Resistance

Corrosion rate measurement of steel in reinforced concrete structures is an electrochemical and non-destructive technique. It requires the determination of corrosion currents between the anode and cathode and may be expressed as corrosion current density (i_{corr}- $\mu A/cm^2$.), mass loss over a given period of time or steel cross-section area reduction over time (Metrohm Autolab, 2011).

The Linear Polarization Resistance (LPR) is the fastest, simplest, relatively inexpensive and most commonly used method for measuring corrosion rates directly, in real time (Kumar, et al., 2013). According to Angst, et al. (2009) the measurement of linear polarization is the most accurate technique to detect corrosion current density, which is inversely proportional to the corrosion current as described by the Stern- Geary Equation 2.27 (Stern & Geary, 1957):

$$R_p = \frac{B}{i_{corr}} \qquad (2.27)$$

where R_p is the linear polarization resistance in $ohms$, B is the proportionality constant for the particular corrosion system determined empirically (calibrated from separate weight loss measurements) and i_{corr} is the corrosion current density in $\mu A/cm^2$.

LPR is based on introducing a small perturbative electrical signal using a surface counter electrode on the reinforcing steel surface so as to disturb the corrosion equilibrium. The corrosion rate is calculated by monitoring the relationship between the electrochemical potential. The auxiliary electrode produces a current that causes a change in the open-circuit potential; this change is termed

"polarization". A perturbation of the open circuit potential results in a linear relationship between the change in voltage and the change in the applied current per unit area of electrodes. This ratio is termed polarization resistance (Andrade & Alonso, 1996).

The LRP test can be performed using either manual or automated methods by first breaking the concrete cover and exposing the reinforcing steel to make positive electrical contact and confirming the electrical conductivity between the contact point and reinforcement in the concrete test area (Kumar, et al., 2013). A three-electrode polarization resistance (3LPR) system is used to collect data for the manual method by first polarizing the reinforcement through manual operations. In this method, the electrical potential value is recorded once a stable potential is achieved, with potential variations of no more than +/- 5 mV per minute (Millard, 2003). Figure 2.15 shows an illustration of the polarization resistance measurement.

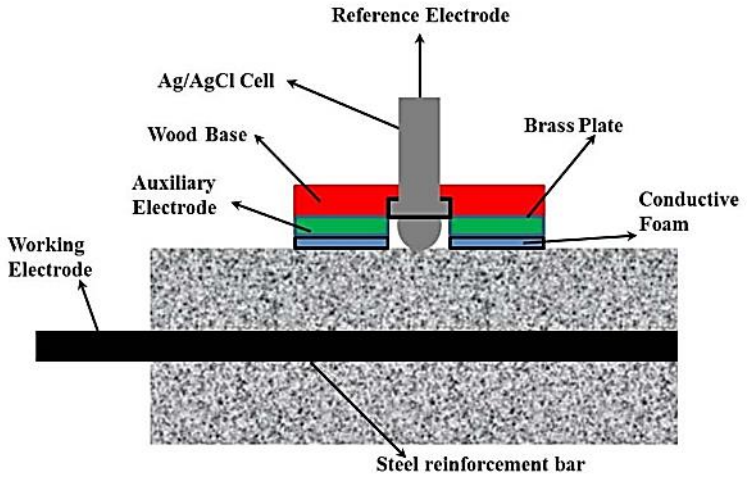

Figure 2.15: Illustration showing Polarization Resistance Measurement (Andrade & Alonso, 1996)

Automated methods perform the polarization process automatically and can be programmed or pre-programmed to linearly perturb the potential to values between +12 mV and +20 mV from the open-circuit potential at a rate of 10 mV per minute. The corrosion rate is calculated as shown in Equation 2.28.

$$i_{corr} = \frac{B}{R_p * As} \quad (2.28)$$

where B is a potential constant, R_p is the polarization resistance and As is the area of steel affected (perturbed) (Stern & Geary, 1957). The data is interpreted by generating a contour map of the measured corrosion rate and reported as a spatial distribution of corrosion activity. Table 2.8 shows the corrosion classification for specific corrosion current densities.

Table 2.8: Typical corrosion rates from LPR measurements (Andrade & Alonso, 1996)

Corrosion classification	Corrosion current density (i_{corr})	Corrosion penetration rate
Passive/Very Low	*Up to 0.2 µA/cm^2*	*Up to 2 µm/year*
Low/Moderate	*0.2 µA/cm^2 to 0.5 µA/cm^2*	*2 µm/year to 6 µm/year*
Moderate/ Low	*0.5 µA/cm^2 to 1.0 µA/cm^2*	*6 µm/year to 12 µm/year*
Very High	*> 1.5 µA/cm^2*	*> 12 µm/year*

The advantages of the LPR technique is that it uses lightweight, portable equipment and provides an indication of real time corrosion rate the time of measurement (Andrade & Alonso, 1996).

The disadvantages of this technique are that it is a semi-non-destructive technique as it requires an electrical connection to the embedded reinforcement, requires a smooth, uncracked, free of impermeable coatings and free of moisture concrete surface. However, despite these limitations LPR is still the most commonly used technique for corrosion rate measurement.

2.7.2. Half-cell potential measurement

The half-cell potential measurement technique is the most widely used method to measure corrosion of steel in concrete and was introduced by Richard Stratfull in the 1970s in North America and was approved in 1980 as a standard by ASTM C876-91 (1999).

In this technique, E_{corr} is measured against a reference electrode, (such as a saturated calomel electrode (SCE)), which can be placed either on the concrete surface above the reinforcement (a wet sponge required for electrolytic connection) or immersed in exposure salts (specifically in laboratory setups). The

reference electrode (SCE) is connected to the negative terminal and the working electrode (reinforcing steel) is connected to the positive terminal of a high-impedance voltmeter (>10 MΩ) (ASTM C876-9, 1999).

The guidelines for the application of the half-cell measurement technique and the interpretation of the results as well as the possible factors influencing the measurements can be found in Elsen er, et al. (2003) and Angst, et al. (2009). While changes in the moisture content (wet surface) shift the potential to more negative values, the potential difference between the position above the anode and a distant cathode becomes smaller with increasing cover depth (Elsener, et al., 2003). This is due to the effect of cover depth on HCP measurements such that, as the cover depth increases, the potential difference increases, this may be useful if the reinforcing steel is deep in the concrete or near the surface.

The potential difference between the working electrode and the reference electrode depends on the type of reference electrode as well as on the passive/active state of the steel. This technique only gives an indication of corrosion risk, unlike the corrosion rate measurement which gives the degree of corrosion. This electrochemical measurement technique is shown in Figure 2.16:

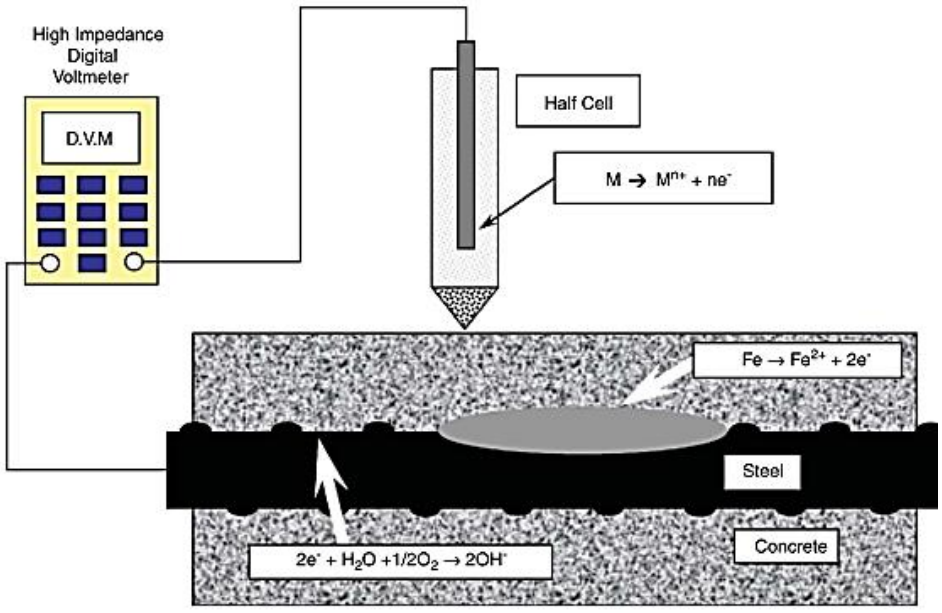

Figure 2.16: Set-up of half-cell potential measurement (Ha, et al., 2007)

Results from this technique can also be analysed based on the Pourbaix diagram by transferring the measured potential to the 'SHE' scale, i.e. by normalising the potentials and expressing them against the standard hydrogen electrode (SHE). For example, if a SCE is used as a reference electrode at 25 ℃, E_{corr} is obtained by adding 244 mV to the measured value on the high-impedance voltmeter or using the conversion factors sown in Table 2.9 for other reference electrodes (Vennesland, et al., 2007). Table 2.10 shows the voltage measured and provides an indication of the probability of active corrosion with the recommended ASTM interpretation of the half-cell potential (HCP) measurements for the $Cu/CuSO_4$ reference electrode. Hansson, et al. (2007) advised that these are only interpretations of corrosion and give no indication of the rate of corrosion or even how long the steel has been corroding for. There are also other possible causes of negative potentials from HCP indicating corrosion activity. For example, de-aerated concrete with normal half-cell potential readings as low as -700 mV in concrete submerged in deep water but the steel remains passive (ASTM C876-91, 1999).

Table 2.9: Standard potentials of reference electrodes used in concrete *(Vennesland, et al., 2007)*

Reference Electrode	Potential (mV vs. SHE)
Manganese Dioxide, MnO_2	*+365*
Copper/Copper Sulfate, $Cu/CuSO_4$	*+316*
Saturated Calomel	*+244*
Silver/Silver Chloride, Ag/AgCl	*+199*

Table 2.10: Probability of Corrosion of Carbon Steel According to Half-Cell Potential Reading *(ASTM C876-91, 1999)*

Half-cell potential reading vs. $Cu/CuSO_4$	Corrosion activity
More positive than -200 mV	*90% probability of no corrosion*
Between -200 and -300 mV	*An increased probability of corrosion*
More negative than -300 mV	*90% probability of corrosion*

Figure 2.17 shows a schematic representation of the typical range of potentials that can be found for concrete under different conditions, with the typical potential values for passive steel in concrete exposed in atmospheric conditions ranging from -200 to 100 mV versus SCE (Bertolini, et al., 2004).

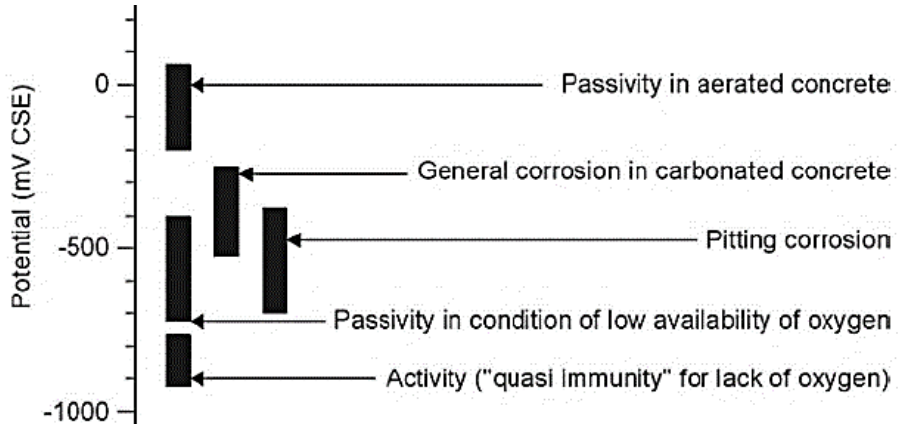

Figure 2.17: Typical range of potentials of steel in concrete *(Bertolini, et al., 2004)*

2.7.3. Pentiostatic measurement technique

In pentiostatic control techniques a pentiostat is used to maintain E_{corr} at a constant level. The steel bar is kept under anodic polarization and the corrosion activity of the steel monitored by measuring the current passing from the working electrode to a counter electrode (Alonso, et al., 2002). This counter electrode can either be immersed in the specimen (Arup and Sorensen, 1995; Sandberg, 1998) or immersed in the exposure solution (Nygaard and Geiker, 2005; Bertolini and Redaelli, 2009) as shown in Figure 2.18. This technique involves shifting the imposed polarisation potential of the steel potential away from its natural E_{corr} which can influence both the characteristics of the passive film and the chloride threshold value. In pentiostatic conditions, depassivation is marked by an abrupt increase in the current (Bertolini & Redaelli, 2009). Alonso and Sanchez (2009) conducted a review on existing literature and found that the potentiostatic measurement method gives lower chloride threshold values as well as narrow scatter when compared to natural methods such as the open circuit conditions.

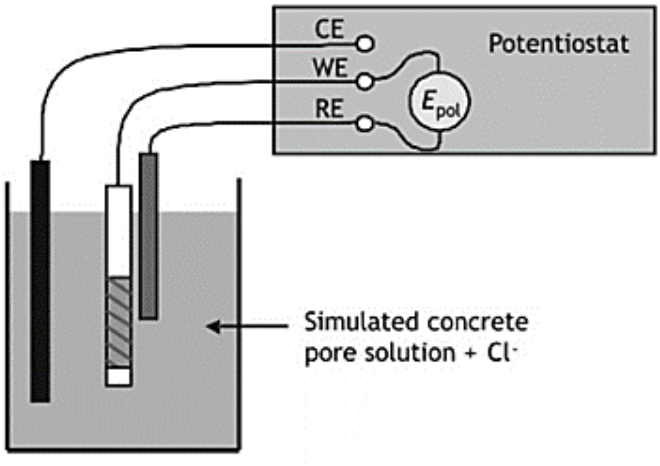

Figure 2.18: Experimental arrangement for potentiostatic measurement on steel immersed in chloride solution (Bertolini and Redaelli, 2009)

Although there is no definite consensus, the literature review shows that values more positive than -250 mV versus SCE are usual. In this range of potentials, the chloride threshold value is not affected by the polarisation and the type of passive layer does not vary significantly. A study by Nygaard and Geiker (2005) showed that under potentiostatic controlled conditions, clear visible pits were found only a few hours after depassivation. This study supports the possible explaination of the lower critical chloride content (chloride threshold value) under potentiostatic control as repassivation of incipient pits is more difficult making stable pit growth achievable earlier. Similary Angst, et al. (2011) were able to reproduce pits of similar size but only after days or even weeks after depassivation. However, a study by Sandberg (1998) showed contrary results where activation-repassivation events were observable under pentiostatic control.

Due to these varying observations, Silva (2013) concluded that there are other factors contributing to the lower critical chloride contents reported under pentiostatic control such as the influence of the polarization current at the steel-concrete interface and that measured on the concrete itself.

2.7.4. Concrete resistivity measurement

The resistivity of concrete is an indirect indication of active corrosion of the steel reinforcement and is evaluated as $\Omega \cdot m$ (Sadowski, 2010). Low resistivity is

always associated with rapid chloride penetration thus the resistivity of concrete exposed to chloride indicates the risk of early corrosion. Subsequently, high resistance of the concrete will result in a slower corrosion process (Polder, 2001).

The advantages of this technique are that it is easy, fast, portable and inexpensive and can be used for routine inspection. The disadvantage of this technique is that the reinforcement in the test region can provide a "short-circuit" path and cause erroneous reduction in the measurement (Zaki, et al., 2015). This method has other limitations due to the heterogeneities (steel reinforcement, resistivity layers, cracks and large aggregates) and weather conditions (moisture, temperature and humidity) which influence the resistivity results (Reichling, et al., 2013). The resistivity of concrete can be related to reinforcing steel corrosion and protection of steel reinforcement while resistivity mapping will show the most permeable spots within a structure with the interpretation of the results is shown in Table 2.11:

Table 2.11: Concrete resistivity and risk of reinforcement corrosion at 20℃ for OPC concrete (Polder, 2001)

Concrete resistivity $\rho_{concrete}$ $(\Omega\, m)$	Risk of corrosion
100	*High*
100-500	*Moderate*
500-1000	*Low*
>1000	*Negligible*

2.7.5. Gravimetric mass loss measurement

The rate of corrosion can be determined by conducting gravimetric mass loss measurements on the steel by weighing it before and after the corrosion process. The mass loss of the steel due to the accelerated corrosion test may be used to determine the rate of corrosion of the steel. Two standards for conducting gravimetric test measurements have been referenced in literature (1) ASTM G1-90 (1999) cited by Huet, et al. (2007); Ahmad (2009) and (2) ISO/DIS 8407.3 (1986) cited by Daflou, et al. (2006) with the former standard being the one favoured by most researchers.

ASTM G1-90 (1999) standard prescribes that only ideal procedures should be used to remove corrosion products so as to avoid removing the base material. According to the standard, after retrieval from the concrete, the steel bars should be cleaned mechanically by lightly brushing (with a non-metallic bristle), thoroughly rinsed in distilled water and hot air dried. For heavily corroded specimens the chemical cleaning procedure should be followed after the mechanical procedure.

The standard prescribes temperatures ranging from 20 to 25 ℃ for the cleaning procedures and involves immersion of the specimen in a chemical solution and intermittent removal of specimens from the chemical solution for light brushing (with a non-metallic bristle) to remove tightly adherent corrosion products.

Once all visible corrosion products had been removed, the rebar specimens should be rinsed thoroughly in distilled water, hot air dried and weighed to determine the mass to the fifth significant figure ASTM G1-90 (1999).

2.8. Accelerated corrosion of steel in concrete

The corrosion initiation phase may take decades to manifest itself in reinforced concrete structures, with the time taken largely dependent on the concrete cover quality as well as the exposure environment.

Thus, in order to study reinforcement corrosion effectively and within a realistic time frame, (reducing the corrosion initiation time from decades, to months, weeks, days and even hours), accelerated corrosion techniques are used to accelerate the initiation phase and sometimes control the propagation phase (Ing, 2003). An accelerated corrosion test is usually defined as any test method from which results are obtained in a shorter period of time than from natural exposure.

The method used to accelerate corrosion depends on the nature of corrosion under investigation. For example, in accelerated carbonation-induced corrosion, the concrete can be placed in a CO_2 chamber at 50% RH to rapidly increase neutralisation of the pore water (Lopez, et al., 1993). For chloride induced

corrosion, three different techniques can be employed, namely admixed chlorides, wet/drying and impressed anodic current or a combination thereof.

The corrosion process occurring under accelerated techniques is not entirely the same as the corrosion process which occurs naturally. In their study Yuan et al. (2007) concluded that the fundamental difference between accelerated and natural corrosion is from an electrochemical aspect which results in different corrosion distribution and characteristics on the surface of the steel bar as well as different deterioration of the bond behaviour. In accelerated corrosion, high degrees of corrosion are achievable within a relatively short period of time (days or even hours). For naturally occurring corrosion processes, the degree and rate of corrosion is influenced by the inherent concrete properties and the environmental exposure the concrete is subject to (Ing, 2003). In these conditions, chloride and carbonation diffusion are gradual process proceeding from the surface of the concrete cover to the steel. As a result, the passivity of the steel bar on the surface facing the concrete cover is at first compromised thus the corrosion reaction is mainly located on the bar surface in the direction of the concrete cover. Corrosion can present itself as localised pitting corrosion or uniform general corrosion, with the steel serving as sites for both anodic and cathodic reactions.

In accelerated corrosion, for example the impressed anodic current, the steel is forced to become the anode which makes the entire steel surface a site for corrosion. Furthermore, the surface characteristics (corrosion products) of corroded rebar from natural conditions are also different from those due to accelerated corrosion. Fischer (2012) noted Ferric hydroxide, which is has a unit volume 4.8 times more than Iron, as the main corrosion product of natural corrosion whilst Lepidocrocite, which has a unit volume 3 times more than Iron, was noted as the main corrosion products for accelerated corrosion.

2.8.1. Methods of accelerating chloride-induced corrosion of steel in concrete

This section will discuss the three main methods of accelerating chloride-induced corrosion which is the main focus of this study, namely admixed chlorides, wet/dry technique and anodic impressed current technique.

a) Admixed chlorides

Accelerated corrosion by means of the admixed chlorides technique is achieved by adding a sufficient percentage of chlorides by weight of cement to the concrete mix (Ing, 2003).

A study by Gonzalez et al.,(1993) found that additions as low as 1% by weight of cement were sufficient to pose a high risk for corrosion in good quality concrete. Levels of chloride concentration used by researchers generally range from 1-5%, and are often selected to simulate chloride concentration of sea water which has a salt concentration of 3.5% (Angst, 2011).

The advantage of this technique is that immediate steel depassivation occurs since chlorides are introduced in the concrete mix. This techinique is also less labourous as it eliminates the need to closely monitor the specimens to ensure that there is sufficient chloride solution available for the ingress of chlorides into the concrete. The disadvantage of this technique is that it does not resemble the usually encountered pitting/localised corrosion formed under natural chloride induced corrosion, instead general/uniform corrosion of the steel bar occurs (Malumbela, Moyo & Alexanderet 2012).

This technique is also less favoured by many researchers as the practise of introducing impurities such as chlorides into concrete is discouraged.

b) Cycling wet/drying technique

This method involves the ingress chlorides into the concrete, post hydration, through alternate cycles of wetting and drying until the passivating layer is destroyed and corrosion commences. The disadvantage of this technique is that it

may take several months for sufficient levels of chloride ions to permeate through the uncracked concrete cover and depassivate the steel.

The advantage of this method is that it closely resembles natural corrosion of reinforced concrete in the natural environment such as in concrete exposed to tidal spray in marine environments. A good correlation between the wet/dry accelerated corrosion technique and the behaviour of steel over time in marine environment was reported by Artigas, et al. (2015) who concluded that the technique allowed adequate prediction of corrosion thickness in steels exposed for years to a marine environment.

c) Anodic impressed current

When a metal is immersed in a given solution, electrochemical reactions characteristic of the metal-solution interface occur at the metal surface, causing it to corrode. For steel embedded in concrete, corrosion occurs due to anodic-cathodic reactions, at the surface of the steel. Electrons are produced at the anode and transferred to the cathode causing steel loss at the anode. This flow of electrons produces a current which is referred to as the corrosion current. Dividing the corrosion current by the surface area of the steel provides a measure of the corrosion causing current density which is often referred to by many reasearchers in literature. According to Alonso and Andrade (2001) the current density due to natural corrosion ranges between 0.1 and 10 $\mu A/cm^2$. Reaserchers take advantage of this natural current density by applying a larger constant direct current in laboratory corrosion tests and adjusting the direction of the current flow by connecting the reinforcing steel they want to corrode to the positive terminal, thus forcing it to become the anode, hence the name of this technique.

The negative terminal of the DC power supply is connected to a counter electrode with good conductivity such as copper or stainless making it the cathode. This metal can be a embedded inside the concrete or in most cases placed in the electrolyte, outside the concrete. The corrosion cell is completed by partially or fully submerging the concrete specimen in an electrolyte made from a salt solution which allows electrons to flow from the anode to the cathode (Ing, 2003).

The disadvantage of this technique is that it is not truly respresentative of the in-service conditions under natural corrosion as it forces the entire surface of the reinforcing steel to be the anode which corrodes whilst in natural corrosion partial surface steel corrosion occurs. The advantages that the impressed current technique has over other techniques for accelerated corrosion is that it saves time and money but more importantly, it allows for the control of the corrosion rate. For the purposes of this study focus will be placed on the accelerated corrosion technique by means of an impressed anodic current. Despite the disadvantages of this technique it is still used by researchers due to the benefits of its advantages.

There is however limited research on the efficiency of this technique which is imperative for applying its findings to real life structures. The impressed current technique can be achieved in two ways, by the potentiotastic or galvanostatic technique. Such experiments are performed with a computer-controlled pentiostat/galvanostat.

i. Pentiostatic method

In this method, the working electrode (WE), rebar, is polarized and held constant at a certain potential during the experiments (Angst, et al., 2009).

When a metal is polarized in a systematic manner and the resulting current measured, the corrosion current can be determined and is directly related to the corrosion rate. A potentiostatic experiment is conducted by mainatining a constant potential and measuring the resulting current as a function of time (Marcus & Mansfiel, 2005). The current required for the steel (WE) to be polarized is monitiored until an increase indicates active corrosion. This method has been used by several researchers such as Hansson and Sorenson (1990), Breit (1998) and Geiker et al. (2005). A critical parameter in this method is the selection of the potential to which the WE is polarized.

ii. Galvanostatic method

The galvanostatic method is employed by impressing a constant direct current (DC) upon the steel-solution interface and monitoring the potential response as a function of time. The galvanostatic experiments generate curves of potential

versus time and can measure passivation rates, evaluate cathodic or anodic protection techniques or gauge the thickness of passive films or electroplated layers.

This method involves connecting the positive terminal of a DC power supply to the steel reinforcing bar so that it becomes an anode and connecting the negative terminal to a counter electrode of good electrical conductivity so that it becomes the cathode, and placing the bars in an electrolyte (Ballim & Reid, 2005). In a study conducted by Taha, et al. (2016) using the galvanostatic method to accelerate the corrosion process, the researchers concluded that it is a reliable method as good correlation was achieved when comparing the accelerated time and real time to reach a certain degree of corrosion. This study will focus on the galvanostatic method from the impressed anodic current technique to induce corrosion of the steel embedded in corrosion. Both techiques have been used by researchers in literature and have been shown to induce corrosion in steel. The galvanostatic techniques was selected based on the availability of data logging resources, which records values of voltage as a function of time.

2.9. Fundamental principles of anodic impressed current

When an electric field is applied to passive steel embedded in concrete, electrolysis of the pore water can occur at both electrodes (Andrade, 1993). In the impressed current technique chloride penetration is also enhanced by an electric field on the steel surface (Care & Raharinaivo, 2007). The primary electrochemical difference of this technique to naturally corroding systems is the raising of the potential to a value greater than E_{tp} (transpassive potential), where the corrosion rate does not correspond with an equilibrium mixed potential or a potential obtainable under usual service conditions without applying an external source of energy (Ing, 2003). Subsequently, the corrosion rate of the impressed anodic current technique is not governed by the mixed potential theory but by the applied current which offers the benefit of reducing the sensitivity to changes in oxygen content, moisture content or temperature thus enabling good control over the corrosion rate for experimental purposes (Ing, 2003).

The corrosion current is a measure of the number of electrons that flow in a given period of time and can thus be used to determine the rate of the electrochemical reaction. Where corrosion is induced by means of impressed current, the amount of mass loss, by the steel, is related to the electrical energy consumed once depassivation has commenced. This can be modelled using Faraday's law which states that the amount of material deposited on an electrode is proportional to the amount of electricity used and that the amount of substances liberated by a given quantity of electricity is proportional to their chemical equivalent weight (Rosemary Gene & Ihde, 1954).

For impressed anodic current, this is done by measuring the electric current generated by the anodic reaction, consumed by the cathodic reaction, and then converting the current flow by Faraday's law to metal loss using Equation 2.29 (El Maaddawy & Soudki, 2003):

$$\Delta m = \frac{MIt}{zF} \tag{2.29}$$

where Δm is mass of steel consumed, M is molar mass (55.847 g/mol for iron (Fe)), I is current (amperes), t is time (seconds), z is number of electrons transferred (2) and F is Faraday's constant (96.487 amperes.second).

Under normal/natural conditions corrosion occurs due to a difference in electrochemical potential between the anode and cathode. The impressed current technique simulates this natural process by using an external electric field to apply an electrochemical potential, between the anode (reinforcing steel) and cathode (stainless steel), that is greater than the equilibrium potential between water and oxygen (El Maaddawy & Soudki, 2003). This accelerates the corrosion initiation phase from several years to several days or even hours depending on the current density.

2.9.1. Efficiency of using impressed current to induce steel corrosion in concrete

According to Ing (2003) the primary objective of any accelerated technique should be to simulate naturally induced corrosion in terms of the type of corrosion products and method of attack.

However, the similarities and deviations between the two mechanisms must be considered in order to determine its effectiveness as a technique. This is particularly important for the impressesd anodic current technique which involves an entirely different electrochemical process for inducing corrosion where the corrosion rate is governed by the applied current.

Currently there is no standardised procedure on the use of the impressed current technique to induce corrosion. Thus the technique has been investigated by several reseachers such as Nossoni and Harichandran (2012). The efficiency of this technique is described as mall loss efficiency which is defined the as the ratio of the actual mass loss (determined used gravimetric measurement) to the mass loss calculated using Faraday's law with efficiency indicated by a value closer to unity (one) (Nossoni & Harichandran, 2012).

The current efficiency is affected by the corrosion current density, salt solution concentration, pH of concrete pore solution, concrete cover and concrete quality. However, for the last two factors, the current literature only focuses on the correleation between concrete cover and concrete quality on the corrosion current density and not the efficiency of the impressed current technique. This study will focus on the effect of these two variables on mass loss efficiency. The following section discusses the factors which influence the current efficiency.

2.9.2. Factors affecting corrosion efficiency of impressed current technique

a) Effect of current density on corrosion efficiency

Current density from natural corrosion ranges from 0.1 to 10 $\mu A/cm^2$, occasionally reaching 100 $\mu A/cm^2$ (Andrade & Alonso, 2001). In the impressed

anodic current technique, an external power supply source is used to apply a larger direct current, thus increasing the rate of the anodic and cathodic reactions. Current density has varied greatly form 3 $\mu A/cm^2$ (Alonso, et al., 1998); 10400 $\mu A/cm^2$ (Almusallam, et al., 1996) to 17000 (Nossoni & Harichandran, 2012) amongst researchers.

El Maaddawy and Soudki (2003) investigated the influence of vaying the impressed current density level between 100 and 500 $\mu A/cm^2$ to accelerate steel reinforcing corrosion in concrete structures. The researchers reported good correlation between the measured mass loss and the predicted mass loss, using Faraday's law, for current densities between 100 and 500 $\mu A/cm^2$. However, they postulated that higher current densities could have an influence on the ability of Faraday's law to predict the actual degree of corrosion as a result of amount of corrosion products around the steel rebars which may hinder the diffusion of OH^- and/or Fe^{2+} ions through the rust layer. This is in agreement with what was reported by Nossoni and Harichandran (2012) who used current densities of 1700 $\mu A/cm^2$ and 17000 $\mu A/cm^2$ and concluded that when the current density is too high Faraday's law is not expected to yield an accurate estimate of the mass loss due to physical barriers (such as expansive corrosion products) which restrict the diffusion of moisture and chlorides into the concrete.

Pourbaix diagrams can also be used to explain the effect of impressed current density magnitude on the current efficiency. At high potentials and subsequently high current densities, it is possible that the oxidation at the anode produces either predominantly Fe^{3+} ions or both Fe^{3+} and Fe^{2+} ions in which case *n* will be greater than 2 in the oxidation reaction of iron and the mass loss calculated using Faraday's will be smaller than that obtained with *n* equal to 2, thus making the calculated current efficiency much higher than 1.0 (Nossoni & Harichandran, 2012). According to Ahmad (2009) the current applied for inducing corrosion is not fully efficient in causing loss of mass equal to that theoretically predicted by Faraday's law due to factors such as need for electrical energy to initiate corrosion, resistivity of concrete, composition of bar, etc., such that I_{corr}

(corrosion causing current) is not equal to I_{app} (applied current from DC power supply). Subsequently Austin, et al (2004) conducted a study to investigate the applicability of applying Faraday's law for calculating reinforcing steel mass loss whilst taking into account the difference between I_{corr} and I_{app}.

The Acoustic Emissions (AE) techique was used to detect the onset of corrosion. Acoustic emissions are generated as a result of microcrack development and their propagation in the concrete during the migration of corrosion products (Idrissi & Limam, 2003). The mechanical stresses induced in the concrete due to crack formation and propagation were converted to electric voltage and connected to a data logger recording hit-and-time driven acoustic amissions data as shown in Figure 2.19. In other words when a microseismis event occurs, such as microcrac development, the sensors detect the AE event as an AE hit.

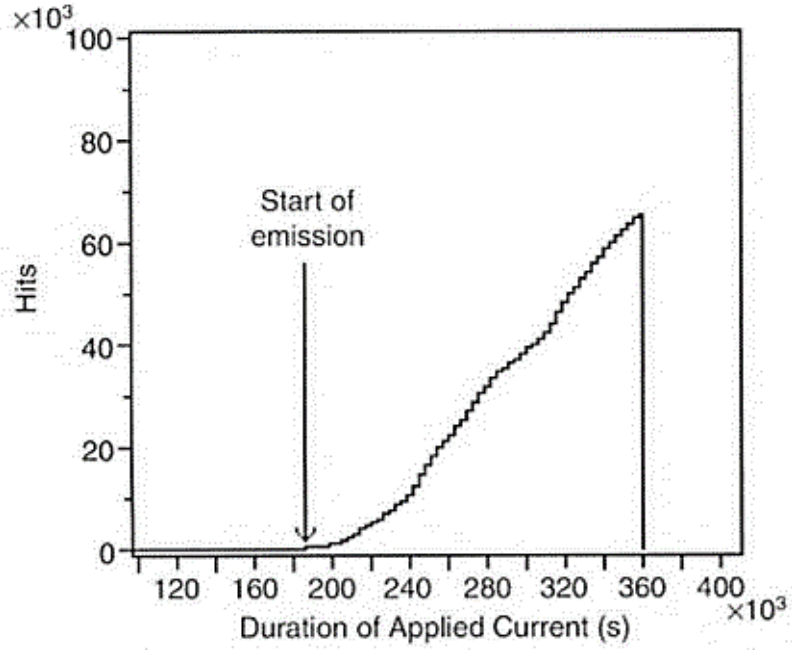

Figure 2.19: Increase in acoustic emission hits indicating onset of corrosion *(Austin, et* al., 2004)

The early detection of corrosion on-set allowed the researchers to propose a modified improved expression based on Faraday's law relating the electrical current to the mass loss. AE has been reported as a suitable laboratory tool that gives reasonably accurate estimates of corrosion initiation without interfering with or being affected by the applied current. In this study the percentage of surface

corrosion ranged between 0.2 – 39.8% with a median value of 4.9% with corrosion products typically localised on the underside of the bar, in the direction of the closest front of the proceeding chlorides in the salt solution.

Results of graphs of E_{sce} (V) versus Days showed that potentials in all cases remained consistently greater than E_{tp} implying that oxygen evolution was probably occurring where passivity had been compromised. According to the researcher's this suggested a split in the applied current used for the oxidation of water and steel. Austin, et al. (2004) suggested that the split anode reactions will influence the theoretical mass loss. The researchers suggested that a more reliable estimate of steel loss requires a modification to the terminilogy used in Faraday's law. Firstly the variable *time*, measured in seconds is not the total time duration of the applied current, but the *duration* (d_c) of corrosion activation until the termination of the test. Secondly, the value used for the *current,* must be proportional to the area of the steel on the bar that has been depassivated (a_c) and not the whole suface area (A_e), assuming that equal charge is used in the reduction of oxygen as in the dissolution of steel and that the area covered in corrosion products has depassivated.

Based on this, Austin, et al. (2004) developed a modified version of Farady's law for their work expressed in Equation 2.30:

$$Theoretical\ Mass\ Loss = \frac{Mid_c a_c}{A_e zF} \qquad (2.30)$$

Based on the results and observation made in this study, Austin, et al. (2004) confirmed that the impressed current technique is an effective and quick method for accelerating chloride-induce corrosion. Accounting for oxygen evolution and passivity when applying Faraday's law (modified version of Faraday's law) significantly improves the correlation between theoretical and gravimetric mass loss.

b) Effect of salt solution concentration

For accelerated corrosion tests, accelerated depassivation of the steel is required and can be achieved by adding chlorides into the concrete mix ranging from 1%

(Mangat & Elgarf, 1999) to 5% (El Maaddawy & Soudki, 2003) by weight of cement. Other researchers, (Cairns, Du and Law 2008), (Cabrera, 1996) opted to immerse their cured concrete specimens in tanks containing NaCl solution with concentrations ranging from 3% (Cairns, et al., 2008) to 5% (Cabrera, 1996) by weight of solution. The salt solution should be regularly replenished with a fresh one to ensure that the salt concentration remains the same throughout the test programme.

In an attempt to better simulate natural steel corrosion, Yoon et al., (2000) contaminated selected concrete faces by creating a NaCl solution reservoir on the top surface of the concrete specimen, whilst some researchers (Zhang et al, 2005; Rio et al, 2005) preferred spraying selected concrete faces with the salt solution. Under this action of contaminating selected faces the researchers found steel corrosion to be localised within the direction of ingress of chloride ions with further implications of larger tensile strains on the contaminated faces (Malumbela, et al., 2012).

The effects of using different chloride concentrations and current levels in accelerated corrosion testing were investigated by Nossoni and Harichandran (2012) in their study on the applicability of using Faraday's law for calculating the steel mass loss. The tests were done using two different constant current densities of 0.071 A/cm^2 (low current) and 0.14 A/cm^2 (high current) on steel embedded in concrete specimens. The specimens were immersed in solutions having chloride concentrations of 0.0% (water), 0.5%, 3.5% and 10% for more than one week to allow corrosion ions to penetrate the concrete and compromise the passive layer prior to accelerated corrosion testing. During the accelerated corrosion testing the specimens were removed from the salt solution and immersed in 100 mM K(OH) solution to increase conductivity since the electrical resistivity of concrete is considerably high.

In their study Nossoni and Harichandran (2012) opted for immersing the specimens in the KOH solution instead of the salt solution for the duration of the impressed current to prevent an increase in the chlorides at steel level due to crack

formation. The study showed that when no chlorides existed in the system the current efficiency (ratio of I_{corr} to I_{app}), was about 0.30 and 0.35 for the lower and higher current densities, respectively and increased to 0.6 and 0.52 when the chloride concentration increased to 0.5%. At medium chloride concentration of 3.5% the current efficiency increased to 1.0 and 0.86 for the low and high current densities, respectively. At chloride saturation of 10% the current efficiency for both low and high current densities reached (one) 1.0.

The results observed by Nossoni and Harichandran (2012) confirmed Care and Raharinaivo's (2007) recommendations that specimens for accelerated corrosion testing should be immersed in salt solution rather than water, as current efficiencies closer to unity were achieved at higher chloride concentrations. Nossoni and Harichandran (2012) concluded that Faraday's law may be used to accurately estimate the mass loss in the accelerated corrosion system as long as the current density is not too high. However, the researchers do not give any indication of what they considered to be a high current density.

c) Effect of concrete quality and concrete cover

Good concrete quality will normally offer excellent chemical protection for the reinforcing steel against corrosion due to the high alkalinity and low permeability of the concrete matrix (Hansson, et al., 1985). Concrete quality can be improved by reducing the water/binder ratio and/or by substituting plain Portland cement with mineral admixtures such as fly ash (FA), condensed silica fume (CSF) and ground granulated blast furnace slag (slag).

Ha, et al. (2007) conducted a study to evaluate the influence of admixture, namely fly ash, on the corrosion performance of steel in mortar. Accelerated short-term techniques such as anodic polarization and impressed voltage technique were carried out to determine the optimum level of replacement of FA with better corrosion resistance properties. Four FA replacement levels, 10%, 20%, 30% and 40% with respect to plain Portland cement (PC) were used and compared with PC specimens without FA. Results from the study showed that the addition of FA reduced the pH values of concrete, but still kept the final pH values above the

critical pH value of the breakdown of the passive film. Overall FA addition improved the permeability characteristics of concrete, delayed corrosion initiation and decreased the corrosion rate. Furthermore it was found that FA up to 30% replacement level improved the corrosion resistance properties of steel in concrete.

Upon retrieval of the reinforcing bars at the end of the experiment it was noted that the bars were uniformly corroded on the under side of the bar, closest to the concrete cover and the direction of the proceeding chloride ingress. Thus supporting the conclusions drawn by several researchers, such as (Ahmad, 2009), that the rebar corrodes mainly on the surface facing the concrete cover. At the same time, this supported the statement made by Yuan, et al. (2007) that corrosion under impressed current technique occurs uniformly on the steel surface.

This study by Yuan, et al. (2007) also investigated the effect of varying the w/b ratio and concrete cover on the time required for chlorides to permeate through the cover, and they found that the thickness of the concrete cover had a greater influence, than the w/b ratio. This is in agreement with what was reported by Palumbo (1991) who investigated the influence of varying the w/b ratio and the concrete cover on the corrosion activity of steel embedded in concrete.

Palumbo (1991) used w/b ratios ranging from 0.30 to 0.70 and found that no discernible distinctions were observed between each w/b ratio on the corrosion activity. On a cautionary note, although the concrete cover is the more predominant variable on the corrosion rate than the w/b ratio, it should not be used as a substitute for concrete quality. This is because the quality of the concrete cover is dependent on the w/b ratio and binder type, a lower w/b ratio results in a concrete with a denser microstructure that increases the resistivity of concrete thus reducing its permeability to the ingress of corrosion causing substances. Thus, a higher quality, less permeable concrete cover, offers a greater protection against corrosion to the steel than a more permeable concrete with a greater cover depth.

Palumbo (1991) also assessed the influence of various concrete covers on the corrosion activity of steel embedded in concrete by testing specimens with nine

different concrete covers ranging from 8 mm to 63.5 mm. Corrosion was accelerated using the pentiostatic technique to impress a constant voltage of 4.5 V on steel bar and the highest observed corrosion current density was 2 $\mu A/cm^2$. The bars were embedded in plain Portland cement with a w/b ratio of 0,45. The test was conducted for a period of 45 days. The results of average theoretical and gravimetric mass loss versus the clear cover depth are shown in Figure 2.20.

From Figure 2.20 it can be seen that the general trend for the increase in concrete cover is a reduction in average mass loss due to a retardation of corrosion initiation. For the cover depth ranging from 0.31 to 1.45 in (8 to 36.83 mm) the estimated theoretical mass loss determined using Faraday's law was higher than the actual mass loss from gravimetric measurement. The results show that at lower cover depths Faraday's law gives a better indication of steel mass loss than at higher cover depths. This is because for the same binder type, at higher cover depths the corrosion initiation phase is increased due to retardation of steel depassivation, through the ingress of chloride ions. The study concluded that the corrosion current i_{corr} is directly proportional to the cover depth and that smaller concrete covers resulted in significant increases in metal loss and average chloride content.

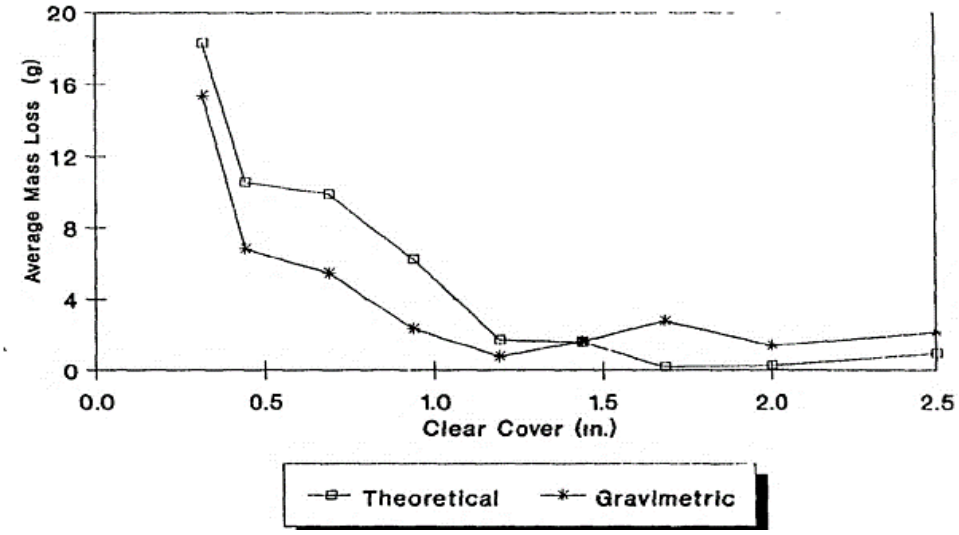

Figure 2.20: Theoretical and gravimetric average mass loss (g) vs. concrete cover (in.) (Palumbo, 1991)

2.9.3. Typical experimental set-ups and research findings

The set-up used for inducing reinforcement corrosion through the impressed current technique generally consists of a DC power supply, a counter electrode, working electrode and an electrolyte connection. The positive terminal of the DC power source is connected to the steel bar (anode) and the negative terminal is connected to the counter electrode (cathode) and the circuit may be connected in parallel or in series. The current is impressed from the counter electrode to the reinforcing steel through the concrete with the help of the electrolyte (usually a salt solution), for transferring ions from one electrode to the other and to close the circuit (Ahmad, 2009).

In a circuit connected in series, the current through each of the components is the same, and the voltage across the circuit is the sum of the voltages across each component. In a circuit connected in parallel, the voltage across each of the components is the same, and the total current is the sum of the currents through each component (Ahmad, 2009). In a parallel circuit, the amount of current flowing through the components is not the same, thus for the impressed anodic current technique, the series circuit is preferred by researchers as it impresses the same amount of current through all the component's (Ahmad, et al., (1997); El Maaddawy and Soudki, (2003)). Since there is no standardised procedure for impressed current experiments, there exist many various set-ups in literature. The main differences on the set up are the shape of the specimen and the method of chloride ingress through the concrete, either through full immersion of specimen, partial immersion or ponding of salt solution on selected faces.

The various experimental set-ups used in literature are discussed below with their similarities and differences compared. Figure 2.21 shows a cylindrical specimen with a single bar in the centre, this type of specimen is sometimes referred to as a "lollypop" specimen. This test set-up was used by Care and Raharinaivo (2007) for their study on accelerated corrosion using the impressed current technique.

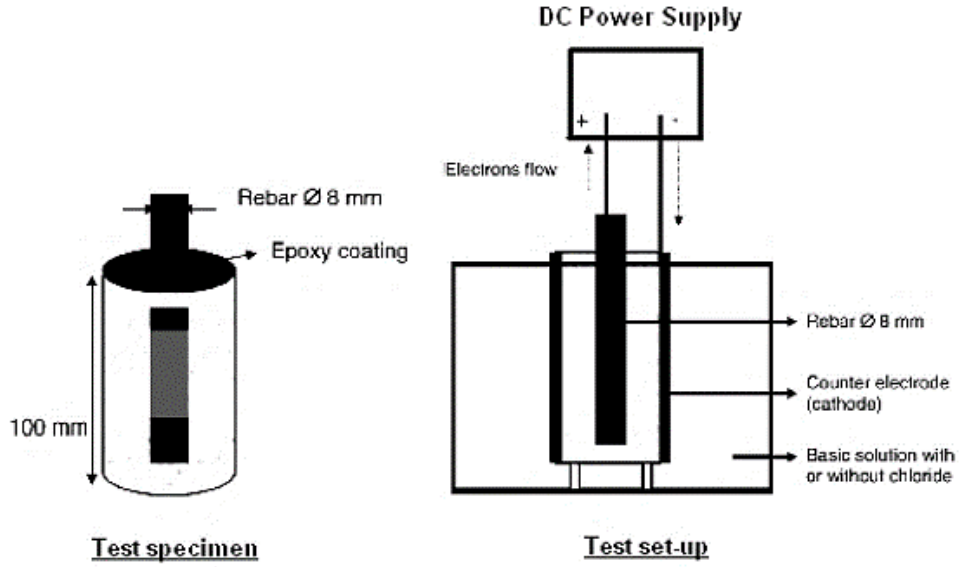

Figure 2.21: Typical lollypop reinforced concrete test specimen and set-up for accelerating reinforcement corrosion. ***(Care and Raharinaivo, 2007)***

This test set-up was also used by Ahmad, et al. (1997) who conducted experiments on 6 "lollypop" specimens conncected in series as shown in Figure 2.22.

The specimens shown in Figure 2.22 were immersed in a salt solution which also functioned as the electrolyte.

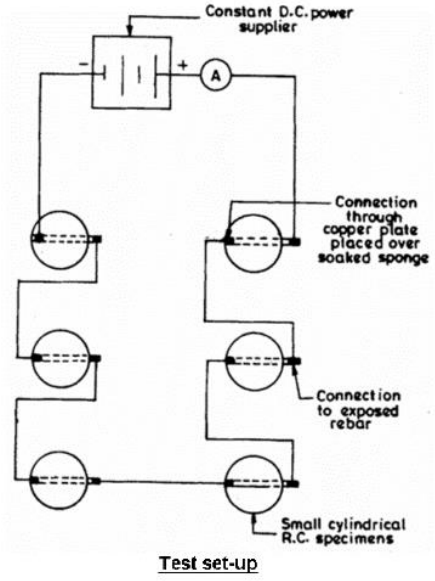

Figure 2.22: Lollypop reinforced concrete test specimens and set-up for accelerating reinforcement corrosion connecting several specimens in series. (*Ahmad et al., 1997)*

Care and Raharinaivo (2007) recommended that the specimens under accelerated corrosion testing should be immersed in solutions containing chloride instead of water. Their study reported that reinforcement corrosion in specimens under impressed current immersed in chloride solution are comparable with Faraday's law whereas when water is used, a more complex process occurs during the corrosion test. Similarly, a study by Raharinaivo's (2007) concluded that specimens for accelerated corrosion testing should be immersed in salt solution rather than water, as current efficiencies closer to unity were achieved at higher chloride concentrations.

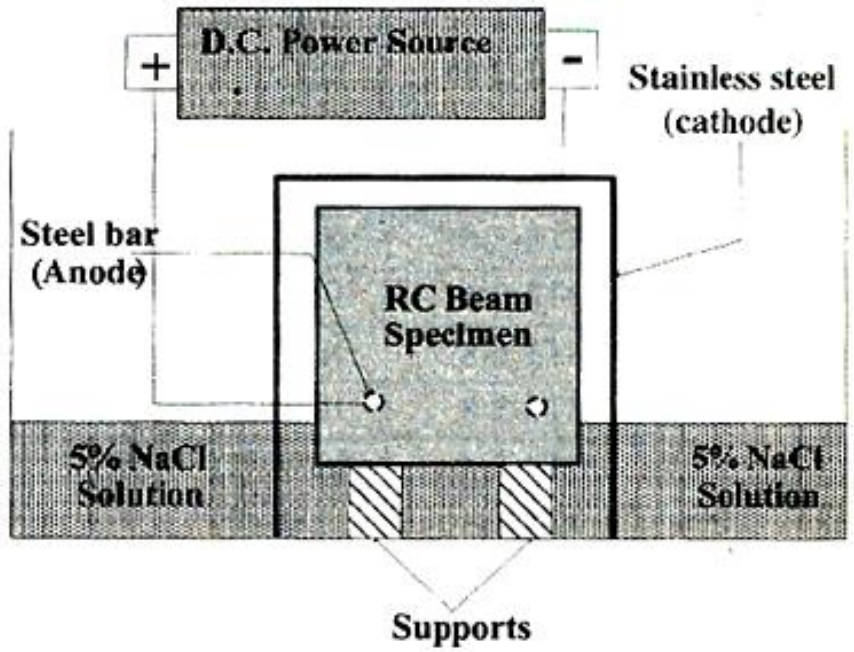

Figure 2.23: Set-up for accelerated reinforcement corrosion in large-sized reinforced concrete beam specimen. ***(Azad, et al. 2007)***

Figure 2.23 shows the set-up used by Azad, et al. (2007) for accelerating reinforcement corrosion testing using 150 x 150 x 1100 mm prisms. In this set-up, a 5% NaCl solution was used as the electrolyte and chlorides were introduced into the concrete through partial submersion of the prisms placed on top of supports so that the salt solution level was below the location of the steel in the concrete. This prevents the protruding steel from being in direct contact with the salt solution. The cathode (stainless steel) was placed outside the concrete in this test set-up.

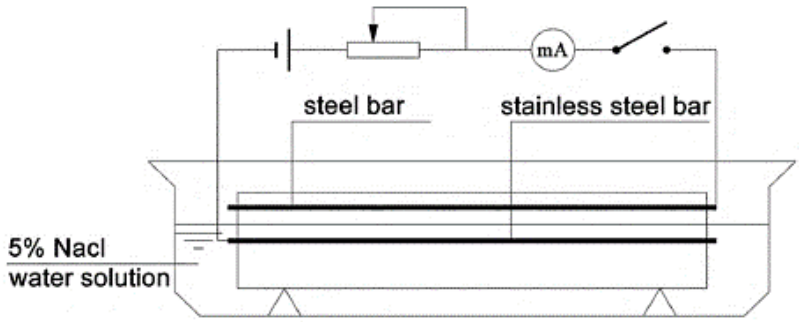

Figure 2.24: Set-up for accelerated reinforcement corrosion in large-sized reinforced concrete beam specimen. ***(Azad, et al. 2007)***

Figure 2.24 shows a similar test set-up used by Yuan, et al. (2007) where the concrete prisms were partially submerged in a 5% NaCl solution and placed on supports such that the level of the salt solution was below the steel level in the concrete. However, the difference in their set-up is that the cathode (stainless steel) was placed inside the concrete. This test set-up also comprised of a variable resistor/potentiometer in the corrosion circuit.

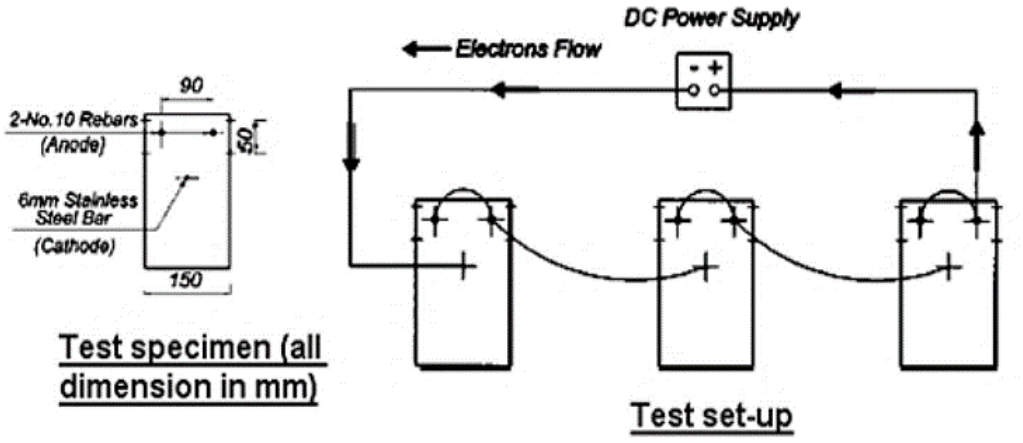

Figure 2.25: Reinforced concrete prism specimens and set-up for accelerating reinforcement corrosion connecting several specimens in series (*El Maaddawy & Soudki, 2003)*

Figure 2.25 shows the test set-up used by (El Maaddawy & Soudki, 2003). In this set-up, the cathode used was a stainless-steel bar placed inside the concrete and the prisms were connected in series. In this set-up, the chlorides were mixed into the concrete during casting.

Adding chlorides into the concrete mix provides direct access of the steel surface to chloride thus resulting in accelerated depassivation. As a result, when the

current is applied to accelerate corrosion, there is reduced time required to depassivate the steel. The total time for applied current can be attributed to the total time for corrosion. Thus, the method of adding chlorides into the concrete mix may address Ahmad (2009) concerns that for the impressed current technique, the time for rebar corrosion, is less than the total time of current application, because some time is required for depassivation of the rebar.

The study conducted by Austin, et al., (2004) attempted to address Ahmad (2009) concerns of differentiating between time required for corrosion depassivation (corrosion initiation) and total time for applied current by making use of a transducer placed on top of the concrete as shown in Figure 2.29.

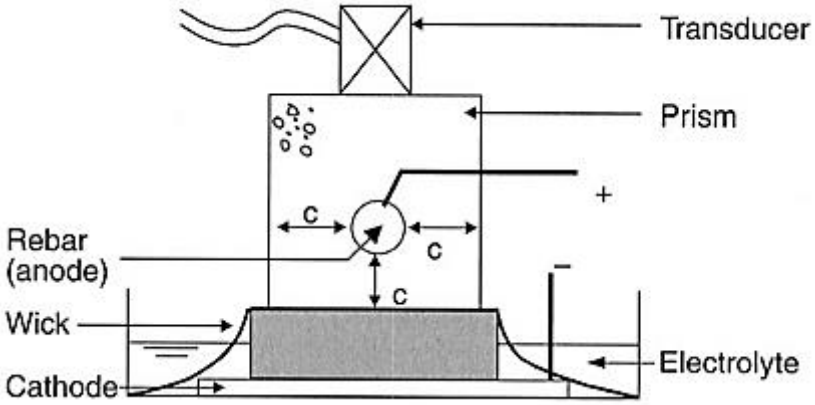

Figure 2.26: Accelerated corrosion cell set-up ***(Austin et al., 2004)***

In the corrosion cell set-up shown in Figure 2.26, corrosion was induced in concrete prisms of different characteristic strengths, and varying cover depths (16, 25, 40 mm) by applying a fixed current density of 100 $\mu A/cm^2$ for a period between 3 and 17 days. Electrical continuity between the cathode (stainless steel plate) and the anode (reinforcing steel) was provided by a wet wick saturated with 5% NaCl solution. A novel non-destructive technique referred to as acoustic emissions (AE) was used to detect corrosion initiation. This technique does not interfere with or becomes affected by the applied current and has been reported as a suitable tool for the detection of corrosion induced concrete damage (Das, 1995).

The force stresses generated in the concrete due to crack formation were measured using a piezoelecric transducer which converts the mechanical stress to electric voltage and recorded on a data logger.

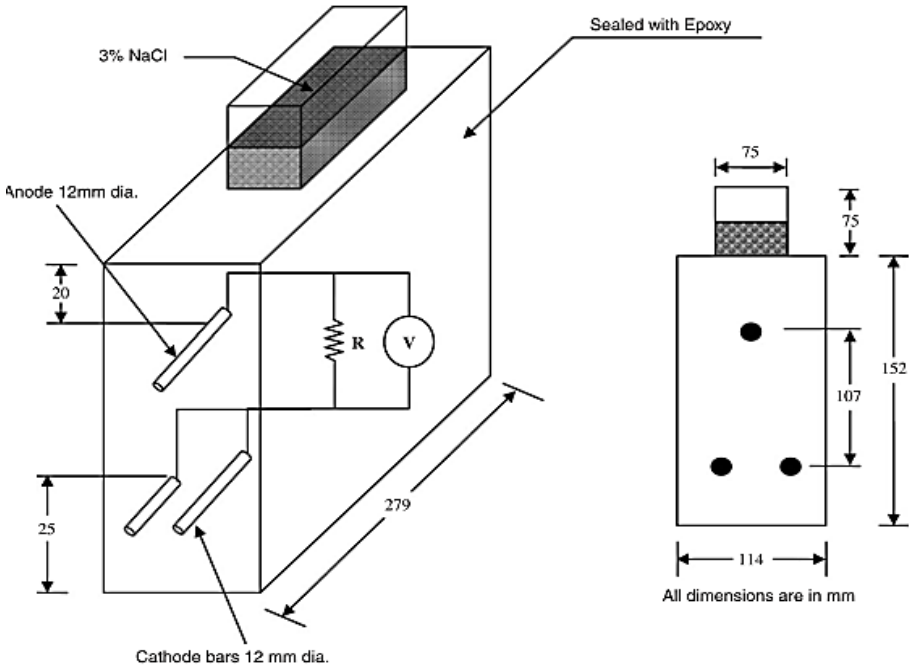

Figure 2.27: Schematic view macrocell specimen adopted from ASTM G109 ACT (Ha, et al., 2007)

Figure 2.27 shows the corrosion cell set-up used by Ha, et al. (2007) in their study on accelerated short-term techniques to evaluate the corrosion performance of steel in fly-ash blended concrete. They used the standard ASTM G109 Accelerated Corrosion Test technique which makes use of a salt solution reservior on the top surface of the prism, a single reinforcing steel bar (anode) and two cathode bars embedded inside the concrete. In this set-up a resistor is connected in series and the voltage across the resistor is measured.

As can be seen there are various set-ups that can be used by the researcher with the selected set-up depending on the variables under investigation, for example researchers investigating the effect of concrete cover will rather use the set-up consisting of a salt solution reservoir as opposed to adding chlorides into the concrete mix. The set-up used in the present study is a combination of the set-up used by various researchers. The corrosion cell in this study consists of a resistor

connected in series and the voltage across the resistor is measured similarly to the ASTM G109 ACT set-up adopted by. Ha, et al. (2007).

The set-up used consists of a salt solution reservoir on the top surface of the concrete as used by Ha, et al. (2007) adopted from ASTM G109 ACT. A 5% NaCl solution was used following the set-ups used by Azad, et al. (2007); Yuan, et al. (2007) and Austin, et al. (2004).

Lastly an external cathode was used as in the case of the research conducted by Azad, et al. (2007) and Austin, et al. (2004). Further details of the test set-up used are provided in the next chapter of this research report

2.10. Summary of literature review

Currently there is no standardised set-up for inducing steel reinforcement corrosion using impressed anodic current thus the various studies found in literature used different set-ups to induce corrosion.

Accelerated corrosion of reinforcing steel through the impressed current technique is achieved by applying a constant current from a DC power source to the steel embedded in the concrete. The procedure is termed accelerated because it induces significant corrosion in the steel over a short period of time, by drastically reducing the initiation period for depassivation from years to days and rapidly increasing the corrosion propagation period (Austin, et al., 2004). In this technique, a DC is applied for a given duration of time and the degree of induced corrosion can be determined theoretically using Faraday's law. Faraday's law relates to electrolysis and how the electrochemical reaction current is associated with the moles of elements under the reaction. Faraday's law is used to compute corrosion rates according to the kinetics of the cathodic and anodic reactions.

Based on this empirical law a linear relationship exists between the rate of corrosion and the corrosion current (CorrosionPedia , 2016). The rate of corrosion can be determined by first determining the corrosion current, this entails identifying the reaction mechanisms involving corrosion reactions (Austin, et al., 2004). By combining Faraday's law and Tafel plot analysis, industries are able to

predict whether a certain setup is likely to lead to corrosion and how fast the rate of corrosion will be in a given setup (CorrosionPedia , 2016).

Thus, Faraday's law is rather significant in corrosion testing and prevention, making the validation of the efficiency of the impressed current technique an important aspect.

The efficiency of this technique can be determined as a ratio of the theoretical mass loss calculated using Faraday's law to the actual mass loss determined by gravimetric weight loss measurements. This section will summarise the various results and observations in literature made by several researchers on studies using impressed current to induce corrosion of reinforcement steel in concrete. Various studies have been encountered in literature such as research by Yuan, et al. (2007) who conducted a study on reinforced concrete beams specimens which were initially immersed in a solution of 5% NaCl for 7 days, then a DC was impressed on the steel according to the set-up as shown in Figure 2.24. The position of the corroding steel bar in concrete was set higher than the level of the solution, (similarly to the set-up used by Azad, et al. (2007) shown in Figure 2.23, so as to avoid the dissolution of oxidation products as indicated by the researchers.

Placing the reinforcing steel above the salt solution is an approriate configuration as it prevents direct contact between the reinforcing bar and the chlorides since the rebar protrudes from the concrete face. Chlorides are purposely excluded from the concrete mix however this is not the approach followed by El Maaddawy and Soudki (2003), in the set-up shown in Figure 2.25, who added 5% NaCl by weight of cement into the concrete mix. This study investigated the influence of varying the impressed current level between 100 and 500 $\mu A/cm^2$on the actual degree of steel rebar corrosion. The results showed that for mass losses ranging from 4 to 7.27%, the measured mass loss based on the gravimetric weight loss was in good agreement with the predicted mass loss based on Faraday's law at different current densities.

The authors recommended that more research is required to investigate the ability of Faraday's law to predict the percentage mass loss at degrees of corrosion higher

than 7.27% mass loss. They suggested that at higher degrees of corrosion the amount of corrosion products around the steel reinforcing bars may hinder the diffusion of OH^- and/or Fe^{2+} ions through the rust layer.

This agrees with what was reported by Nossoni and Harichandran (2012) in their conclusion that when the current density is too high Faraday's law is not expected to yield an accurate estimate of the mass loss due to physical barriers (corrosion products) restricting the diffusion of water into the concrete. However the rearchers did not give an indication of what is considered as a current density that is too high. Another effect of corrosion is the reduction of cross-sectional area of reinforcing steel and loss of residual bond strength. This was investigated by Ayop and Cairns (2014) who studied the effect of using two different current densities; 0.08 $\mu A/cm^2$ (slow) and 0.4 $\mu A/cm^2$ (fast) impressed current to corrode 10 mm and 16 mm diameter reinforcing steel bars. The degree of corrosion was limited to 8% theoretical section loss of the steel and determined by applying Faraday's law.

The researchers observed a significant difference on the section loss between 10 mm and 16 mm bar diameters on both impressed current densities which contradicted with the almost similar amount of impressed current applied throughout the test. The results showed that most of the tested bars had a lower mass loss than the desired 8%, thus the reaseracher's concluded that 100% efficiency was not achieved in their study.

On the other hand good correlation between theoretical and experimental mass loss rates have been observed in literature by researchers such as El Maaddawy and Soudki (2003), Austin, et al. (2004), (Scott, 2004) and Yuan, et al. (2007) who investigated the effect varying variables such as the corrosion current density, concrete cover cracking, w/b ratio and binder types on the impressed current technique. This study will focus on the effect of concrete cover depth and concrete quality on the efficiency of the impressed current technique, which has not been covered in literature. The following chapter will provide details on the experimental set-up used in order meet the objectives of this research.

2.11. References

Ahmad, S., 2009. Techniques for inducing accelerated corrosion of steel in concrete. *The Arabian Journal for Science and Engineering,* 34(2), pp. 95-104.

Almusallam, A., Al-Gahtani, A., Aziz, A. & Rasheeduzzafar, F., 1996. Effect of reinforcement corrosion on bond strength. *Construction Building & Materials,* 10(2), pp. 123-129.

Alonso, C., Andrade, C., Rodriguez, J. & Diez, J., 1998. Factors affecting the cracking of concrete affected by reinforcement corrosion. *Materials & Structures,* Volume 31, pp. 435-441.

Andrade, C., 1993. Calculation of chloride diffusion coefficients in concrete from ionic migration measurements. *Cement and Concrete Research,* 23(3), pp. 724-742.

Andrade, C. & Alonso, C., 1996. Corrosion rate monitoring in the laboratory and on-site. *Construction and Building Materials,* 10(5), pp. 315-328.

Andrade, C. & Alonso, C., 2001. On-site measurements of corrosion rate of reinforcements. *Construction & Building Materials,* 15(2-3), pp. 141-145.

Andrande, C. & Alonso, C., 2004. Test methods for on-site corrosion rate measurement of steel reinforcement in concrete by means of the polarization resistance method. *Materials and Structures,* Volume 37, pp. 623-643.

Angst, U., 2011. *Chloride induced reinforcement corrosion in concrete,* Norway: Norwegian University of Science and Technology.

Angst, U., Elsener, B., Larsen, C. & Vennesland, O., 2009. Critical chloride in reinforced concrete - A review. *Cement and Concrete Research ,* 39(8), pp. 1122-1138.

Angst, U., Elsener, B., Larsen, C. & Vennesland, O., 2011. Chloride induced reinforcement corrosion: Electrochemical monitoring of initiation stage and chloride threshold values. *Corrosion Science,* 53(4), pp. 1451-1464.

Artigas, A. et al., 2015. Development of accelerated wet-dry cycle corrosion test in marine environment for weathering steels. *Corrosion Engineering, Science and Technology* , 50(8), pp. 628-632.

ASTM C876, 2015. *Test m-ethod for corrosion potentials of uncoated reinforcing steel in concrete* , s.l.: ASTM International .

ASTM G1-90, 1990. *Standard practice for preparing, cleaning and evaluating corrosion test specimens* , West Conshohocken: ASTM International.

Austin, S. A., Lyons, R. & Ing, M. 2., 2004. Electrochemical behaviour of steel reinforced concrete during accelerated corrosion testing. *Corrosion,* 60(2), pp. 203-212.

Azad, A., Ahmad, S. & Azher, S., 2007. Residual strength of corrosion-damaged reinforced concrete members. *ACI Matrials Journal* , 104(1), pp. 303-310.

Azarsa, P. & Gupta, R., 2017. Electrical Resistivity of Concrete for Durability Evaluation: A Review. *Advances in Materials Science and Engineering,* Volume 2017, pp. 1-30.

Ballim, Y., Alexander, M. & Beushausen, H., 2009. Durability of Concrete. In: G. Owens, ed. *Fulton's concrete technology.* ninth Edition ed. Midrand(Gauteng): Cement and Concrete Institute, pp. 155-188.

Ballim, Y. & Reid, J., 2005. Reinforcement corrosion and the deflection of RC beams - an experimental critique of current test methods. *Cement & Concrete Composites,* Volume 25, pp. 625-632.

Bardal, E., 2004. *Corrosion and Protection. Engineering Materials ans Processes.* 1st ed. London, UK: Springer.

Bell, T., 2017. *The balance: What is corrosion?.* [Online]
Available at: https://www.thebalance.com/what-is-corrosion-2339700
[Accessed 24 August 2017].

Bentur, A., 1991. Microstructure, interfacial effects and microchemics of cementitious composites. In: S. Mindess, ed. *Advances in Cementitious Materials.* USA: The American Ceramic Society, pp. 523-547.

Bentur, A., Diamond, S. & Steven, B., 1997. *Steel corrosion in concrete: Steel corrosion in concrete: Fundamentals and civil engineering practice.* 1st ed. London, UK: EFN Spon.

Bertolini, L., Elsener, B., Pedeferri, P. & Polder, R., 2004. *Corrosion of steel in concrete: prevention, diagnosis, repair,* Weinheim: Verlag GmbH & Co.

Bertolini, L. et al., 2016. *Corrosion of steel in concrete and it's prevention in aggressive chloride-bearing environments.* Shenzhen, P.R. China, 5th International Conference on Durability of Concrete Structures.

Bertolini, L. & Redaelli, E., 2009. Depassivation of steel reinforcement in case of pitting corrosion: detection techniques for laboratory studies. *Materials and Corrosion ,* 60(8), pp. 608-616.

Bird, R., Stewart, W. & Lightfoot, E., 2007. *Transport Phenomena.* 2nd ed. Wiley & Sons, Inc.

Bockris, O., Reddy, A. & Gamboa-Aldeco, M., 2000. *Modern Electrochemistry 2a, Fundamentals on Electrodics.* 2nd ed. New York: Kluwer Academics/Plenum Publishers .

Boddy, A., Bentz, E., Thomas, M. & Hooton, R., 1999. An overview and sensitivity study of a multi-mechanistic chloride tranport model. *Cement and Concrete Research,* 29(6), pp. 827-837.

Broomfield, J., 1996. Field measurement of the corrosion rate of steel in cincrete using a microprocessor controlled unit with a monitored guard ring for signal confinement. *ASTM Spec. Tech. Publ.,* 1276(1), pp. 91-106.

Byfors, K., 1990. *Chloride initiated reinforcemet corrosion, chloride binding,* Stockholm: Swedish Cement and Concrete Research Institute .

Cabrera, J., 1996. Deterioration of concrete due to reinforcement steel corrosion. *Cement & Concrete Composistes,* 18(1), pp. 47-59.

Cairns, J., Du, Y. & Law, D., 2008. Structural performance of corrosion-damaged concrete beams. *Magazine of Concrete Research,* 60(5), pp. 359-370.

Callister , W. & Callister , D., 2000. *Fundamentals of Materials Science and Engineering.* 5th ed. New York, USA: Wiley .

Care, S. & Raharinaivo, A., 2007. Influence of impressed current on the initiation of damage in reinforced mortar due to corrosion of embedded steel. *Cement and Concrete Research,* Volume 37, pp. 1598-1612.

Christensen, B. et al., 1994. Impedance spectroscopy of hydrating cement based materials: Measuremt, interpretation and application. *Journal of American ceramic Society,* 77(11), pp. 2789-2804.

Cigna, R. et al., 2002. *Corrosion of steel in reinforced concrete structures* , Luxenbourg : COST 521.

Corrosion Science, 2011. *Principles of Corrosion.* [Online]
Available at: http://www.corrscience.com/products/corrosion/intro-to-corrosion/principles-of-corrosion/
[Accessed 4 January 2017].

CorrosionPedia , 2016. *CorrosionPedia: Corrosion 101.* [Online]
Available at: https://www.corrosionpedia.com/definition/1475/faradays-law
[Accessed 20 August 2016].

Daflou, E., Rakanta, E. & Batis, G., 2006. *Corrosion protection methods of structural steel against atmospheric corrosion ,* Greece: National Technology University of Athens.

Dao, L. T., Dao, V. T., kim, S. H. & Ann, K. Y., 2010. Modeling steel corrosion in concrete structures - PART 1: A new inverse relation between current density and potential for the cathodic reaction. *International Journal of Electrochemical Science ,* 5(3), pp. 302-313.

Das, S., 1995. *Computer-aided quantitave interpretation of electropotential survey results for RC structures.* Edinburg, Scotland, Engineering Technics Press.

Dhir, R., McCarthy, M. & Newlands, M., 2002. *Challenges of Concrete Construction: Concrete for Extreme Conditions:*. Scotland, UK, Thomas Telford Publishing.

DuraCrete R17, 2000. *Probabilistic performance based durability design of concrete structure, includes general guidelines for durability design and redesign* , Gouda: Tech.Rep. BE95-1347/R17, The European Union - Brite EuRam .

El Maaddawy, T. A. & Soudki, K. A., 2003. Effectiveness of impressed current technique to simulated corrosion of steel reinforcement in concrete. *Jounal pf Materials in Civil Engineering,* 15(1), pp. 41-47.

Fagerlund, G., 1993. *On the service life of concrete exposed to frost action,* Sweden: Lund University.

Feliu, S., Gonzalez, j., Andrade, C. & Feliu, V., 1987. On-site determination of the Polarization Reistsnace in reinforced concrete beam. *Corrosion,* 43(9), pp. 1-9.

FIB, 2006. *Model code for servive life design - FIB Bulletin No 34,* .

Gehlen, C., 2000. *Probability-based service life design of reinforced concrete structures - Reliability studies for preventio of reinforced corroion.* 1st ed. Berlin, Germany: DAfStb Heft.

Ghosh, P. & Tran, Q., 2015. Correlation Betwen Bulk and Surface Resistivity of Concrete. *International Journal of Concrete Structures and Materials* , 9(1), pp. 119-132.

Gillespie, R., Humphreys, D., Baird, N. & Robinson, E., 1989. *Chemistry.* 2nd ed. Massachusetts : Allyn and Bacon Inc.

Glass, G., Hassanein, N. & Buenfeld, N., 1997. Neural network modelling of chloride binding. *Magazine of concrete research,* Volume 49, pp. 323-335.

Glass, G., Wang, Y. & Buenfeld, N., 1996. An investigation of experimental methods used to determine free and total chlorides contents. *Cement and Concrete Research,* Volume 26, pp. 1443-1449.

Gonzalez, J. & Andrade, C., 1982. Effect of carbonation, chlorides and relative humidity on the corrosion of galvanised rebars in concrete. *Britis Corrosion Journal,* 17(1), pp. 21-28.

Gulikers, J., 1996. *Experimental investigations on macrocell corrosion in chloride-contaminated concrete ,* Rotterdam: Delft University of Technology .

Gulikers, J., 2006. Considerations on the reliability of service life predictions using a probalistic approach. *Journal of Physics ,* 136(4), pp. 233-241.

Hansson, C., Frolund, T. & Markussen, J., 1985. The effect of chloride cation type on the corrosion of steel in conccrete by chloride salts. *Cement and Concrete Research,* 15(1), pp. 65-73.

Hansson, C. M., Poursaee, A. & Jaffer, S. J., 2007. *Corrosion of Reinforcing Bars in Concrete,* Canada: University of Waterloo.

Hansson, C. M., Poursaee, A. & Laurent, A., 2006. Macrocell and microcell corrosion of steel in ordinary Portland cement and high performance concretes. *Cement and Concrete Research,* 36(11), pp. 2098-2102.

Hansson, C. & Sorensen, B., 1990. *Threshold concentration of chloride in concrete for the initation of reinforcement corrosion,* Denmark: ASTM STP 1065.

Ha, T.-H.et al., 2007. Accelerated short-term techniques to evaluate the corrosion performance of stel in fly ash blended concrete. *Building and Environment ,* 42(1), pp. 78-85.

Huet, B. et al., 2007. Steel corrosion in concrete: Deterministic modeling of cathodic reaction as a function of water saturation degree. *Corrosion Science ,* Volume 49, pp. 1918-1932.

Idrissi, H. & Limam, A., 2003. Study and characterizaion by acoustic emission and electrochemical measurements of concrete deterioration caused by reinforcement steel corrosion. *NDT & E International*, 36(8), pp. 563-569.

Ing, M. J., 2003. *Detection of Reinforcement Corrosion by an Acoustic Technique,* Leicestershire: Loughborough University.

ISO/DIS 8407.3, 1986. *Procedures for removal of corrosion products from corrosion test specimen ,* Geneve, Switzerland : ISO/DIS.

Jones, D., 1996. *Principles and Prevention of Concrete.* 2nd ed. New Jersey, USA: Prentice Hall.

Kear, G. & Walsh, F. C., 2005. The characteristics of a True Tafel Slope. *Corrosionn and Materials*, 30(6), pp. 1-4.

Khadom, A. et al., 2009. The effect of temperature and acid concentration on corrosion of low carbon steel in hydrochloric acid media. *American Journal of Applied Sciences ,* 6(7), pp. 1403-1409.

Krajci, L. & Jerga, J., 2015. Assessment of steel reinforcement corrosion state by parameters of potentiodynamic diagrams. *Civil and Environmental Engineerin - De Gruyter,* 11(2), pp. 95-102.

Kumar, V., Singh, R. & Quraishi, M., 2013. A study on corroion of reinforcement in concrete and effect o inhibitor on service life of RCC. *Journal of Material and Environmental Science ,* 4(5), pp. 726-731.

Kumar, V., Singh, R. & Quraishi, M., 2013. A study on corrosion reinforcement in concrete and effect of inhibitor on service life of RCC. *Journal of Materials and Environmental Science,* 4(5), pp. 726-731.

Küter, A., 2009. *Managemnt of reinforcement Corrosion ,* Denmark: DTU Department of Civil Engineering .

Lambert, P., Page, C. & Vassie, P., 1991. Investigations of corrosion: electrochemical monitoring of steel in chloride-contaminated concrete. *Materials and structures,* Volume 24, pp. 351-358.

Layssi, H., Ghods, P., Alizadeh, R. & Salehi, M., 2015. Electrical resistivityof concrete. *Concrete International,* pp. 41-46.

Lim, T., Teng, S., Bahador, D. & Gjorv, E., 2016. Durability of very high strength concrete with supplementary cementitious materials for marine environments. *ACI Materials and Journal,* 113(1), pp. 95-103.

Lopez, W., Gonzalez, J. A. & Andrande, C., 1993. Influnce of temperature on service life of rebars. *Cement Concrete Resources* , pp. 1130-1140.

Lower, S., 2007. *All about Electrochemistry.* [Online]
Available at: http://www.chem1.com/acad/webtext/elchem/ec1.html
[Accessed 30 october 2016].

MacPhee, D. & Cao, 1993. Theoretical description of impact of blast furnace slag (BFS) on steel passivation in concrete.. *magazine of Concrete Research,* 45(162), pp. 63-69.

Malumbela, G., Moyo, P. & Alexander, M., 2012. A step towards standardising accelerated corrosion tests on laboratory reinforced concrete specimens. *Journal of the South African Institute of Civil Engineering,* October , 54(2), pp. 78-85.

Mangat, P. & Elgarf, M., 1999. Flexural strength of concrete beams with corroding reinforcement. *ACI Structural Journal,* 96(1), pp. 149-158.

Mangat, P. & gurusamy, K., 1987. Chloride diffusion in steel fibre reinforced concrete containing PFA. *Cement and Concrete Research,* 17(2), pp. 385-396.

Mangat, P. & Molloy, B., 1994. Prediction of long term chloride concentration in concrete. *Journal of Materials and Structures,* 27(7), pp. 338-346.

Marcotte, T. D., 2001. *Characterization of chloride-induced corrosion products that form in steel-reinforced cementitious materials,* Waterloo, Canada: University of Waterloo.

Marcus, P. & Mansfiel, F. B. eds., 2005. *Analytical methods in corrosion science and engineering.* 1st ed. s.l.:CRC Press.

McDonald, M., 2009. Control of concrete quality . In: *Fulton's Concrete Technology.* Midrand : Cement and Concrete Institute, pp. 287-295.

McKee, R., 1981. A generalization of the nernst-Einstein equation for self-diffusion in high defect concentration solids. *Solid Sate Ionics,* 5(10), pp. 133-136.

Metrohm Autolab, 2011. *Corrosion Part 2 - Measurement of corrosion rates,* Switzerland: Metrohm Autolab.

Millard, S., 2003. Measuring the corrosion rate of reinforced concrete using linear polrization resistance. *Concrete - Good Practice Guide No 132,* pp. 36-38.

Morris, W., Moreno, E. & Sagues, A., 1996. Practical evaluation of resistivity of concrete in test cylinders using a Wenner array probe. *Cement Concrete Research,* Volume 26, pp. 1779-1787.

Neville, A., 1995. *Properties of Concrete.* 4th ed. Essex, UK: Longman.

Neville, A., 1998. Concrete cover to reinforcement - or cover up?. *Concrete International ,* 20(11), pp. 25-29.

Nielson, E. & Geiker, M., 2003. Vhloride diffusion in partially saturated cementitious material. *Cement and Concrete Research ,* 33(1), pp. 133-138.

Nilsson, L. et al., 1996. *Chloride penetration into concrete, State of the Art, Transport processes, corrosion initiation, test methods and prediction models ,* Denmark: HETEK.

Nimmo, B. & Hinds, G., 2003. *Beginners Guide to Corroion ,* Middlesex: NPL.

Nokken, M., Boddy, A., Hooton, R. & Thomas, M., 2006. Time dependent diffusion in concrete - three laboratory studies. *Cement and Concrete Resources ,* 36(1), pp. 200-207.

Nossoni, G. & Harichandran, R., 2012. Current efficiency in accelerated corrosion

Page, C. L. & Treadaway, K. W., 1982. Aspects of the electrochemistry of steel in concrete. *Nature,* 297(5), pp. 109-115.

Palumbo, N., 1991. *Accelerated corrosion testing of steel reinforcement in concrete,* Montreal, Canada: McGill University.

Parra & Valcuende, M., 2010. Natural carbonation of self-compacting concretes. *Construction and Building Materials ,* 24(5), pp. 848-853.

Pettersson, K., 1993. *Corrosion of steel in high performance concrete.* Proceedingz from 3rd International Symposium on Utilization of High Strength Concrete , Lillehammer, Norway.

Polder, R., 2001. Test methods for on site measurement of resisitivity of concrete. *Construction and Building Materials,* 15(2-3), pp. 125-131.

Polder, R., 2001. Test methods for on-site measurement of resistivity of concrete - A RILEM TC-154 technical recommendations. *Construction and Building Materials ,* Volume 15, pp. 125-131.

Pourbaix, M., 1973. *Lectures on electrochemical corrosion.* New York(New York): Plenum Press.

Pourbaix, M., 1974a. Applications of electrochemistry in corrosion science and practice. *Corrosion Science ,* 14(2), pp. 25-85.

Poursaee, A. & Hansson, C. M., 2009. Potential pitfalls in assessing chloride-induced corrosion of steel in concrete. *Cement and Concrete Research,* 39(5), pp. 391-400.

Poyet, S., 2009. Experimental investigation of the effect of temperature on the first disorption isotherm of concrete. *Cement and Concrete Research,* 39(11), pp. 1052-1059.

Presuel-Moreno, F. & Liu, Y., 2012. *Temperature effect on electrical resistivity measurements on mature saturated concrete.* Salt Lake City, Utah, USA, NACE - International Corrosion Conference Series 7 .

Princeton Applied Research, 2000. *Electrochemistry and corrosion: overview and technques,* Illinois: Ametek.

Rajabipour, F., 2006. *Insitu electrical sensing and material health monitoring in concrete structures,* West Lafayette, Indiana: Purdue University .

Rajabipour, F. & Weiss, J., 2006. *Linking health monitoring in concrete structures with durability performace simulations.* St. Loius, Missouri, ASCE Structures Congress.

Ranade, R., Zhang, J., Lynch, J. & Li, V., 2014. Influence of micro-cracking on the composite resistivity of Enguneered Cementitious Composites. *Cement and Concrete Research,* 59(1), pp. 1-12.

Reen, E. & Carritt, D., 1976. Oxygen solubility in sea water: thermodynamic influence of sea water. *Science,* 157(7), pp. 191-193.

Reichling, K. et al., 2013. Full surface inspection methods regarding reinforcement corrosion of concrete structures. *Material Corrosion,* Volume 64, pp. 116-127.

Ries, H., 1983. Complete and Reversible Absorption of Radiation. *Applied Physics B,* 32(7), pp. 153-156.

RILEM, 1994. Draft recommendation for repair strategies for concrete structures damaged by reinforcement corrosion. *Materials and Structures* , Volume 27, pp. 415-436.

Rosemary Gene, E. & Ihde, A., 1954. Faraday's Electrochemical Laws and the Determination of Wquivalent Weghts. *Journal of Chemical Educaton,* 31(5), pp. 226-232.

Rostam, S., 2003. Reinforced concrete structures - Shall concrete remain the dominating means of corrosion prevention. *Materials and Corrosion ,* 54(6), pp. 369-378.

Rupnow, T. & Icenogle, P., 2012. *Evaluation of surface resistivity measurements as an alterntive to the rapid chloride permeability test for quality assurance and acceptance ,* Baton Rouge, LA, USA: Transportation Research Center .

Sadowski, L., 2010. New non-destructive method for linear polarisation resistance corrosion rate measurement. *Arch. Civ. mech. Eng,* Volume 10, pp. 109-116.

Sandberg, P., 1995. *Critical evaluation of factors affecting chloride initiated reinforcement corrosion in concrete,* Lund, Sweden: LTH.

Sandberg, P. & tang, L., 1993. *A field study if the penetration of chlorides and other ions into a high quality concrete marine bridge column.* Nice, International Conference of Durability of Concrete .

Sato, N., 2012. *Basics of corrosion chemistry.* 1st ed. Weinheim, Germany : Wiley-VCH VerlagGmbH& Co.KGaA..

Schiessl, P. & Breit, W., 1995. *Time to depassivation depending on concrete composition and envitonmental conditions.* Saint-Remy-les-Chevreuse, France, RILEM International Workshop on Chloride Penetration into Concrete .

Schiessl, P. & Lay, S., 2005. *Influence of conecret composition.* 1st ed. Cambridge: Woodhead Publising Limited .

Schiessl, P. & Raupach, M., 1990. *Influence of concrete composition and microclimate on the critical chloride content in concrete.* UK, Wishaw, Elsevier Applied Science, pp. 49-58.

Scott, A. N., 2004. *The influence of binder type and cracking on reinforcing steel corrosion in concrete,* Cape Town: Department of Civil Engineering University of Cape Town.

Sengul, O., 2014. Use of electrical resistivity as an indicator fordurability. *Construction and Building Materials,* 73(1), pp. 434-441.

Sengul, O. & Gjorv, O., 2009. Effect of embedded steel on electrical resistivity measurements on concrete structures. *ACI Materials Journal,* 106(1).

Shane, J. et al., 1999. Microstructural and pore solution changes induced by the rapid chloride permeability test measured by impedence spectoscopy. *Concrete Science Enginineering ,* 1(1), pp. 110-119.

Shi, X. et al., 2009. *Corrosion of deicers to metals in transportation infrastructure: introduction and recent developments,* Montana: Western Transportation institute.

Shreir, L., Jarman, R. & Burstein, G., 1994. *Corrosion.* 3rd ed. Butterworth: Oxford.

Silva, A., Neves, R. & de Brito, J., 2014. Statistical modelling of carbonation in reinforced concrete. *Cement and Concrete Composites ,* 50(1), pp. 73-81.

Silva, N., 2013. *Chloride Induced Corrosion of Reinforcement Steel in Concrete,* Gothenburg, Sweden: Chalmers University of Technology .

Sirivivatnanon, V., Bucea, L., Meck, E., Yozghatli, S., & Cao, H. (1994). Influence of Fly Ash, Ground Granulated Blastfurnace Slag ans Silica Fume on Chloride Induced Corrosion of Steel Reinforcement. *2nd International Symposium on Blended Cements* (pp. 114-120). Malaysia: Symposium on Blended Cements.

Spragg, R. et al., 2013. *Electrical testing of cement-based materials: role of testing techniques, sample conditioning,* Purdue: FHWA/IN/JTRP.

Spragg, R. et al., 2013. Factors that influence electrical resistivity measurements in cementitious systems. *Journal of the Transportation Research Board,* 2342(1), pp. 90-98.

Stern, M. & Geary, A., 1957. Electrochemical Polarization: A theoretical analysis of the shape of polarization. *Journal of the Electrochemical Society* , 104(1), pp. 56-63.

Stillwell, J., 1983. *Concrete in the Oceans. Exposure tests on concrete for offshore structures.* , Middlesex, UK: Wimpey Laboraties Ltd.

Stratfull, F., 1972. *Half-cell potential and the corrosion of steel in concrete.* 1st ed. California, USA: Division of Highways, State of California.

Taha, N. & Morsy, M., 2016. Study of the behaviour of corroded steel bar and convenient method of repairing. *Housing and Building National Research Center,* 12(1), pp. 107-113.

Tan, K. & Gjorv, O., 1996. Performance of concrete under different curing conditions. *Cement and Concrete Research,* 26(3), pp. 355-361.

Thomas, J., 1996. *The Electrochemistry of Corrosion.* [Online]
Available at:
http://www.npl.co.uk/upload/pdf/the_electrochemistry_of_corrosion.pdf
[Accessed 07 August 2016].

Torrent, R., Alexander, M. & Kropp, J., 2007. *Introduction and problem statement, Chapter one: State of the art report, non-destructuve evaluation of the penetrability and thickness of the cover,* s.l.: RILEM TC 189-NEC.

Tuutti, K., 1982. *Corrosion of steel in concrete.* 82 ed. Sweden: Swedish Cement and Concrete Research.

Vennesland, O., Raupach, M. & Andrade, C., 2007. Recommendaton of RILEM TC 154-EMC: Electrochemical techniques for measuring corrosion in concrete -

measurements with embedded probes. *Materials and Structures* , 40(8), pp. 745-758.

Virmani, Y. & Clear, K., 1983. *Time-to-corrosion of reinforcing steel in concrete,* Washington: FHWA.

Vivas, E., Boyd, A. & Hamilton, H., 2007. *Permeability of concrete-comparison of conductivity and diffusion methods* , Tallahassee, FL, USA: Tech. Rep. 4910, Florida Department of Transportation .

Wenner, F., 1916. A method of measuring earth resistivity. *Bulletin of the Bureau of Standards,* 36(261), pp. 461-471.

West, J., 1980. *Basic Corrosion and Oxidation* , London: Ellis Horwood Limited.

Whitting, D. A. & Nagi, M. A., 2003. *Electrical resistivity of concrete,* Skokie, USA: Portland Cement Association .

Yuan, Y., Ji, Y. & Shah, P., 2007. Comparison of two accelerated corrosion techniques for concrete structures. *ACI Structural Journal,* 104(3), pp. 344-347.

Zaki, A., Chai, H., Aggelis, D. & Alver, N., 2015. Non-destructive evaluation for corrosion monitoring in concrete: A review and capability of acoustic emission technique. *Sensors,* 15(8), pp. 19069-19101.

Zemajtis, J., 2002. *Portland Cement Association.* [Online]
Available at: http://www.cement.org/learn/concrete-technology/concrete-construction/curing-in-construction
[Accessed 13 July 2017].

Zhang, Y., Sun, W., Chen, S. & Guo, F., 2011. Two and three dimensional chloride ingress into fly ash concrete. *Journal Wuhma Unoversity of Technology, Materials and Science,* 26(5), pp. 978-982.

Zhou, Y., Gencturk, B., William, K. & Attar, A., 2014. Carbonation-induced and chloride-induced corrosion in reinforced concrete structures. *Journal of Materials in Civil Enginering* , 27(9), pp. 847-864.

CHAPTER 3: EXPERIMENTAL DETAILS

3.1. Introduction

This Chapter will provide a detailed overview and description of the laboratory experiments conducted in this study. Firstly, the variables under investigation and the properties of the materials used will be discussed. Secondly the concrete mix design and preparation of concrete prisms will be discussed. Lastly the accelerated corrosion set-up using anodic impressed current will be discussed. Figure 3.1 shows a flow chart diagram of the experimental detail set-up.

RESEARCH AIMS
To study the effect of varying the concrete quality and cover on the efficiency of impressed anodic current to induce corrosion of steel embedded in concrete.

↓

TEST SET- UP	
Variables	**Constants**
Cover depth: 20, 35 and 50 mm	w/b ratio: 0.55 Salt solution concentration: 5% NaCl
Binder type: 100% PC 50/50 PC/SL, 70/30 PC/FA	Reinforcing steel: 12 mm diameter high yeild bar Aggregates: Andesite

↓

TEST PARAMETERS			
Test	**Specimen type**	**Test technique**	**Standards/protocol**
Accelerated corrosion	100 x 100 x 500mm beams	Impressed anodic current (galvanostatic method)	Adapted from literature (Maaddawy et al., 2003); Azad et. al, (2007) ASTM G109 ACT; Austin et al, (2004)
Compressive strength	100 x 100 x 100mm cubes	Concrete cube crushing	SANS 5863:2006
Concrete bulk electrical resistivity	100 x 100 x 100mm cubes	4 Point Modified Wenner probe	Adapted from literature (Polder, 2001); (Spragg et al, 2011)
Durabilty index test	30mm thick, 70 +/- 2mm diameter cores	OPI, CCI, WSI	Concrete durability testing manual (Alexander et al, 2017)

Figure 3.1: Flow chart showing experimental details

3.2. Experimental variables

3.2.1. Concrete cover to reinforcing steel

Concrete cover is the distance from the surface of the concrete to the centre reinforcing bar (Middel, 2009). The South African concrete design code recommends a minimum cover of 20, 30, 40 and 50 mm for mild, moderate,

severe and very severe exposure conditions respectively (SANS 10100-2, 1992). Mild conditions refer to concrete that is exposed to generally unpolluted air; moderate conditions refer to concrete that is subject to polluted air; severe conditions refer to concrete that is exposed to salt laden air and very severe conditions refer to concrete exposed to wet conditions in which the water is mildly to fairly aggressive (SANS 10100-2, 1992). Three concrete covers were investigated in this study namely 20, 35 and 50 mm. All concrete specimens were exposed to the same condition of exposure i.e. very severe condition in the form of a salt solution ponded on the concrete surface in the direction of the investigated concrete cover.

3.2.2. Degree of steel corrosion

The degree of corrosion may be expressed in terms of the percentage mass loss (P), calculated using Equation 3.1:

$$P = \frac{M_i - M_f}{M_i} \times 100 \qquad (3.1)$$

where M_i is the initial mass of the reinforcing steel determined before the accelerated corrosion process and M_f is the final mass determined after accelerated corrosion process.

In this study, the amount of impressed current (I_{app}) required to induce corrosion for a certain duration and the degree of corrosion (P) was calculated. The duration of accelerated corrosion was determined by the time taken for first visible cracks to develop on surface of the concrete specimen. Setting the duration of accelerated corrosion to the time taken for crack formation to occur allowed for confirmation of corrosion activity as corrosion products exuded to the surface of the concrete prisms.

3.2.3. Binder types

The concrete quality was varied by using three different types of cement/binder blends. The South African design code recommends that the cement type can be any cement complying with SANS 50197-1 and cements blends of at least 50% plain Portland cement (PC) and 50% ground granulated blast furnace slag (SL) or

70% PC and 30% Fly Ash. For this study three different binder types were used, namely:

a) 100% plain Portland cement (100% PC)

This binder type consists of 100% plain Portland cement which has a particle relative density of 3.14 (Addis & Goodman, 2009). CEM I 52.5, rapid hardening cement was used to reduce the waiting period required before stripping the formwork.

b) 70% PC and 30% Fly Ash blend (70/30 PC/FA)

This binder type consists of a 70% plain Portland cement and 30% fly ash blend. Fly ash (FA) is a pozzolanic binder i.e. it contains high reactive SiO_2 which forms stable cementitious compounds in reaction with the calcium hydroxide released during the hydration of cement (Grieve, 2009). FA has a particle relative density of 2.3 (Addis & Goodman, 2009). FA content of 30% or more enhances the concretes resistance to chloride attack of reinforcement steel (SANS 1491-2, 2005). Thus a 70/30 PC/FA blend was selected for this study.

c) 50% PC and 50% Ground Granulated Blast-furnace Slag blend

This binder type consists of 50% Ground Granulated Blast-furnace Slag (GGBS/SL) and 50% plain Portland cement. GGBS is a latent hydraulic binder that is used in concrete as a partial cement replacement material that can replace up to 90% Portland cement with at least 50% replacement prescribed by SANS 1491-1 (2005). GGBS captures chlorides and enhances the concretes resistance to chloride attack. Thus, in this study 50% GGBS replacement of plain Portland cement was used with a relative density of 2.9 (Addis & Goodman, 2009).

3.3. Materials used

3.3.1. Reinforcing steel (rebar)

Ribbed high yield tensile strength steel bars, 12 mm in diameter and machine cut to 500 mm lengths were used in this study. The rebar was first cleaned with Acetone to remove grease stains, before use. The reinforcing steel functioned as the anode in the accelerated corrosion cell.

3.3.2. Stainless steel

Grade 304, 8 mm diameter stainless steel bars, 300 mm long, were used in this study. The stainless steel performed the function of the cathode in the accelerated corrosion cell.

3.3.3. Salt solution

A 5% NaCl solution was used to serve as an electrolyte for the transfer of ionic charge and the accelerated depassivation of the steel. Depassivation is the loss of the passive protective layer on the steel surface. The 5% NaCl solution was used in this study to represent very severe exposure environmental conditions. For 10 L of NaCl solution, 10 litres of tap water and 500g of NaCl salt was used to make 5% NaCl solution.

3.4. Aggregates

Crushed andesite rock of good quality was used for both coarse and fine aggregate. The aggregate quality was used to determine the amount of water required in the concrete mix to achieve a slump of 25 mm which is a measure of the concrete's workability. The workability of the fresh concrete can be improved by using rounder and smoother aggregates which can be described as aggregates of good quality.

3.4.1. Coarse aggregate

The coarse aggregate refers to stone of particle size such that is retained on a sieve having square apertures of nominal size 4.75 mm (South African National Standards 201, 2008). Coarse aggregate used in conventional concrete production has maximum typical sizes of 9.5, 13.2, 19.0, 26.5 and 37.5 mm. According to SANS 10100-1 (2000), the maximum nominal size of stone used should at least be equal to the concrete cover depth to reinforcement. In this study, three cover depths were used, 20, 35 and 50 mm. For all cover depths under investigation, stone a maximum size of 13.2 mm was used. A sieve analysis, in accordance to SANS 201 (2008), was conducted on the stone to determine the stone size and grading. The sample size required for conducting sieve analysis tests on course aggregate was determined in accordance to SANS 197 (2006) sampling methods.

The sieve analysis results show that the stone has a maximum diameter of 13.2 mm and minimum diameter of 9.5 mm and is continuously-graded.

3.4.2. Fine aggregate

The fine aggregate content in conventional concrete production refers to sand of particle size such that at least 90% passes a sieve having square apertures of nominal size 4.75 mm and is retained on a sieve having square apertures of nominal size 0.075 mm (Grieve, 2009). The typical sizes of fine aggregates are 4.75, 2.36, 1.18, 0.60, 0.30, 0.15 and 0.075 mm. The South African National Standards have specified several requirements for fine aggregates, namely:

i. not less than 90% shall pass a 4.75 mm sieve and between 5 and 12% shall pass a 0.15 mm sieve,
ii. the material passing a 0.075 mm sieve shall not exceed 5% by mass and
iii. a fineness modulus (FM), a dimensionless parameter which is a measure of the average particle size.

Similarly, to the coarse aggregate, the sample size required for conducting FM test on fine aggregate was determined in accordance to SANS 197 (2006) sampling methods. Figure 3.2 shows the grading curve of the fine aggregate determined from the sieve analysis test.

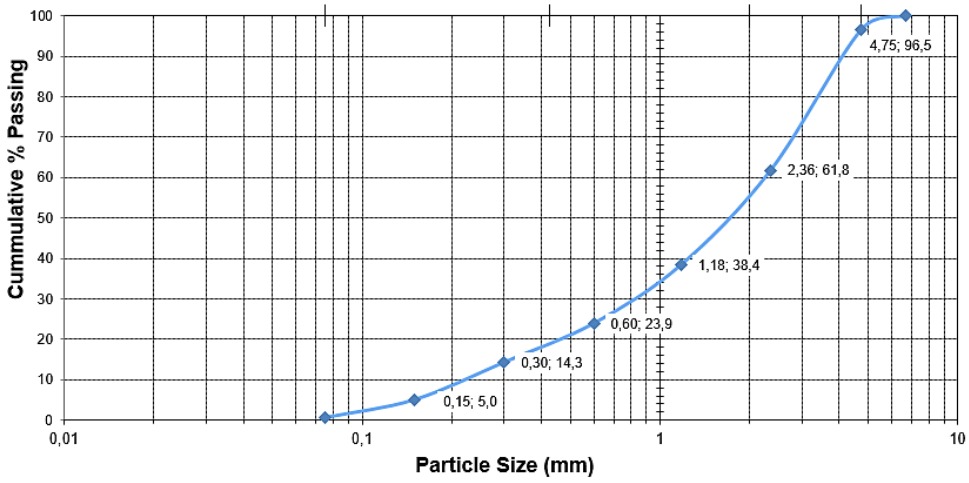

Figure 3.2: Grading curve of coarse aggregate

The grading curve shows that 96.5% of the sand passes through the 4.75 mm sieve. The sand had a continuous grading and a fineness modulus of 3.6.

3.5. Concrete mix design

Concrete mix design is a way of proportioning the concrete making materials, namely binder type, water, sand and stone so as to achieve the required properties of the fresh and hardened state of concrete, at the lowest cost. Concrete mix design is often a matter of trial and error with calculations based on formulae developed from empirical relations, graphs and charts. Kosmatka and Panarese (1988) from the Portland Cement Association outline the concrete mix design process objective as determining the most practical and economical combination of readily available materials to produce concrete that will satisfy the performance requirements whilst being a designer-independent process as well.

Most countries have standardised their own concrete mix design methods, in South Africa the volumetric mix design from the Cement and Concrete Institute is used (Addis & Goodman, 2009).

This method is derived from the ACI Standard 211.1-91 (1999) and was adopted for this study. The procedure prescribed by the ACI Standard for a volumetric concrete mix design is shown in Figure 3.3:

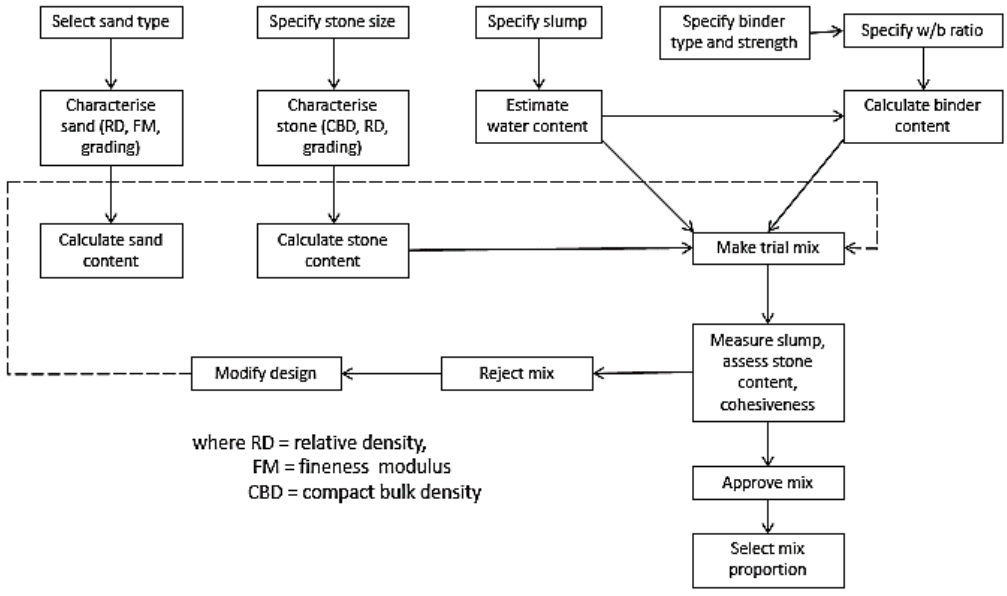

Figure 3.3: Concrete mix design flow chart modified *ACI Standard 211.1-91 (1999)*

The mix design process shown in Figure 3.3 involves specifying the concrete properties and characteristics; selecting, characterising and proportioning materials; specifying mix proportions and lastly, producing and assessing the trial mix. The amount of water required for the concrete mix is determined per unit volume of concrete. The volume of compacted concrete is equal to the sum of absolute volumes of binder, aggregate, water and entrained air (if applicable otherwise negligent). The amount of constituents required for each mix is determined per cubic metre of concrete. As such the concrete mix design proportions are given in kg/m^3.

The South African concrete design code recommends a maximum water/binder (w/b) ratio of 0.55 and minimum cover depths of 25 mm and 50 mm for concrete structures in non-polluted and highly corrosive environments, respectively (SANS 10100-2, 1992). In this study, a w/b ratio of 0.55 was used for the different binder types and concrete cover depths. The strength and permeability of the hardened concrete is dependent on the w/b ratio of the paste such that the strength decreases and permeability increases with increasing w/b ratio (Grieve, 2009). The w/b ratio is an intrinsic factor of concrete durability which is a function of concrete quality.

In this study, the w/b ratio was kept constant and the concrete quality was varied by using three different the binder types. The mix proportions per cubic metre for the three different concrete mixes are shown in Table 3.1:

Table 3.12: Concrete mix proportions (kg/m^3)

Material	100% PC blend	50/50 PC/SL blend	70/30 PC/FA blend
PC	391	195	274
GGBS	-	195	-
FA	-	-	117
Stone	896	896	940
Sand	806	793	730
Water	215	215	215

3.6. Formwork

18 mm Thick plywood was used to make formwork moulds of 100 x 100 x 500 mm in size. The plywood forms were assembled using 8 x 40 mm chip board screws so that the formwork can be easily stripped thus allowing preservation of the wood for reuse. Form oil was applied to the inside surfaces of the formwork moulds to prevent the moisture from the concrete from absorbing into the wood and allow for easy stripping. Figures 3.4 and 3.5 show the arrangement of the reinforcing steel bar inside the concrete prisms.

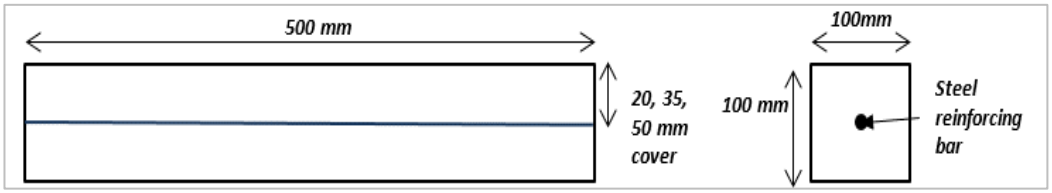

Figure 3.4: Side elevation view and cross-section view of rebar in concrete prism.

Figure 3.5: Photograph of reinforcing bar (with conductive electrical wire attached) in the formwork mould.

3.7. Casting of specimens

The concrete was poured in two layers and each layer vibrated using a mechanical vibration table for two minutes. Concrete is compacted to expel entrapped air, thereby achieving maximum density, strength and impermeability, for every 1% excess voids, the concrete strength is reduced by approximately 5 to 6% (Kellerman, 2009). Mechanical vibration in most cases is the most effective way

of compacting concrete in order to ensure that the maximum potential strength and minimum permeability is achieved when the concrete is fully cured (Kellerman, 2009). Casting comprised of nine beams for accelerated corrosion tests, nine cubes for compressive strength test, three cubes for electrical resistivity tests and four cubes for durability index tests from each concrete mix. The formwork was stripped after 24 hours of casting.

3.8. Curing

Concrete curing is the process of maintaining satisfactory moisture content and temperature in the concrete during its early stages so that the desired properties may develop (Kellerman, 2009). Cementing reactions in the hydration of concrete can only properly take place when capillaries are filled with water.

Curing should also be initiated as soon as the concrete is exposed to the atmosphere, if it is delayed; calcium hydroxide is deposited in the entrances of the capillaries by the evapourating pore water. The carbon dioxide carbonates the calcium hydroxide which seals the capillaries and makes it difficult to get water back into the concrete to replace the evapourated water (Kellerman, 2009).

During the first 24 hours setting period, all specimens were covered with plastic sheeting to prevent excessive moisture loss. The exposed ends of the accelerated corrosion specimen were coated in silicone glue to prevent premature corrosion during the curing process. All specimens were cured in a water bath at temperature of $22 \pm 2℃$. Cubes for concrete compressive strength test were cured for 7, 14 and 56 days before crushing while cubes for durability index tests, bulk electrical resistivity tests and accelerated corrosion tests were cured for at least 56 days.

3.9. Accelerated corrosion

Accelerated corrosion of reinforcement steel embedded in concrete was achieved by means of using impressed anodic current to drive the corrosion process. The theoretical amount of mass lost by the steel, due to corrosion, is related to the

electrical charge consumed once passivity has been compromised and can be modelled using Faraday's Law.

3.9.1. Accelerated corrosion cell set-up

There are four items required to form a corrosion cell: an anode, cathode, electrolyte, and an ionic path. Corrosion was accelerated by connecting the positive terminal of a Direct Current (DC) power source to the reinforcing steel bar thereby forcing it to become the anode. The negative terminal was connected to the stainless-steel rod forcing it to become the cathode. The ionic path flows through the power supply and the connecting wires, with the current impressed moving from the reinforcing steel bar to the stainless-steel rod. A reservoir pond was placed on the top surface of the concrete and was filled with 5% NaCl solution and the stainless-steel rod (cathode) was placed inside the salt solution pond. The salt solution supplied the chlorides which were required to accelerate steel depassivation as well as functioned as an electrolyte completing the corrosion cell.

A DC power supply unit with a capacity of 0 to 30 *Volts* and 0 to 3 *A* was used to impress the anodic current. The power supply unit was set to supply a maximum DC of 0.4 *A* for all the specimens. The arrangement of the accelerated corrosion cell is shown in Figure 3.6.

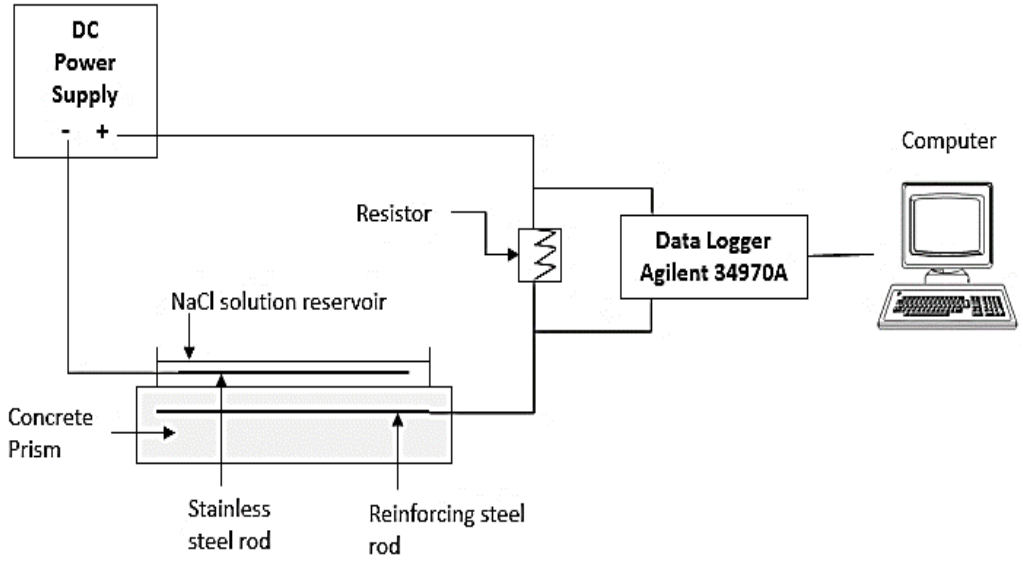

Figure 3.6: Schematic diagram of the accelerated corrosion cell set-up

Figure 3.6 shows a schematic diagram of the accelerated corrosion set-up. Each concrete beam specimen was connected to its own power supply unit. Insulated copper wires were used to connect the positive terminal of the power supply unit to the reinforcing steel, and to connect the negative terminal to the counter electrode (stainless steel rod). A resistor of known resistance was connected in series to the concrete prism. The Agilent 34970A data logger was connected to the circuit to record the voltage across the resistor. The data log was connecting to a computer with Agilent 34970A software and was set to record voltage readings every five seconds. The current flowing through the resistor was determined by dividing the voltage across the resistor (from data logger) with the resistance of the resistor. The salt solution was poured into reservoir before switching on the power supply. For the duration of the experiments, the corrosion tanks were monitored on a regular basis, checking on the progress of corrosion activity and replenishing the salt solution when necessary. As the corrosion process progresses, corrosion products protrude to the surface of the concrete changing the colour of the salt solution from clear to rusty brown. The accelerated corrosion cell set-up is shown in Appendix C.

3.9.2. Gravimetric mass loss measurement

The gravimetric test method was used to determine the actual mass loss of the reinforcing steel bar at the end of the accelerated corrosion test. The corrosion process was terminated when the first visible surface crack was observed as shown in Figure 3.7.

Figure 3.7: Photograph showing crack on surface of concrete

Figure 3.7 shows the longitudinal cracks that formed on the surface of the concrete. After the corrosion process, the steel bars were retrieved, by crushing the concrete specimen, and cleaned using mechanical procedures according to ASTM G 1-90 (1999) cleaning procedures. Figure 3.9 shows the rebar in the concrete during the retrieval process. As seen in Figure 3.8 the corrosion products are concentrated on the concrete cover, between the rebar and the salt solution reservoir. However, the rebar was corroded uniformly along its surface.

Figure 3.8: Photograph showing corrosion products within the concrete cover depth

After retrieval from the concrete, the steel bars were cleaned mechanically by lightly brushing with a wire brush and thoroughly rinsing with tap water.

The gravimetric test was conducted in accordance with the American Society for Testing and Materials (ASTM G1-90, 1999) as shown in Equation 3.2:

$$m_{actual} = M_i - M_f \quad (3.2)$$

where M_i is the initial mass in grams and M_f is the final mass loss in grams.

3.10. Number of specimens

The concrete specimens were cast in three separate batches according to the binder type used starting with 50/50 PC/SL followed by 70/30 PC/FA, and lastly 100% PC.

There are three unique series for each binder type. For each series, 3 specimens were cast resulting in a total number of 27 specimens. Due to the large number of specimens and limited resources, the study was split into three sets, Set 1, Set 2 and Set 3. Set 1 was conducted on the 50/50 PC/SL, Set 2 was conducted on the 70/30 PC/FA and Set 3 was conducted on the 100% PC blend.
Due to the number of variables investigated, the binder type, cover depth and corrosion degree for each specimen were named according to the convention shown in Table 3.13:

Table 3.13: Nomenclature for the different specimen

Binder Type	Cover Depth (mm)	Series Label
100% PC	20	PC -20
	35	PC - 35
	50	PC - 50
50/50 PC/SL	20	SL - 20
	35	SL - 35
	50	SL - 50
70/30 PC/FA	20	FA - 20
	35	FA - 35
	50	FA - 50

3.11. Other tests

In addition to the accelerated corrosion tests, other tests such as concrete durability, compressive strength and resistivity tests were conducted on the different concrete specimens. The additional test procedures are discussed below.

3.11.1. Durability Index tests

Researchers in South Africa have developed an approach to improving the durability of reinforced concrete. The South African Durability Index approach has adopted the strategy of providing 'deemed to satisfy' rules, which limit durability index values, cover depths and selected binder types with test methods that have been shown to be sensitive to material, constructional and environmental factors that influence durability (Gouws, Alexander & Maritz 2001). This approach is based on the philosophy that durability will be improved only when measurements of appropriate concrete cover properties can be made. The approach links the durability index parameters, service life prediction models, and performance specifications with concrete quality.

Durability index parameters are characterised in-situ by conducting durability index tests for oxygen permeation, water absorption and chloride conductivity on laboratory specimens. The tests provide reproducible engineering measures of the microstructure of the concrete as well as characterise the quality of concrete in relation to the choice of material mix proportions, compaction and curing and environment. The discussion which follows focuses on the basic principles of the South African durability index test procedures conducted in this research (Alexander, Mackechnie & Ballim 1999).

a) Oxygen permeability index test

In this study the Oxygen Permeability Index (OPI) test was conducted according to SANS 3001-C03-2 (2015) test standards. The OPI test method measures the pressure decay of oxygen passed through a 30 mm thick, 70 mm +/- 2mm diameter disc, placed in a falling head permeameter. Figure 3.8 shows the permeability cell arrangement used for measuring the pressure decay.

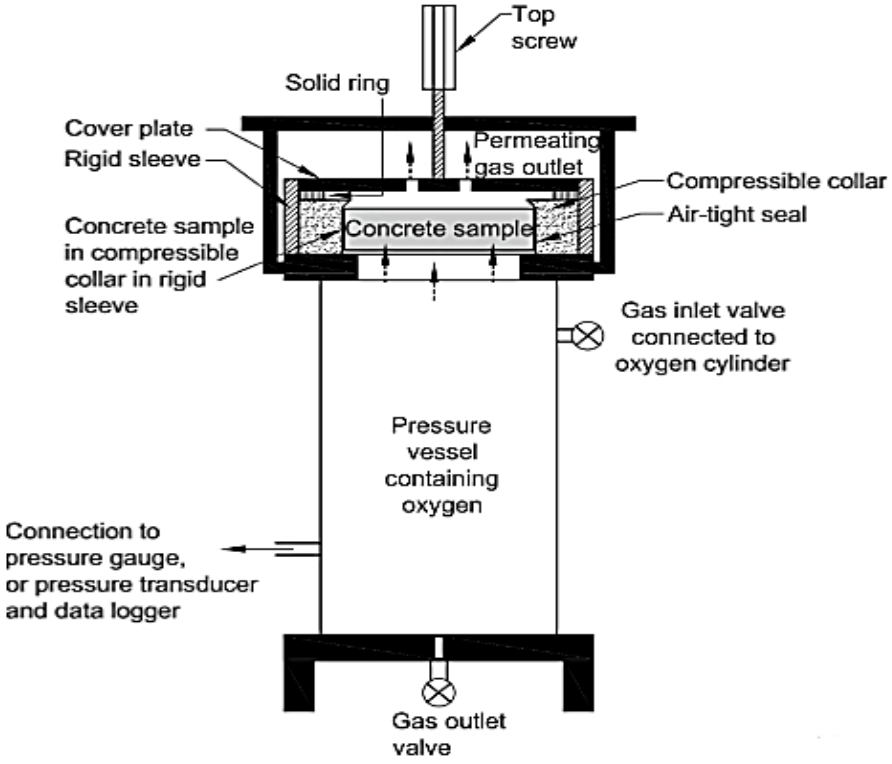

Figure 3.9: Permeability cell arrangement used for measuring pressure decay *(SANS 3001-C03-2, 2015)*

The oxygen permeability coefficient is calculated from the D'arcy coefficient of permeability as shown in Equation 3.3 (Alexander, 2017):

$$k = \frac{\omega \cdot V \cdot g \cdot d}{R \cdot A \cdot T} \times \frac{\Sigma\left[ln\left(\frac{P_0}{P_t}\right)\right]^2}{\Sigma\left[ln\left(\frac{P_0}{P_t}\right)t\right]} \quad (3.3)$$

where: k = coefficient of permeability of the test specimen (in m/s);

ω = molecular of oxygen (0.032 kg/mol);

V = volume of the permeability cell which includes the volume of the opening in the top plate and the rubber annulus below the sample. The volume is recorded to the nearest 0.01 litre and shall be determined by determined by dimensional measurement, accurate to the nearest mm, or by the volume of water contained at 23 $\pm$ 2 ℃;

g = the gravitational acceleration (9.81 m/s^2);

d = the average specimen thickness to the nearest 0.02 mm (in m);

t = the time since the start of the test, recorded to the nearest minute (in $seconds$);

P_0 = the pressure reading at start of test (i.e. time t_0) to the nearest 0.5 KPa

P_t = the pressure reading at time t, measured from t_0, to the nearest 0.5 KPa

R = the universal gas constant (8.313 Nm/KPa);

A = the cross-sectional area of the specimen (in m^2);

T = the absolute temperature (K);

The oxygen permeability index (OPI) of the test specimen is determined as the negative log value of the coefficient of permeability as shown in Equation 3.4:

$$OPI = -log_{10}(k) \quad (3.4)$$

The OPI of the concrete is given as the geometric mean of the OPI values of four specimens, or at least three specimens. Typical OPI values from South African concretes range from 8.5 to 10.5. The higher the value, the higher the impermeability and the higher the quality of the concrete. The OPI test assesses the overall micro- and macrostructure of the outer surface of cast concrete and is sensitive to macro-voids and cracks which act as short circuits for the permeating gas (Alexander, Mackechnie & Ballim 1999). As the OPI assess the microstructure of concrete, the influence of different binder types on the microstructure of various concrete can also be compared. Oxygen is also an important parameter in the study of reinforcement corrosion as it is required at the steel level for the corrosion process to occur. Thus, an understanding of the movement of oxygen through the concrete cover is invaluable knowledge for any meaningful estimation of the concrete's susceptibility to reinforcement corrosion.

b) Chloride conductivity index test

Under natural conditions, diffusion is a slow process, even when using high concentration gradients. Diffusion tests may take months or even years to yield useful results. Hence, in order to obtain results rapidly in the laboratory, accelerated diffusion tests using an applied potential difference have been

developed to measure the coefficient of diffusion. In this study the CCI test will be conducted according to SANS 3001-C03-3 (2015) test standards.

The South African Chloride Conductivity Index (CCI) test apparatus consists of a two-cell conduction rig in which concrete disc samples are exposed on either side to a 5M NaCl chloride solution as shown in Figure 3.10:

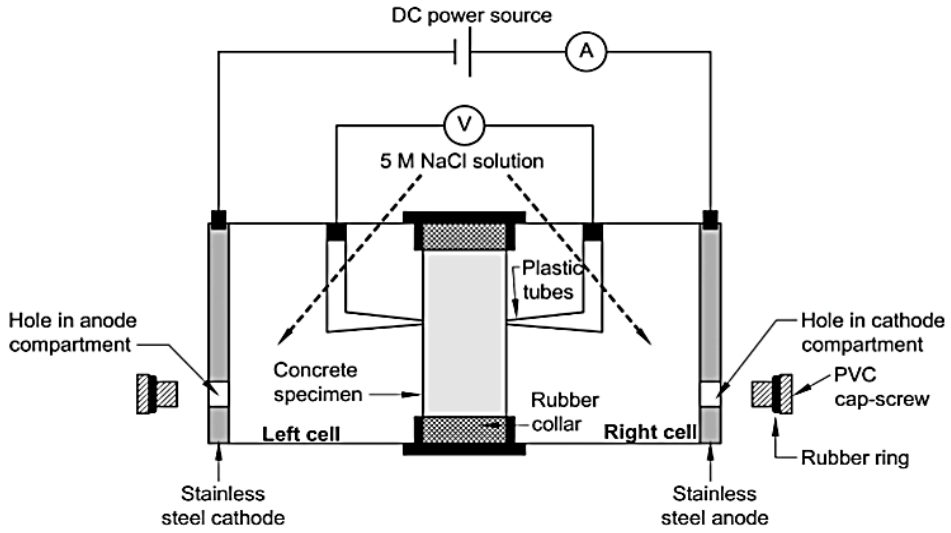

Figure 3.10: Longitudinal section of simple cell arrangement *(SANS 3001-C03-3, 2015)*

A 10 V potential difference was applied across the sample disc to facilitate the movement of chloride ions. The chloride conductivity was determined by measuring the current flowing through the concrete specimen using the Equation 3.5:

$$\sigma = \frac{id}{VA} \tag{3.5}$$

where: σ = chloride conductivity of the specimen (mS/cm);

i = the electric current (mA);

d = the average thickness of the specimen (cm);

V = the voltage different (V);

A = cross-sectional area of the specimen (cm^2)

The chloride conductivity index was determined as the average of four test specimens. The chloride solution porosity was determined using Equation 3.6:

$$n = \frac{(M_s - M_d)}{Ad\rho_s} \times 100 \qquad (3.6)$$

where: n = the porosity as a fraction of the volume of the specimen that is occupied with the solution (%);

M_s = the vacuum saturated mass of the specimen determined to the nearest 0.01 g;

M_d = the mass if the dry specimen determined to the nearest 0.01 g;

A = cross-sectional area of the specimen determined to the nearest 0.02 mm^2;

d = the average thickness of the specimen determined to the nearest 0.02 mm;

ρ_s = the density of the salt solution i.e. 1.19 x 10^{-3} g/mm^3

Experimental results have shown that the porosity determined from the chloride conductivity test is normally lower than that determined by the sorptivity test.

c) Water sorptivity index test

The Water Sorptivity Index (WSI) test is used to determine the water-penetrable porosity of the specimen which is then used to interpret the water sorptivity value. The test may be performed using two set ups; (a) 10 layers of paper towel or (b) roller/pin supports. For this research the former test set-up was employed and the tests were performed on specimens that had been previously tested in the oxygen permeability cells. The test was performed by sealing the curved edges of the test specimen with packaging tape to create a water tight seal but without blocking the test face of the specimen and to ensure uni-directional absorption, under the action of capillary rise, from the test face which was exposed to a few millimetres of solution (Kelham, 1988). A solution of calcium hydroxide (5 grams of $CaOH_2$ per 1 litre of water) was poured into a tray with 10 sheets of paper towels such that the final solution level was a maximum on 2 mm above the edge of the specimen

when the test face of the specimen was placed on top the paper sheets as shown in Figure 3.11:

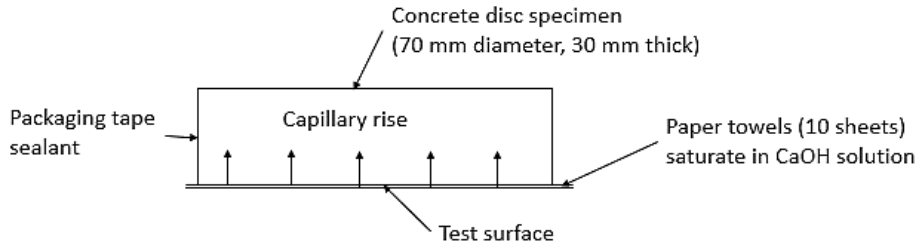

Figure 3.11: Schematic diagram of WSI test. ***(Alexander, 2017)***

The sealed specimens were weighed (M_{s0}) at time t_0 and subsequently at intervals of 3, 5, 7, 9, 12, 20 and 25 minutes after exposure of the test face to the solution and were patted with tissue to appear surface dry before weighing. After weighing the specimen were placed in a -80 kPa vacuum for approximately 3 hours and afterwards vacuum saturated with calcium hydroxide for approximately 18 hours. The porosity (n) of each specimen was determined, as a percentage, by using the Equation 3.7:

$$n = \frac{M_{sv} - M_{s0}}{Ad\rho_w} \times 100 \qquad (3.7)$$

where:

M_{sv} = the vacuum saturated mass of the specimen to the nearest 0.01 g;

M_{s0} = the mass of the specimen at time t_0 (start of the test) to the nearest 0.01 g;

A = cross-sectional area of the specimen determined to the nearest 0.02 mm^2;

d = the average thickness of the specimen determined to the nearest 0.02 mm;

ρ_w = the density of water i.e. 10-3 g/mm^3

The water sorptivity of the specimen(S), in $mm/\sqrt{h}$ is may be determined by Equation 3.8:

$$S = \frac{Fd}{M_{sv} - M_{s0}} \qquad (3.8)$$

where F = the slope of the best fit line, determined by linear regression analysis, from plotting the mass gain against square root of hour, in $g/\sqrt{h}$ and d, M_{sv} and M_{s0} are as described in Equation 3.8.

The measured values for water sorptivity (WS) and porosity are inter-related, a low WS value may be due to a high porosity value and vice versa thus care should be taken when interpreting and reporting and the values. Water sorptivity cannot be viewed in isolation of porosity as ideally both low WS and porosity are indicative of a potentially durable concrete.

Detailed literature on the Durability Index tests in terms of sample preparation and equations used is provided in the Durability Index Testing Procedure Manual (Alexander, 2017). A standard spreadsheet has been developed to perform the calculations described in the procedure manual and was used to determine the OPI, WSI and CCI for the test specimens. The spreadsheet is available for free download from Concrete Institute website.

3.11.2. Compressive strength

The compressive strength of concrete was determined by conducting the cube (100 x 100 x 100 mm) crushing test in accordance with SANS 5860 (2006). The strength of hardened concrete was used as an index of the concrete quality (Perrie, 2009) and confirmation of concrete mix. The concrete cubes were tested for compressive strengths after 7, 14 and 56 days of curing. The compressive strength of each specimen was calculated in accordance to (SANS 5863, 2006), using Equation 3.9:

$$f_{cc} = \frac{F}{A_C} \qquad (3.9)$$

where f_{cc} is the compressive strength in megapascals, F is the maximum load at failure in newtons and A_C is the cross-sectional area (in mm) of the specimen on which the compressive force asts.

3.11.3. Bulk Electrical Resistivity

Bulk electrical resistivity was determined by measuring the current passing through all the phases of the concrete specimen i.e. the cement paste, fine and coarse aggregate. The test was performed on 56 day 100 x 100 x 100 mm cubic specimens at saturated surface dry (SSD) conditions. The test was performed in a humidity controlled room with tempertaure $\pm$ 21℃.

The test was perfomed by placing two eletrodes (two parallel stainless steel plates, 100 mm x 100 mm) with moist sponge in between, on opposite sides of the concrete specimen.

The sponge was saturated with water to ensure electrode contact between the specimen and the metal plates. The test is non-destructive and only took a few minutes. The bulk resistivity was measured using the 2-Plate method.

In this technique the Resipod four-point probe device with probe spacing of 50 mm was used to meausure the bulk resistivity of the concrete specimen. The four-point probe device is intended to measure surface electrical resistivity but can be reconfigured to measure bulk electrical resistivity. For surface resistivity measurements the two outer probes apply an AC current to the concrete surface while electrical potential is measured from the two inner probes as shown in Figure 3.12.

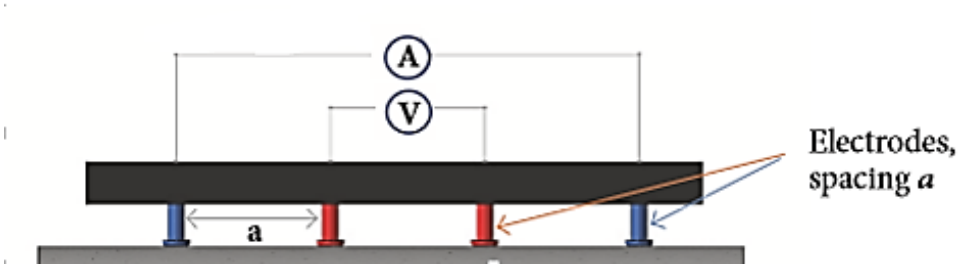

Figure 3.12: 4 Point surface resistivity measurement device configuration.

For bulk electrical resistivity measurements the instrument was reconfigured by connecting the first two probes that generate the current and measure the potential to one of the stainless steel electrode plates and likewise for the other two probes. Figures 3.13 and 3.14 show the 2-plate method configuration.

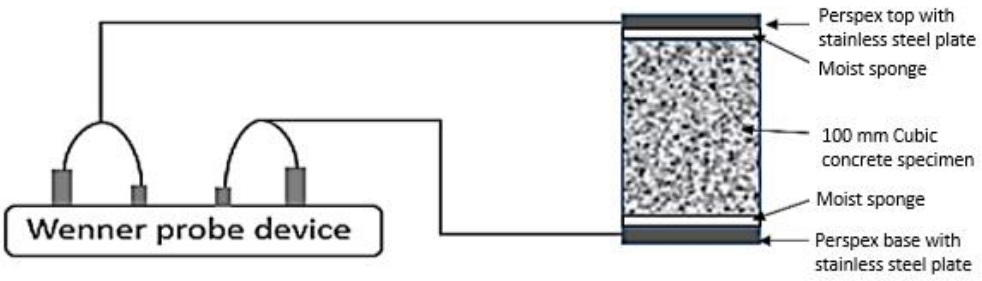

Figure 3.13: Schematic diagram of 2-plate resistivity measurement device set-up.

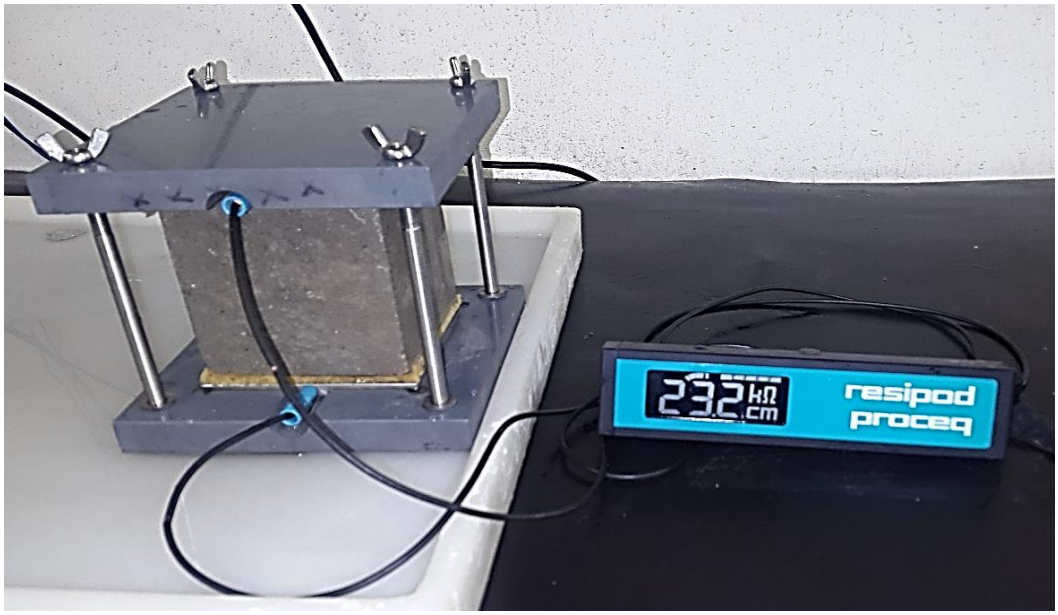

Figure 3.14: Photograph showing 2-plate resistivity measurement set-up

The Resipod Wenner probe device calculates the surface resistivity using Equation 3.11:

$$\rho = 2\pi a \cdot R \tag{3.11}$$

where ρ is resistivity of the system in $k\Omega cm$ and a is the probe spacing. Thus the resistance of the concrete is simply the resitsitivity reading from the Wenner probe device divided by $2\pi a$.

Accelerated corrosion is based on the principles of electric current flow which are dependent on the electrical conductivity of the system. Electrical conductivity is the inverse of electrical resistivity. The electrical resistivity of the concrete cannot be measured directly but can however be inferred based on the electrical resistivity measurements. Thus electrical resistivity measurements provide a holistic assessment of the concretes susceptibility to corrosion especially due to electrical current flow. Eletrical resistivity is also an inherent property of concrete thus concretes made from different binder types will have diffetrent electrical resistivity values. The chapter that follows will present the analysis of the results obtained from the experiments discussed in this chapter.

3.12 References

ACI 211.1-91, 1999. *Standard practice for selecting proportions for normal, heavyweight, and mass concrete,* Farmington Hills, Michigan: America: American concrte institue .

Addis, B. & Goodman, J., 2009. Concrete mix design. In: G. Owens, ed. *Fulton's concrete technology.* ninth ed. Midrand(Gauteng): Cement and Concrete Institue, pp. 219-228.

Alexander, M. G., 2017. *Durabiliity Index Testing Procedure Manual ,* cape Town: University of Cape Town.

Andrade, C. & Alonso, C., 2001. On-site measurements of corrosion rate of reinforcements. *Construction & Building Materials,* 15(2-3), pp. 141-145.

ASTM G 1-90, 1999. *Standard practice for preparing, cleaning and evaluating corrosion test specimens,* West Conshohocken: American Society for Testing Materials.

Gouws, S., Alexander, M. & Maritz, G., 2001. Use of durability index tests for the assessment and control of concrete quality on site. *Concrete Beton,* Issue 98, pp. 5-16.

Grieve, G., 2009. Aggregates for Concrete. In: G. Owens, ed. *Technology, Fulton's Concrete.* Pretoria: Concrete and Cement Institue, pp. 25-55.

Heiyantuduwa, R., 2008. *Service life modeling using the durability index approach,* Cape Town: Principles of Chemical Engineering Processes.

Kelham, S., 1988. S.A water absorption test for concrete. *Magazine of Concrete Research,* 40(143), pp. 106-110.

Kellerman, J., 2009. Manufacturing and handling of concrete. In: G. Owens, ed. *Fulton's Concrete Technology* . Pretoria: Concrete and Cement Institute, pp. 229-250.

Kellerman, J. & Crosswell, S., 2009. Properties of fresh concrete. In: G. Owens, ed. *Fulton's concrete technology.* 9th Edition ed. Pretoria(Gauteng): Cement and Concrete Institute, pp. 83-95.

Kosmatka, S. & Panarese, 1988. *Design and control of concrete mixes,* USA: Stokie.

Middel, C., 2009. Formwork. In: G. Owens, ed. *Fulton's Concrete Teechnology.* Pretori: Concrete and Cement Institute, pp. 251-284.

SANS 10100-2, 1992. *Code of practice for the structural use of concrete. Part 2: Materials and execution of work,* Pretoria: The South African Bureau of standards.

SANS 10100-2, 1992. *The structural use of concrete. Part 2: Materials and execution of work,* Pretoria: The South African Bureau of standards.

SANS 1491-1, 2005. *Portland cement extenders Part 1: Ground Granulated Blastfurnace Slag ,* Pretoria: South African Bureau of Standards.

SANS 1491-2, 2005. *Portland cement extenders. Part 2: Fly Ash,* Pretoria: South African Bureau of Standards.

SANS 201, 2008. *Sieve analysis, fines content and dust content of aggregates,* Pretoria, 1994: South African Bureau of Standards.

SANS 5860, 2006. *Concrete tests - dimensions, tolerances and uses of cast test specimens,* Pretoria: South African Bureau of Standards.

SANS 5863, 2006. *Concrete tests - compressive strength of hardened concrete ,* Pretoria: South African Bureau of Standards.

SANS 920, 2011. *Steel bars for concrete reinforcement,* Pretoria: South African Bureau of Standards.

SANS, 2000. *SANS-10100-1: The Structural Use of Concrete,* Pretoria: South African Bureau of Standards.

SANS, 2006. *Preperation of test samples of aggregates* , Pretoria: South African Bureau of Standards.

CHAPTER 4: RESULTS AND DISCUSSION

4.1. Introduction

This chapter presents the analysis and discussion of the results obtained in the various tests performed in the experimental testing phase of this research. These include concrete compressive strength, concrete durability, bulk electrical resistivity and accelerated corrosion tests. The visual assessments of the accelerated corrosion tests are also presented.

4.2. Determining outliers in the data set

All experimental tests were conducted on triplicate samples for each binder type, except for durability index tests which were conducted on quadruplicate samples. It is expected that triplicate and quadruplicates results for each test would yield similar results, however there is a possibility that outliers may be present in the data set. Outliers are observation points that are inexplicable or significantly distant from the other observations of the same data set. In this study, the Grubbs test method was chosen as a suitable method for determining outliers. Grubbs test is based on the difference of the mean of the sample and the most extreme data considering the standard deviation (Grubbs, 1950). The test is suitable for small sample sizes, such as in the present study where n = 3 or n = 4. Equation 4.1 is used to define the Grubbs test statistic:

$$G_{exp} = \frac{|\bar{x} - questinable\ value|}{s} \quad (4.1)$$

where $\bar{x}$ is the sample mean and s is the sample standard deviation. The Grubb's test is defined for the hypothesis:

H_0: There are no outliers in the data set
H_a: There is exactly one outlier in the data set

The hypothesis is tested by comparing values of G_{exp} with $G_{critical}$, which is based on the sample size and level of significance. The value for $G_{critical}$ for a

specific level of significance can be selected from Grubb's critical value table (see Appendix A). The null hypothesis is rejected when $G_{exp} \geq G_{critical}$.

The inclusion of outliers in the analysis of results leads to a misleading interpretation of the results therefore all observations that were identified as outliers were not considered in the analysis of the results.

4.3. Concrete compressive strength tests

Concrete compressive strength tests were conducted on the three binder types under investigation at 7, 14 and 56 days of concrete age. The compressive strength development graph of the different binder types is shown in Figure 4.1.

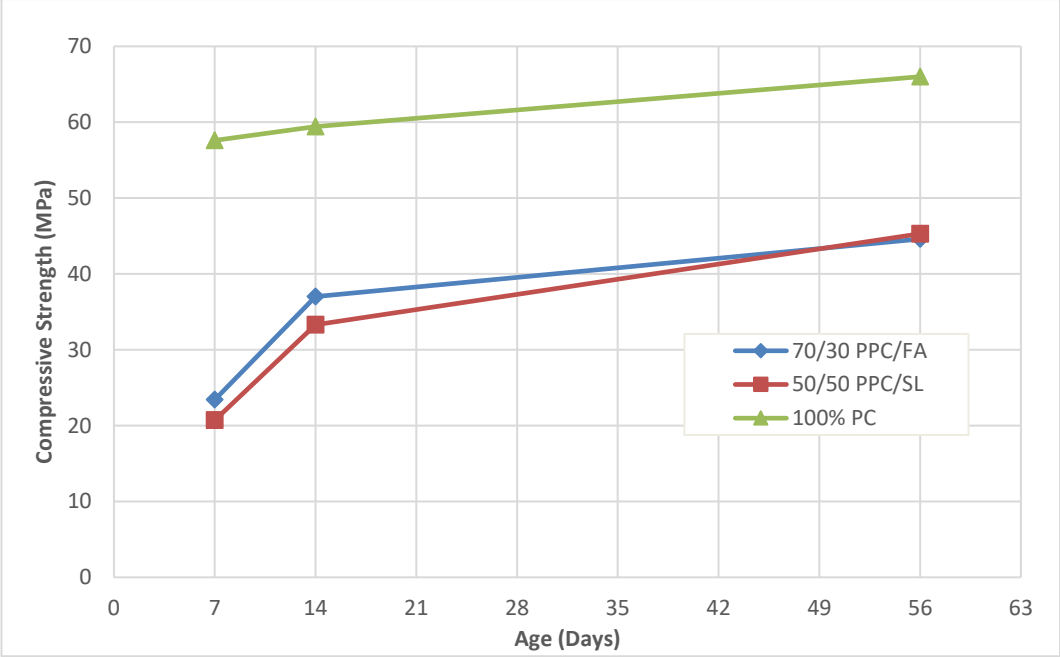

Figure 4.1: Compressive strength development curve for the different binder types

The results show that the highest strength development curve was for the 100% PC concrete, followed by a relatively similar compressive strength development curve for the fly ash and slag blended binders. The 56-day compressive strength is approximately 65 MPa for the plain Portland cement whereas the 56-day compressive strength for both the fly ash and slag blends is approximately 45 MPa. The difference in compressive strength development between the plain

Portland cement concrete and blended cement concrete may be attributed to the slow early age strength development of both blended cement concretes.

The strength of hardened cement paste is attributed to the formation of $C_3S_2H_3$, Calcium Silicate Hydrate (C-S-H), which is in the form of very fine needles and plates (Grieve, 2009). The differences in compressive strength development is due to the difference in the formation of the C-S-H compound. The C-S-H compound for plain Portland cement is formed through the hydration reaction of C_3S/C_2S (tricalcium silicate/dicalcium silicate) whilst the C-S-H compound for the slag blended cement is formed through the hydration reaction of calcium oxide and silica. Fly ash is a latent hydraulic binder i.e. it is not hydraulic but reacts with silica and calcium hydroxide (produced from the hydration of Portland cement) to form C-S-H (Grieve, 2009).

Similar results of higher 56-day compressive strength for 100% plain Portland cement when compared to 50/50 PC/SL cement blend were obtained by Samad, et al. (2017). The researchers reported a compressive strength of 79 MPa and 74 MPa for the 100% PC and 50/50 PC/SL blend respectively, for a w/b ratio of 0.35. A report published by the Portland Cement Association (Thomas, 2007) comparing the compressive strength development of plain Portland cement and fly ash blended cement showed a compressive strength of approximately 55 MPa for both binder types, however at 90 days the compressive strength was higher for the fly ash blended cement concrete. The compressive strength tests were used as a performance measure of the concrete. The target compressive strength for the three different concrete mixes was 25 MPa at 28 days concrete age. If the target compressive strength was not achieved than the concrete mix design would have been modified and a new batch of concrete cast. In addition to the concrete compressive strength test, the Durability Index (DI) tests were also conducted to characterise the quality of the concrete. The results from the DI tests are presented below.

4.4. Durability Index tests

This section presents a summary of the results obtained from the Durability Index test of companion cubes from each binder type, tested at 56 days of concrete age. The DI tests measure the quality of the concrete as a function of its resistance to the ingress of deleterious substances such as moisture, chlorides and oxygen.

4.4.1. Oxygen Permeability Index

The Oxygen Permeability Index test measures the ingress of oxygen through a concrete sample and is presented as the negative log of the coefficient of oxygen permeability *($-log_{10}$ k (m/s)).* A highly porous concrete with a greater pore connectivity will therefore have a high coefficient of permeability and a low OPI value. Oxygen is required at the steel level for corrosion to occur, thus high OPI values would increase the concrete's resistance to the ingress of oxygen and thus limit the rate of the corrosion. The results of the 56 day OPI test for the different binder types are graphically presented in Figure 4.2.

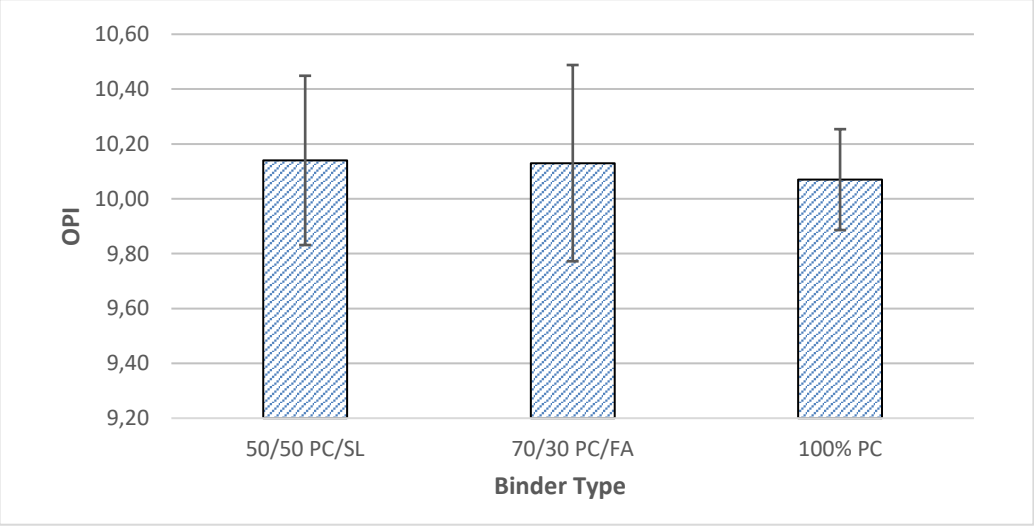

Figure 4.2: 56-Day OPI results for the different binder types

The standard deviation error bars at 95% confidence interval (CI) indicate a measure of scatter of the data. The fly ash blended binder had the highest scatter and therefore the highest standard deviation. An OPI value higher than 10 is considered to provide excellent durability in severe exposure conditions where

concrete is exposed to chlorides such as cyclic wetting and drying in tidal zones (alexander et al., 1999). The three different binders had an average OPI values greater than 10 and can thus be considered to offer excellent durability.

Based on the results shown in Figure 4.2 the OPI of the different binder types can be graded based on the ingress of oxygen into concrete as PC/SL ≈ PC/FA > PC. The results are as expected and depicted in literature as the inclusion of cement extenders in concrete increases the OPI value. This is because fly ash and slag alter the microstructure of the bulk cement paste and the interfacial transition zone (ITZ) between the aggregates and hardened cement paste (HCP). The ITZ is usually more porous than the HCP and the increase in permeability in concrete is attributed to the presence of micro-cracking of the cement paste in the ITZ, due to fewer hydration products such as CSH (Mehta and Monteiro, 1993).

The benefit of adding slag as a cement extender is achieved in the increased thickness of the ITZ due to the nucleation of numerous small and randomly orientated CH crystals on the slag particles (Nilsen et al., 1992). There is also a relative reduction in the concentration of CH crystals compared to plain Portland cement, indicating an increase in CSH which results in reduced permeability. Research by Berry et al. (1989) has shown that the inclusion of FA, similarly to slag, results in a less permeable material as it tends to block the pore structure and increases the discontinuity of the pore structure.

4.4.2. Chloride Conductivity Index

The chloride conductivity describes the concretes predisposition to the ingress of chlorides. The results from the Chloride Conductivity Index (CCI) test are graphically presented in Figure 4.3. The 95% CI standard deviation error bars on the graph in Figure 4.3 indicate a measure of scatter of the results with the higher scatter observed for the fly ash blended cement. It is expected that the lower the chloride conductivity, the more resistant the binder is to chloride ingress. According to work done by Alexander et al. (1999), CCI values less than 0.75 mS/cm indicate excellent durability quality; values between 0.75 and 1.5

mS/cm indicate good durability quality; and values between 1.5 and 2.5 mS/cm indicate poor durability quality, relative to severe exposure environment to chlorides.

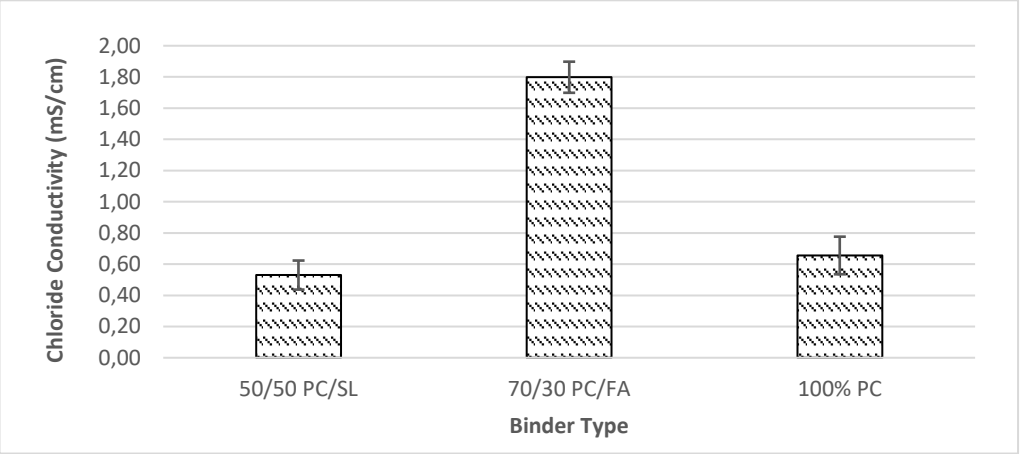

Figure 4.3: 56-Day CCI results for the different binder types

A grading of the results based on concrete quality (increasing with reducing CCI value) is as follows; SL>PC>FA. The results are not as expected as the blended concrete is expected to have a lower CCI value than the plain Portland cement concrete (Alexander et al.,1999). Results from work done by Scott (2004) showed an improvement in CCI values with the inclusion of FA and SL when compared to plain Portland cement.

Scott (2004) reported average CCI values of 0.5; 0.55 and 0.9 mS/cm for the slag, fly ash, and plain Portland cement blends respectively, at 56 day concrete age and a w/b ratio of 0.58. In this study the average 56 day CCI values, at a w/b ratio of 0.55, are 0.53; 1.80 and 0.66 mS/cm for the slag, fly ash, and plain Portland cement blends respectively. The results presented by Scott (2004) for SL and PC concrete are similar to the ones achieved in the present study, however the results for the fly ash concrete in the present study are not as expected based on what has been reported in literature.

The addition of FA is expected to reduce the ingress of chlorides through the chemical binding of chloride due to the high aluminate content of FA, which is approximately three to five times higher than in PC (Ash Resources, 2011).

Previous studies have shown that the pozzolanic reaction of FA is effective around 90 days and beyond, such that the mechanical and durability properties of FA concrete show considerable improvement (Bouzoubaâ, et al. (2001); Atis (2005); Liu, et al. (2014)). Thus, it is believed that the 56-day chloride conductivity value of the FA concrete in the present study is only an indication as FA concrete still had the potential to improve its chloride binding capacity, given more time for the pozzolanic reaction to come into full effect.

4.4.3. Water Sorptivity Index (WSI)

Sorptivity is defined as the rate of movement of a wetting front through a porous material. The water sorptivity test involves the uni-directional absorption of water into one face of a concrete disc sample with a lower sorptivity indicating a higher resistance to moisture penetration (Ballim, 1993). Thus, sorptivity provides information on the general pore structure of the concrete. The results from the water sorptivity index test are presented in Figure 4.4.

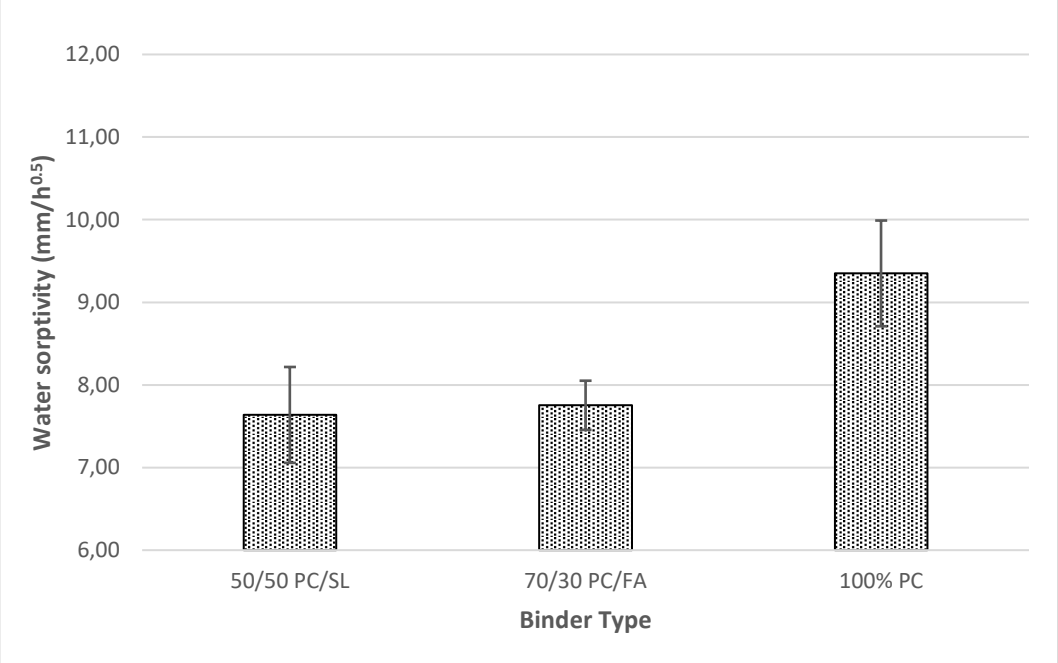

Figure 4.4: 56-Day water sorptivity results for the different binder types

The 95% Confidence Index standard deviation error bars indicate that slag blended cement had the greatest scatter of sorptivity values.

According to work done by Alexander et al. (1999), WSI values between 6 and 10 $mm/h^{0.5}$ are considered to indicate good durability in severe exposure environments.

The results the sorptivity of the different binder types can be graded based on increasing resistance to moisture penetration into the concrete as SL > FA > PC. This trend of increasing resistance to moisture penetration with the addition of FA and SL is as expected and reported in literature by Scott (2004); Ballim (1993) and Alexander et al. (1999). The movement of water into concrete is associated with the pores in the concrete. Hardened cement paste contains two types of pores, capillaries and gel pores. Gel pores are inherent in concrete as they are a result of the hydration process and do not affect permeability. Whereas capillary pores are formed when there in as excess of mixing water (w/b > 0.36) and insufficient gel volume to occupy all the available space (Scott, 2004). Thus, the improvement in the sorptivty of the concrete with the inclusion of FA and SL can be attributed to a more refined pore structure characterized by an increase of fine gel pores and a reduction of connectivity of the capillary pores.

4.5. Concrete bulk electrical resistivity

The bulk electrical resistivity measures the current passing through all the phases of concrete i.e. cement paste and aggregates, thus it gives a good indication in one measurement. Surface electrical resistivity measurements on the other hand are more variable as they are affected by the near surface variations in temperature, moisture condition as well as nearby rebar and cover thickness (Polder, 2001).

The electrical resistivity of concrete hinders the ionic current flow between the anode and the cathode in the steel bar. In the present study, the bulk electrical concrete resistivity was measured using the two – plate method. The experimental set-up for this test was discussed in Chapter 3. Figure 4.5 shows the results obtained for the 56-day concrete resistivity values for the different binder types.

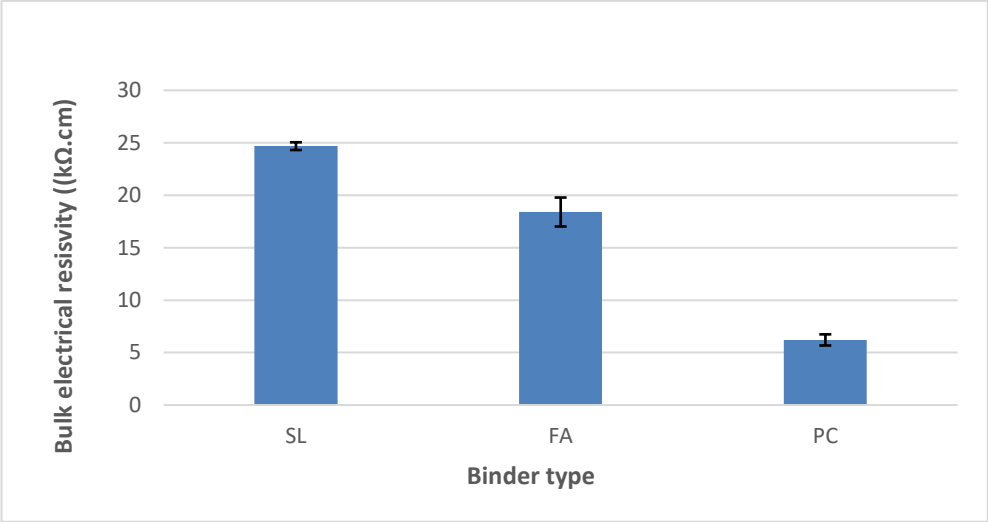

Figure 4.5: 56 - Day electrical resistivity measurements for different binder types.

The standard deviation error bars indicate the scatter of the results at 95% CI. The SL blended concrete had the highest resistivity followed by the FA blended and lastly the PC concrete. The trend of increasing resistivity values with the addition of SL and FA is expected and has been reported in literature by various researchers such as Polder and Peelen (2002); Scott (2004); Kessler, et al. (2008) and Bryant, et al. (2009).

The bulk electrical resistivity of concrete is affected by the resistivity of the fluid in the pores, the concretes degree of saturation and the volume and connectivity of the pore network (Spragg, et al., 2013). The electrical resistivity decreases with a higher pore volume and more open pore network. The pore size and connectivity is reduced by the hydration products in the cement matrix, which block the pores. Plain Portland cement, slag and fly ash blended concrete have different reactions due to the difference in the concrete forming reactants. PC and SL undergo hydration reactions whilst FA is a latent hydraulic binder that undergoes a pozzolanic reaction. Thus, blended cements have different potentials to fill the pores. Berodier and Scrivener (2015) conducted a study on the evolution of pore structure in blended cements and reported that slag is more reactive and contributes more strongly to porosity reduction whilst fly ash needs to react to a much larger extent before impacting the total pore volume.

Ultimately, slag and fly ash reactions lead to reduced solid volume than the reaction of plain Portland cement.

Based on the electrical resistivity for the different concrete blends obtained in this study and the factors that affect resisitivity, one can conclude that the pore size and connectvitiy increase in the order of PC > FA > SL.

4.6. Accelerated corrosion results

4.6.1. Visual observations

This section presents the visual observations of the concrete beams at the end of the accelerated corrosion experiments. Corrosion was terminated when the first visible surface crack on the beam was observed. The cracking of the concrete is due to the stresses from the expansive corrosion products, thus the experiment is terminated under the assumption of active corrosion rates due to the visible corrosion products and cracking of the concrete. The steel bars were extracted from the beams by crushing the concrete. Sample figures showing the post - corrosion conditions observed for the different beams are presented in Appendix C. In general, dark-green to black corrosion products exuding through the surface crack were observed. According to Vassie (1979) this green/black coloured corrosion product suggests that the corrosion product was a type of iron chloride complex formed as an intermediate stage of chloride-induced corrosion. Corrosion products originated from the steel/concrete interface, however they migrated through the concrete cover in the direction of the concrete surface exposed to the sodium chloride solution.

Upon retrieval of the bars a greenish black corrosion product with a reddish brown oxide on the periphery, around the aggregates was also observed. When the corrosion current was applied for a shorter duration as in the case of the plain Portland cement beams, no corrosion products were observed on the surface of the concrete and very little corrosion products were observed on the steel/concrete interface. This is because the plain Portland cement concrete is more porous than FA and SL blended concrete, thus the corrosion products of the PC concrete migrated into the pore solution of the concrete.

The morphology of the corrosion attack on the steel surface resembled general corrosion. For the slag blended concrete beams, the corrosion current was applied over a longer duration (average of 6 weeks for the SL beams) and pitting corrosion was observed on the surface of the bar. Pitting corrosion under the action of impressed current was also reported by Gonzalez, et al. (1995) when corrosion was continued for a longer duration (more than 1 month).

The average duration for impressed current to induce corrosion and surface cracking for the different binder types and cover depths is shown in Table 4.1. The time to corrosion cracking is influenced by the corrosion initiation and propagation period. The corrosion initiation period is associated with the concrete's resistance to the ingress of chloride ions. Corrosion propagation is associated with active corrosion rates which may lead to crack development and spalling of concrete cover.

Table 4.14: Average time to cracking for the different beams.

Cover depth (mm)	**Time to initial surface crack on beams (days)**		
	50/50 PC/SL	70/30 PC/FA	100% PC
20	38	11	5
35	26	10	5
50	72	40	11

The slag and fly ash blended concrete beams took longer to crack than the plain Portland cement concrete beams. This result was expected as various studies in literature have shown that plain Portland cement concrete is more susceptible to corrosion attack than blended concrete. The addition of cement extenders such as fly ash and slag has been shown to have an influence corrosion initiation period and an even greater influence on the corrosion propagation period (Scott, 2004; Mangat et al., 1995). This can be attributed to the denser and finer pore structure of the hardened concrete which is related to the concrete's resistivity. The resistivity is inversely proportional to the corrosion rate such that the higher resistivity results in lower corrosion rates which in turns increases the corrosion propagation period. In the present study resistivity increased in the order SL >

FA > PC. This was the same trend followed by the time to first surface development which increased in this order SL > FA > PC.

The beams with the larger cover depth also took longer to crack, this trend was as expected as it has been reported in literature (Mangat et al., 1994; Nieves-Mendoza, et al., 2012). This due to the increased distance for the migration of chloride ions from the salt solution reservoir to the steel surface in order to depassivate the steel and initiate corrosion. The combination of blended concrete and larger cover depth increases the corrosion initiation corrosion propagation period thus increasing the time to concrete cracking.

4.6.2. Gravimetric mass loss results

At the end of the accelerated corrosion test, the steel bars were retrieved, cleaned and weighed with the mass recorded to the nearest two decimal places. The average results from the gravimetric mass loss for the different beam series are presented in Figure 4.6.

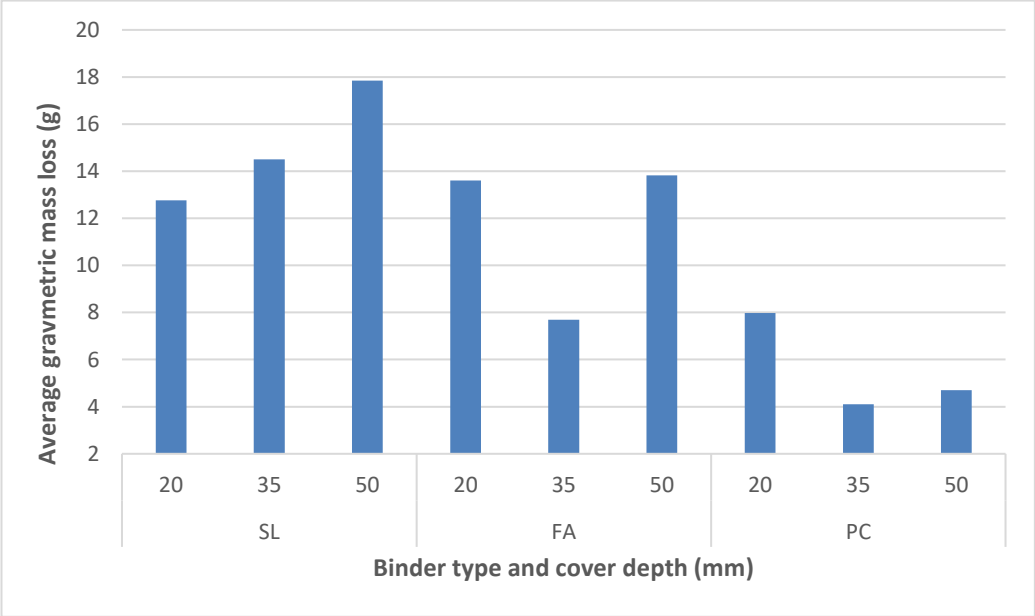

Figure 4.6: Average gravimetric mass loss at cracking for the different binder types and cover depths

The trend observed with gravimetric mass loss is an increase in mass loss with the addition of slag and fly ash cement extenders. With respect to binder type, the blended cement concrete beams were under the influence of impressed

current for longer periods, thus the higher mass loss values. There was no apparent trend observed for the different cover depths, this is because concrete cover influences the corrosion initiation period which results in negligible mass loss.

4.7. Descriptive analysis of accelerated corrosion results

This section presents the descriptive analysis of the results of the bar mass loss, corrosion rates and mass loss efficiency.

4.7.1. Calculation of corrosion current and Faraday's mass loss

Corrosion was accelerated by applying direct current on the steel bars inside the concrete beams. For the impressed current the technique the corrosion current is assumed to be equal to the applied current. The voltage across each beam was recorded at 5 second interval using a data logger. A resistor was connected to the system and the current was calculated using Ohm's Law as shown in Equation 4.2.

$$I_{corr} = I_{app} = \frac{V}{R} \tag{4.2}$$

where I_{corr} is the corrosion current (A); I_{app} is the applied current (A); V is the voltage (V) and R is the resistance (Ω). The voltage and time readings from the data logger were used to plot graphs of voltage versus time (V-T). The area under the V-T graphs was calculated using OriginLab v.18 statistical analysis software using the area integral method. Sample V-T curves are shown in Appendix C. The theoretical mass loss was calculated using Faraday's Law as shown in Equation 4.3:

$$M_{th} = \frac{M}{zF} . \frac{V.T}{R} \tag{4.3}$$

where M_{th} is the theoretical mass loss (g); M is the molar mass of iron (g/mol); z is the valency of iron (2); F is Faraday's constant (A.s); $V.T$ is the area under the V-T graph and R is the resistance (Ω).

4.7.2. Corrosion current density (i_{corr}) results

The corrosion rate in accelerated corrosion by impressing current is described by the corrosion current density, with values greater than 0.1 $\mu A/cm^2$ indicating active corrosion rates.

Values of corrosion current densities ranged from as little as 8 $\mu A/cm^2$ for the SL#2 – 35 mm beam to as high as 1328 $\mu A/cm^2$ for the PC#9 – 20 mm beam. Various corrosion current densities values have been used in literature, from as little as 3 $\mu A/cm^2$ (Alonso, et al., 1998) to as much as 17000 $\mu A/cm^2$ (Nossoni and Harichandran, 2012). The trend observed with cover depths and i_{corr} is a deacrease in i_{corr} with an increase in cover depth. This trend was as expected as increasing the cover depth reduces the corrosion rate as shown by Ing (2003), who reported that the applied electrical field aided the migration of chloride ions through the concrete cover. The i_{corr} is also influenced by also influenced by concrete electrical resistivity (Bentur, et al., 1997).The addition of fly ash and slag led to a decrease in corrosion rates due to the higher resistivity of the blended concrete in comparison with the PC concrete. The relationship between the average i_{corr} and concrete resistivity values for the different binder types and cover depths in the present study are shown in Figure 4.7.

In this graph, i_{corr} values that were identified as outliers using the Grubb's tests have not been plotted. There was an anomaly observed for the FA – 20 beams where two of the beams were connected in series and thus had the same i_{corr} value of 6.6 $\mu A/cm^2$. However, the third beam from this series had an i_{corr} vale of 1457 $\mu A/cm^2$. The decision was made to exclude the i_{corr} results of the FA – 20 beams from the analysis due to the conflicting results obtained. Furthermore, the three SL 20 beams were connected in series and thus had a less than expected corrosion current density of 23.9 $\mu A/cm^2$. This is because the three beams connected in series functioned as resistors in the circuit thereby increasing the overall resistivity and reducing the corrosion current density. Based on findings in literature the corrosion current density is expected to increase with reducing cover depth. Due to the anomaly in the i_{corr} results for the FA 20 and SL 20

beams the expected trend was not observed for the FA and SL blended cement concrete but observed for the PC concrete. However, when the FA 20 and SL 20 results are excluded from this analysis the trend of increasing i_{corr} with decreasing cover depth is observed for the 35 and 50 mm cover depths for the FA and SL blended cement concrete. As such the corrosion current density versus resistivity results for the 20 mm are not presented in Figure 4.7.

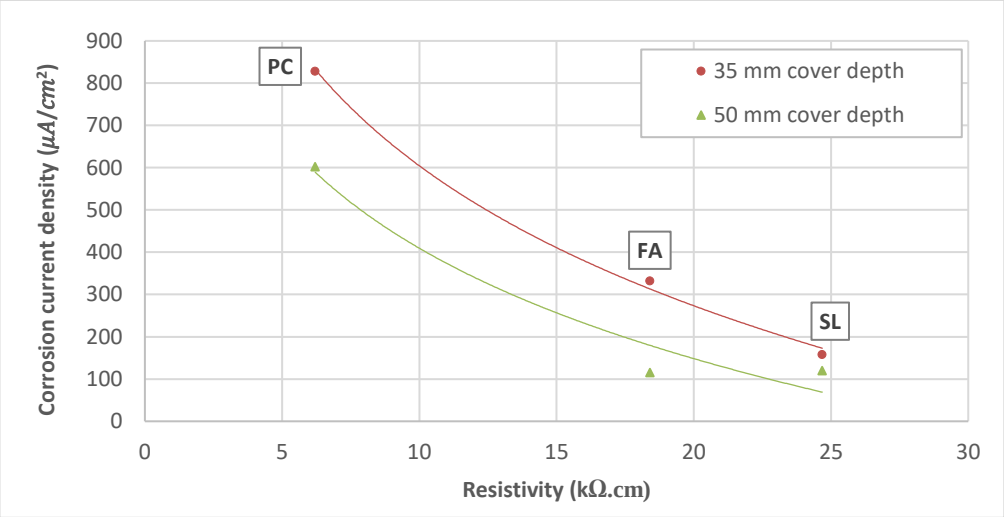

Figure 4.7: Relationship between average corrosion rates and concrete resistivity

4.8. Comparison between gravimetric and faradaic mass loss results

Figure 4.8 shows a scatter plot graph of the faradaic mass loss (theoretical mass loss) calculated using Faradays Law versus the measured mass loss (actual mass loss), determined by gravimetric measurement of the extracted bars for the different cover depths. Values identified as outliers by Grubb's test are not presented. The reference line of equality in Figure 4.8 represents the points on the graph where the Faradaic mass loss is equal to the gravimetric mass loss. All the data points for the plain Portland cement concrete are scattered below the line of equality. This indicates that the Faradaic mass loss for all the PC beams was greater than the gravimetric mass loss. Only a few of the data points for the slag and fly ash blended concrete are clustered above the line of equality whilst the rest of the data points are scattered below the line of equality. In general, the

mass loss results indicate an overestimation in theoretical mass loss for all the binder types. The factors causing the overestimation are discussed in detail in the following section.

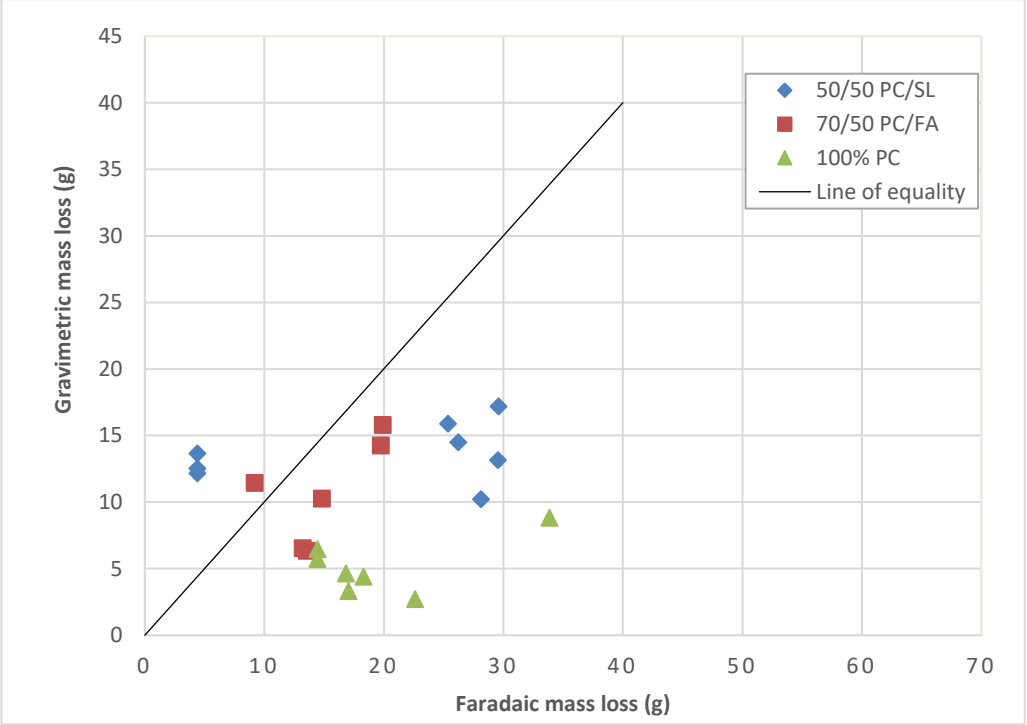

Figure 4.8: Gravimetric mass loss vs. Faradaic mass loss

4.8.1. Determination of efficiency of accelerated corrosion using impressed current

The results from the faradaic and gravimetric mass loss measurements were used to determine the efficiency of the impressed anodic current technique to induce corrosion. The efficiency was determined as the percentage ratio of faradaic (theoretical) mass loss to the gravimetric (measured) mass loss. Figure 4.9 shows the average mass loss efficiency values for the different binder types and cover depths. The standard deviation error bars indicate the scatter of the results at a 95% Confidence Interval. An efficiency value closer to 100% indicates good correlation between the measured (gravimetric) mass loss and faradaic (theoretical) mass loss measurements. The closer the efficiency value is to 100% than it can be said that the impressed anodic current technique is an efficient

technique to accelerate corrosion. An under-estimation is depicted by a mass loss efficiency below 100%.

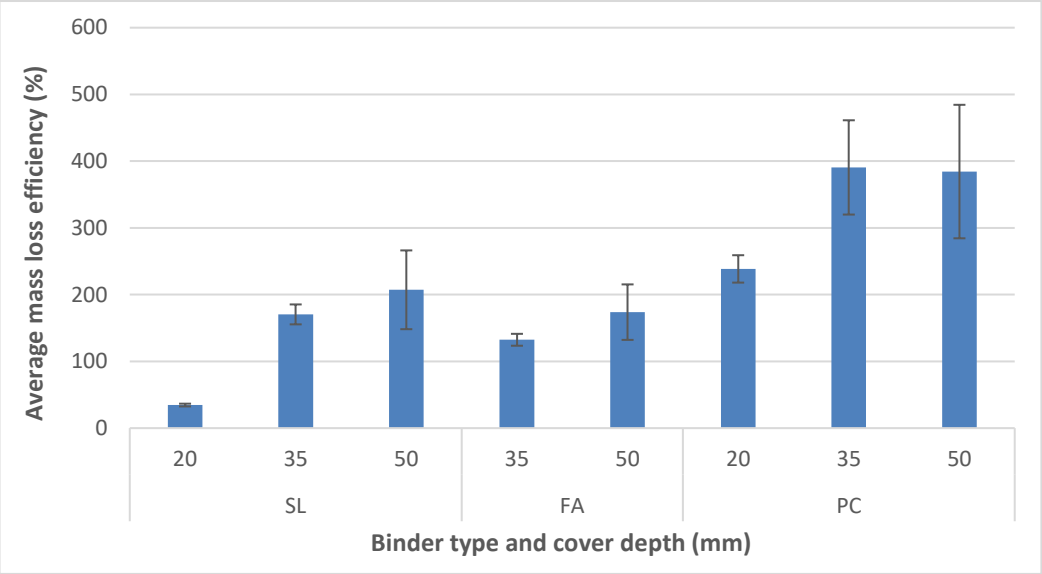

Figure 4.9: Average mass loss efficiency for the different binder types and cover depths

The purpose of this study was to not only determine the efficiency of the impressed anodic current technique to induce corrosion but to investigate the effect of the two independent variables (factors) on the efficiency of the technique. The efficiency of the technique is determined as the mass loss efficiency of the theoretical and gravimetric mass loss. The two variables under investigation in this study were; cover depth, related to the use of three cover depths, 20 mm, 35 mm and 50 mm; and concrete quality, related to the use of three binder types, 50/50 PC/SL, 70/30 PC/FA and 100% PC. The effect of these two factors is discussed below.

a) Effect of cover depth on mass loss efficiency

The effect of cover depth on the mass loss efficiency is shown in Figure 4.9. The results shown in Figure 4.9 indicate that as the cover depth increases, the mass loss efficiency increases to values much higher than 100%. The trend observed of increasing overestimation of faradaic mass loss with increasing cover was also reported in a previous study by Palumbo (1991). The researcher reported that at cover depths greater than 36.5 mm, there was an overestimation of Faraday's mass loss. He concluded that at lower cover depths the mass loss efficiency is

improved for the same binder type. This is because at higher cover depths, the corrosion initiation and propagation period are increased due to the increased time required for chlorides to migrate through the concrete cover and reach the steel. Similarly, Nossoni and Harichandran (2012) reported that when physical barriers, such as cover depth, restrict the migration of chlorides, Faraday's law is not expected to give an accurate estimation of mass loss.

In the equation to calculate theoretical mass loss using Faraday's law the variable *time* refers to the time taken for corrosion propagation. The time taken for corrosion initiation is not accounted for even though the corrosion current is first used to initiate corrosion. This lapse in time between corrosion initiation and corrosion propagation is not taken into account when applying Faraday's law and it is one of the causes for the over estimation of mass loss values. Previous research by Austin, et al. (2004) attempted to compensate for the time taken for corrosion initiation. This was achieved by the using the acoustic emissions technique to detect the start of corrosion propagation and using that as the variable for *time* in Faraday's law. Thus the time take for corrosion intiation was not included when applying Faraday's law to calculate theoretical mass loss and a better estimation of Faraday's mass loss was achieved.

The over estimation of mass loss due to the time taken for corrosion initiation can be corrected by applying Faraday's law when the duration for active corrosion rate is known. This can be achieved by introducing chlorides into the concrete mix at a value equal to or greater than the critical chloride threshold in order to reduce the corrosion initiation period or even depassivate the steel immediately. Following the steel depassivation the probability of active corrosion activity would then be assessed using a suitable technique such half-cell potential (HCP) or Linear Polarization Resistance (LPR) tests. Once probability of active corrosion activity is confirmed by HCP or LPR, then the impressed current technique would be applied to accelerate corrosion.

b) Effect of binder type on mass loss efficiency

The results shown in Figure 4.19 indicate that the mass loss efficiency increases, with an overall mass loss overestimation in the order: PC > FA > SL. The blended cement concrete had a closer approximation to 100% mass loss efficiency, with the SL blended cement concrete giving a better approximation than the FA blended cement concrete.

The blended cement concrete has been shown to have higher electrical resistivity than the plain Portland cement concrete. The higher resistivity of the blended cement concrete is due to a more refined and denser pore structure which results in a less penetrable concrete, thus hindering the ingress of chlorides, and subsequently increasing the time to beam surface cracking.

The electrical resistivity of concrete is also inversely proportional to corrosion rates (Polder, 2001). As such the blended cement concrete had lower corrosion rates than the PC concrete, due to their higher electrical resistivity. The influence of the concretes resistivity is such that higher corrosion currents which translates to higher corrosion current densities, are required to overcome the resistivity of the concrete and induce corrosion rates that lead to crack formation.

The influence of corrosion rates on accelerated corrosion was investigated by, El Maaddawy and Soudki (2003) and they reported good correlation between the measured mass loss and the predicted mass loss, using Faraday's law, for current densities between 100 and 500 $\mu A/cm^2$. In their study chlorides were added into the concrete mix thus depassivating the steel immediately and eliminating the time and taken for corrosion initiation. They postulated that at higher corrosion rates, the ability of Faraday's law to predict corrosion would be influenced by the amount of corrosion products around the steel which may hinder the diffusion of OH^- and/or Fe^{2+} ions through the rust layer. In the present study corrosion current densities as hiigh as 828 $\mu A/cm^2$ were observed for PC concrete. Even higher corrosion rates from 1700 $\mu A/cm^2$ to 17000 $\mu A/cm^2$ were used by Nossoni and Harichandran (2012) and they came to the conclusion that when the corrosion rates are too high, Faraday's law is not expected to yield

an accurate estimate of the mass loss due to physical barriers (such as expansive corrosion products) which restrict the diffusion of moisture and chlorides into the concrete. The results indicate that the overestimation of Faraday's mass loss is due to high corrosion currents which are influenced by the concretes resistivity. The corrosion current is not equal to the applied current due to the current required to overcome the resistivity of the concrete. A better estimation of the corrosion current is required to best determine the theoretical mass loss. This can be achieved by accounting for the resistivity of the concrete by adding it to the overall resistivity of the corrosion cell circuit which in turn reduces the applied current. The results of the corrected corrosion current are presented below.

4.9. Corrected corrosion current

4.9.1. Accounting for the resistance of concrete in the corroson cell

Due to the resistivity of the concrete, not all the applied corrosion current is utilised to induce corrosion, some of the current is used up by the concrete as it functions as a resistor in the corrosion cell circuit. Ohm's law which states that the resistance in a circuit is inversely proportion to the current was used to correct the corrosion current by accounting for the increased resistance in the circuit because of the concrete beam. Figure 4.10 shows a comparison between the mass loss efficiency obtained for the initial corrosion current and the corrected corrosion current.

The blended cement concrete with the higher quality, i.e. higher resistivity had a reduced mass loss efficiency. The reduction of corrosion current by accounting for resistivity resulted in an underestimating of mass loss. This is because the correction of current was done in retrospect and can be more effective applied at the start of the experiment. This can be achieved by adding the amount of current required to overcome resistivity of the concrete to the amount of current required to obtain the desired current density and degree of corrosion.

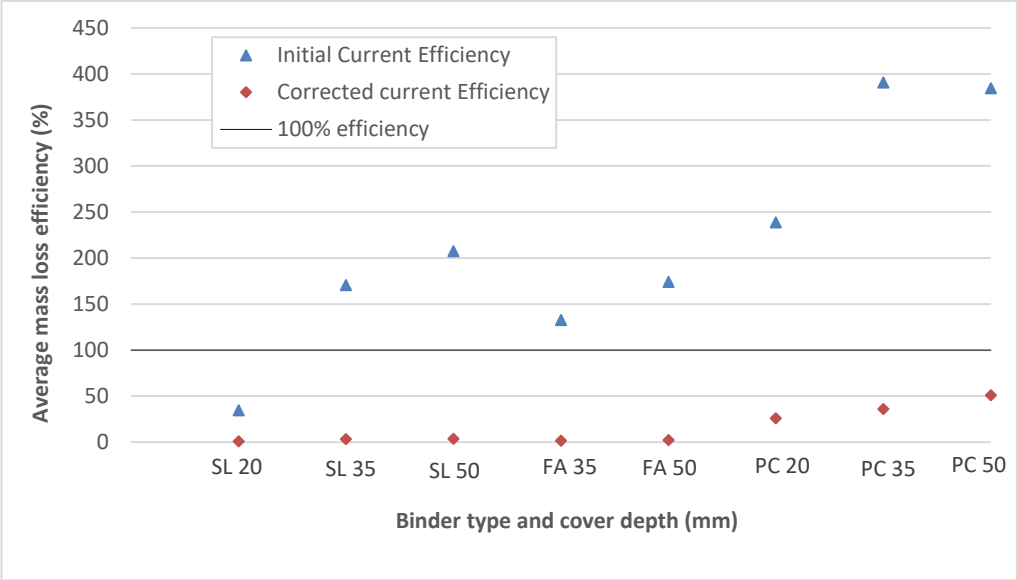

Figure 4.10: Average mass loss efficiency for the initial and corrected current efficiency for the different cover depths and binder types

The results obtained in this study show that the applied current is not equal to the corrosion current, thus when the applied current is used in Faraday's law it leads to on overestimation of theoretical mass loss. A better estimation of the corrosion current is required for application in Faraday's law. The corrosion current can be determined using the gravimetric mass loss results. The calculation of the corrosion current and correction of the applied current is shown below.

4.9.2. Calculating the corroson causing current

The overestimation of theoretical mass loss indicates that the corrosion current density is less than the applied current density. The actual corrosion current density was determined by substituting the actual mass loss from the gravimetric tests results into Faradays law as shown in Equation 4.4:

$$i_{calc} = \frac{M_{ac} z F}{M T} \qquad (4.4)$$

where i_{calc} is the corrosion current density $\mu A/cm^2$; M_{ac} is the actual mass loss in g/cm; z is the valency of iron; F is Faraday's constant in $A.s$; M is the molar mass in g/mol and T is the time in s. Using the results from the present study, the average corrosion current for each binder types can be related to the applied current density using Equation 4.5:

$$i_{calc} = \kappa . i_{app} \quad (4.5)$$

where κ is a constant and be related to the resistivity of the concrete using Equation 4.6:

$$\kappa = \alpha . \rho \quad (4.6)$$

where ρ is the resistivity of concrete and α is as shown for the different binder types:

Plain Portland cement: α_{PC} = $0.043/k\Omega.cm$

Slag blended cement: α_{SL} = $0.023/k\Omega.cm$

Fly ash blended cement: α_{FA} = $0.032/k\Omega.cm$

Taking the concretes resistivity into account by using it to determine the corrosion current led to a modified express of Faraday's law which reduces the overestimation error of theoretical mass loss. The modified expression of Faraday's law is shown in Equation 4.7:

$$M_{th} = \frac{MT(\alpha.\rho.I_{app})}{zF} \quad (4.7)$$

where M_{th} is the theoretical mass loss; z, F, T are as defined in Equation 4.4; I_{app} is the applied current; ρ is the resistivity of concrete and α is a corrosion correction factor.

The modified expression of Faraday's law does not take into account the effect of the cover depth which also causes an overestimation of theoretical mass loss as a result of its influence on the corrosion initiation. However, the influence of cover depth can be reduced by accelerating steel depassivation (e.g. using admixed chlorides) before applying accelerate corrosion. Similarly, a previous study by Austin, et al. (2004) has also presented a modified expression of Faraday's law (see Equation 2.30) which excludes the time taken for corrosion initiation by using acoustic emissions to determine the start of corrosion propagation. The researchers were able to get a better approximation of theoretical mass loss using their modified expression of Faraday's law. However, unlike in the present study, their modified expression does not take into account the effect of the concrete's resistivity on corrosion propagation. As such the

modified expression of Faraday's law shown in Equation 4.7 should give a better estimation of theoretical mass loss for 100% PC, 50/50 PC/SL and 70/30 PC/FA concrete.

4.10. General discussion of results

This section provides a brief summary of the results presented in the section above. In general, there was an overestimation of Faradays mass loss for the different binder types and cover. The current applied for inducing corrosion in the impressed current technique was not found to be entirely efficient in predicting mass loss. This is because not all the current applied was used to induce corrosion as some was lost in overcoming the resistivity of the concrete.

The corrosion rate is inversely proportional to the concrete's electrical resistivity. The electrical resistivity of fly and slag was shown to be higher than that of plain Portland cement. As such the PC concrete had the higher corrosion rates which resulted in their higher overestimation of mass loss. Simply reducing the corrosion current by accounting for resistivity is not enough as it results in mass loss underestimation. Thus, the corrosion current can be further corrected by adding the current required to overcome resistivity to the desired corrosion current density. The applied current should be increased so that not all the current is used up in overcoming resistivity. This ensures that there is enough current in the system for corrosion to prevent under estimation of mass loss when the resistivity of concrete is considered.

In this study, the variable *time* used in Faraday's law for mass estimation includes the corrosion initiation and propagation period. The corrosion initiation period has been shown to increase with increasing cover depth. This is due to the increased distance that chlorides must travel to reach the steel. The time for corrosion initiation can be eliminated by adding chlorides into the concrete to cause immediate steel depassivation. After that the impressed current can be used to induced corrosion once active corrosion rates have been confirmed by LPR and HCP.

CHAPTER 5: CONCLUSIONS AND RECOMMENDATIONS

5.1. Conclusions

This section provides a summary of the findings presented in Chapter 4 and concludes the work done in this research. The aim of this study was to investigate the effect of concrete quality and cover depth on the efficiency of the impressed current technique to induce corrosion. The concrete quality was varied using three different binder types namely SL, FA, PC cement blends. Durability index tests were conducted to make inferences on the quality of the concrete. Based on a ranking of the durability index test results and the electrical resistivity results it was determined that the concrete quality increased in the order: SL > FA > PC.

The impressed anodic current technique was used to accelerate corrosion of the steel. Presently there is no set protocol available in literature for the application of impressed anodic current to accelerate corrosion. As such the set-up employed was a combination of the various set-ups adopted by various researchers.

The applied current was calculated and assumed to be equal to the corrosion current which was used to determine the theoretical mass loss of the steel using Faraday's Law. At the end of the accelerated corrosion experiments the steel bars were extracted from the concrete and their actual mass loss was determined using gravimetric measurements. The mass loss efficiency of the impressed current technique was determined as the mass loss ratio of the theoretical (faradaic) mass loss over actual (gravimetric) loss measurement. A mass loss efficiency ratio of 1 (unity) is equivalent to 100% efficiency. This indicates that the faradaic and gravimetric mass loss values compare well indicating that the impressed current technique is efficient in inducing corrosion.

The results presented in this study showed a general overestimation of Faraday's mass loss. A closer approximation to 100% efficiency was obtained in the

blended cement concrete for the SL, followed by the FA and lastly the PC concrete. In terms of cover depth, a closer approximation to 100% efficiency was obtained for the 20, followed by the 35 and lastly the 50 mm cover depths. The mass loss efficiency can be improved by correcting the corrosion current and eliminating the time to corrosion initiation. A modified equation of Faraday's law was developed to reduce theoretical mass loss overestimation by accounting for the concretes resistivity and correcting the corrosion current as shown in Equation 5.1:

$$M_{th} = \frac{MT(\alpha.\rho.I_{app})}{zF} \quad (5.1)$$

where M_{th} is the theoretical mass loss in g; z is the valency of iron; F is Faraday's constant in $A.s$; M is the molar mass in g/mol and T is the time in $s.$; I_{app} is the corrosion current density A; ρ is the concretes resistivity in $k\Omega.cm$ and α is the correction factor $0.043/k\Omega.cm$, $0.023/k\Omega.cm$, $0.032/k\Omega.cm$ for plain Portland cement, slag blended and fly ash blended cement concrete respectively.

5.2. Recommendations

The following recommendations are made based on the experiments conducted and the findings from Chapter 4 for consideration for future work.

a) Impressed current set-up

Many challenges were encountered with the set-up of the impressed current technique. The initial plan was to connect the beams in series to one power supply but the set-up resulted in the corrosion rates being too low due to the resistivity of the concrete beams. Thus, the set-up was modified and each beam was connected to its own power supply which presented a resource problem. Due to the limited availability of power supply units, the concrete beams with the low 20 mm cover depth were connected in series, thus they had the same theoretical mass loss as they have the same current. The recommendation is to take cognisance of the effect of the concretes resistivity when connecting beams in series as it will increase the overall resistivity of the corrosion cell.

b) Applying Faraday's Law

The time for corrosion duration in Faraday's law refers to the time for active corrosion rates and not passive corrosion rates. The time taken for chlorides to depassivate the steel is dependent on the concrete quality. This time is referred to as the corrosion initiation period where the steel undergoes passive corrosion rates.

This lapse in time between corrosion initiation and active corrosion propagation is not taken into account in Faraday's law and it may be the cause for the over estimation of mass loss values. Accelerated corrosion should be applied once the steel has been depassivated.

c) Concrete electrical resistivity

It is recommended that more work be conducted to develop the bulk electrical resistivity into a potential indicator of the ability of concrete to resist corrosion. More work is required to determine at which concrete age, binder type, w/b ratio and sample conditioning the two factors can be correlated.

d) Steel tensile strength

Corrosion of reinforcing steel results in the conversion of the solid iron into various corrosion products on the surface of the steel. Not only does this, to some degree, reduce the bond strength between the steel and concrete interface but it also reduces the mass and cross-sectional area of the steel. A reduction in the steel cross sectional area reduces the tensile strength of the steel. More work is required to determine the degree of corrosion required to cause a reduction of the ultimate and yield tensile strength of the steel below the acceptable values for structural reinforced concrete members. The degree of corrosion can be determined for real life structures when the impressed current technique is used to estimate corrosion when it is not feasible to conduct gravimetric tests. In the present study tensile strength test were not conducted as mass loss efficiency was not achieved, indicating that for the present study Faraday's law could not be used to estimate actual degree of corrosion. As a result, no inferences could be made between the tensile strength and the faradaic mass loss.

e) Future research

The scope of this study can be extended to investigate the effect of varying other variables of interest such as salt solution concentration, crack widths, binder types and accelerated steel depassivation. The purpose is to obtain a test set-up and combination of variables required to obtain good correlation between real and theoretical mass loss.

5.3. References

Almusallam, A., Al-Gahtani, A., Aziz, A. & Rasheeduzzafar, F., 1996. Effect of reinforcement corrosion on bond strength. *Construction Building & Materials,* 10(2), pp. 123-129.

Alonso, C., Andrade, C., Rodriguez, J. & Diez, J., 1998. Factors affecting the cracking of concrete affected by reinforcement corrosion. *Materials & Structures,* Volume 31, pp. 435-441.

Andrade, C. & Alonso, C., 2001. On-site measurements of corrosion rate of reinforcements. *Construction & Building Materials,* 15(2-3), pp. 141-145.

Ash Resources, 2011. *Fly Ash: Techical Bulletin 3.* [Online]
Available at: www.ashresources.co.za
[Accessed 20 March 2018].

Atis, C., 2005. Strength properties of high-volume fly ash roller compacted and workable concrete, and influence of curing condition.. *Cement and Concrete Research,* 35(12), pp. 1112-1121.

Ballim, Y., 1993. Curing and the durability of OPC, fly ash ans blast-furnace slag concretes. *Materials and Strucures,* 26(158), pp. 238-244.

Bentur, A., Diamond, S. & Steven, B., 1997. *Steel corrosion in concrete: Steel corrosion in concrete: Fundamentals and civil engineering practice.* 1st ed. London, UK: EFN Spon.

Berodier, E. & Scrivener, K., 2015. Evolution of pore structure in blended systems. *Cement and Concrete Research,* 73(1), pp. 25-35`.

Bouzoubaâ, N., Fournier, B., Malhotra, M. & Golden, D., 2001. *Mechanical properties and durability of concrete made with HVFA blended cement produced in a cement plant.* [Online]
Available at: www.ecosmartconcrete.com
[Accessed 20 March 2018].

Gonzalez, J., Andrade, C., Alonso, C. & Feliu, S., 1995. Comparison of rates of general corrosion and maximum pitting penetration on concrete embedded steel reinforcement. *Cement and Concrete Resources,* 25(2), pp. 257-264.

Grieve, G., 2009. Cementitious materials. In: G. Owens, ed. *Fulton's concrete technology* . Pretoria: Cement and Concrte Institute, pp. 1-16.

Grubbs, F., 1969. Sample criteria for testing outlying observations. *Annals of Mathematical Statistics,* 21(1), pp. 27-58.

Hair, j., Anderson, R., Tatham, R. & Black, W., 1998. *Multivariate Data Analysis.* New Jersey : Prentice Hall.

Liu, J., Qiu, Q., Xing, F. & Pan, D., 2014. *Permeation properties and pore structure of surface layer of fly ash concrete.*. [Online]
Available at: www.mdpi.com/journal/materials
[Accessed 20 March 2018].

Nieves-Mendoza, D. et al., 2012. Identifying factors influcencing the corrosion rate of steel using nonparametric statistics. *International Journal of Electrochemical Science,* pp. 6343-6352.

Polder, R., 2012. *Effects of fly ash pn reinforcement corrosion in chloride environment,* Delft, Netherlands: TNO Technical Sciences.

Samad, S., Shah, A. & Limbachiya, M., 2017. Strength development characteristics of concrete produced with blended cement using ground granulated blast furnace slag (GGBS) under various conditions. *Sadhana,* 42(7), pp. 1203-1213.

Spragg, R. et al., 2013. Factors that influence electrical resistivity measurements in cementitious systems. *Journal of the Transportation Research Board,* 2342(1), pp. 90-98.

Thomas, M., 2007. *Optimising the use of fly ash in concrete,* Washington DC: Portland Cement Association.

Vassie, P., 1979. *Non-destructive evaluation of the corrosion of concrete reinforcement by chlorides.* London, Corrosion of reinforcements in concrete construction symposium.

APPENDIX A: IDENTIFYING OUTLIERS

Outliers are observation points that are in explicable or significantly distant from the other observations of the same data set. In this study, the Grubbs test method was chosen as a suitable method for determining outliers. Grubbs test is based on the difference of the mean of the sample and the most extreme data considering the standard deviation (Grubbs, 1969) extreme data considering the standard deviation (Grubbs, 1969). The test is suitable for small for small sample sizes, such as in the present study where n = 3 or n = 4. Equation A.1 is used to define the Grubbs test statistic:

$$G_{exp} = \frac{|\bar{x} - questinable\ value|}{s} \quad \text{(A.1)}$$

where $\bar{x}$ is the sample mean and s is the sample standard deviation. The Grubb's test is defined for the hypothesis:

H_0: There are no outliers in the data set
H_a: There is exactly one outlier in the data set

The hypothesis is tested by comparing values of G_{exp} with $G_{critical}$, which is based on the sample size and level of significance. The value for $G_{critical}$ can be selected from Grubb's critical value Table A.1. The null hypothesis is rejected when $G_{exp} \geq G_{critical}$, in other words the questionable value is indeed an outlier. In this study $G_{critical}$ was determined at a 95% confidence interval.

Table A.1: Sample G critical values for various samples sizes and levels of significance

n	g_{crit} α=0.05	g_{crit} α=0.01	n	g_{crit} α=0.05	g_{crit} α=0.01	n	g_{crit} α=0.05	g_{crit} α=0.01
3	1.1543	1.1547	15	2.5483	2.8061	80	3.3061	3.6729
4	1.4812	1.4962	16	2.5857	2.8521	90	3.3477	3.7163
5	1.7150	1.7637	17	2.6200	2.8940	100	3.3841	3.7540
6	1.8871	1.9728	18	2.6516	2.9325	120	3.4451	3.8167
7	2.0200	2.1391	19	2.6809	2.9680	140	3.4951	3.8673
8	2.1266	2.2744	20	2.7082	3.0008	160	3.5373	3.9097

APPENDIX B: EXPERIMENTAL RESULTS

B.1 Compressive strength and density results

Table B.1: Compressive strength and durability results for slag blended cement concrete

50/50 PC/ SL Concrete Age	Compressive Strength	Range/Average	Density	Ave. Compressive Strength
	(MPa)	(%)	(kg/m3)	(MPa)
7 days	20.9	1.45	2500	20.7
	20.1		2460	
	21.2		2500	
14 days	35	1.20	2580	33.3
	32.3		2500	
	32.7		2540	
56 days	44.6	3.75	2540	45.3
	45		2530	
	46.3		2480	

Table B.2: Compressive strength and durability results for fly ash blended cement concrete

70/30 PC/ FA Concrete Age	Compressive Strength	Range/Average	Density	Ave. Compressive Strength
	(MPa)	(%)	(kg/m3)	(MPa)
7 days	23.3	3.42	2460	23.4
	23		2440	
	23.8		2500	
14 days	37.3	3.78	2460	37.0
	36.2		2480	
	37.6		2480	
56 days	45.5	7.85	2450	44.6
	42.4		2420	
	45.9		2470	

Table B.3: Compressive strength and durability results for plain Portland cement concrete

100% PC Concrete Age	Compressive Strength (MPa)	Range/Average (%)	Density (kg/m3)	Ave. Compressive Strength (MPa)
7 days	56.8	2.61	2580	57.6
	58.3		2550	
	57.6		2510	
14 days	59.4	3.87	2560	59.4
	58.2		2570	
	60.5		2630	
56 days	65.3	5.75	2470	66.0
	68.3		2540	
	64.5		2530	

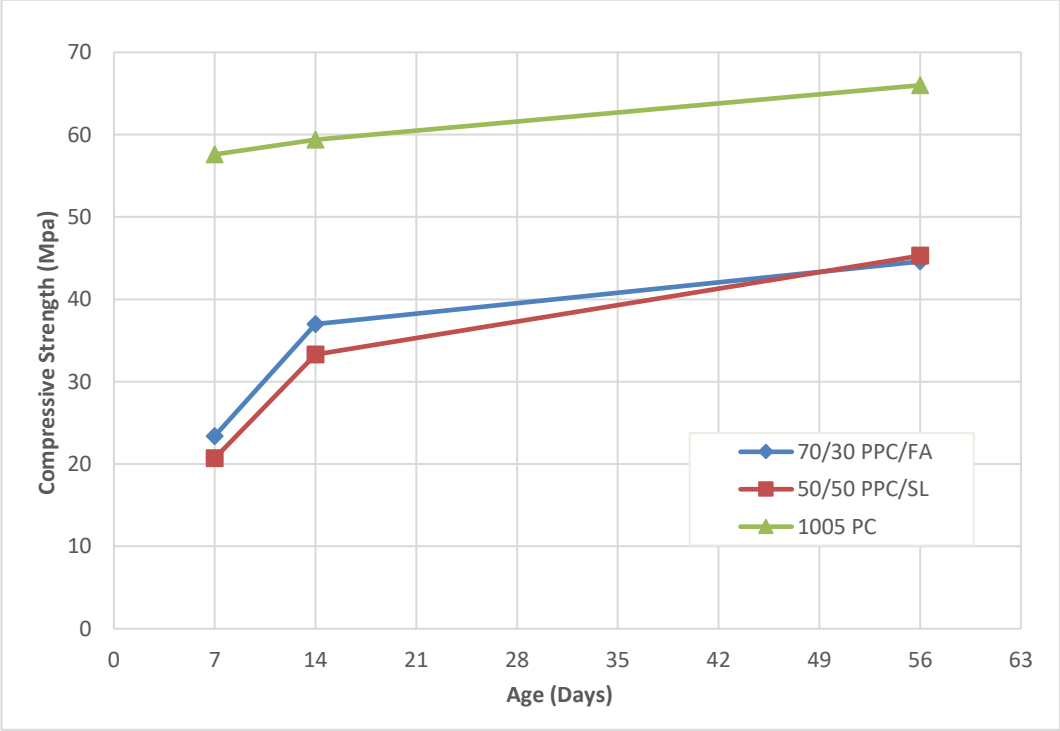

Figure B.1: Compressive strength and durability results for plain Portland cement concrete

B.2 Durability Index Test Results

B.2.2 Oxygen Permeability Index

Table B.4: 56 Day OPI for slag bended cement concrete

50/50 PC/SL		
Disk Number	**k (m/s)**	**OPI**
1	3.865E-11	10.41
2	4.042E-11	10.39
3	1.712E-10	9.77
4	9.985E-11	10.00
Mean	**8.753E-11**	**10.14**
S.D.	6.262E-11	0.31
COV (%)	72	3.10

Table B.5: 56 Day OPI for fly ash blended cement concrete

70/30 PC FA		
Disk Number	**k (m/s)**	**OPI**
1	4.280E-11	10.37
2	3.307E-11	10.48
3	1.002E-10	10.00
4	2.093E-10	9.68
Mean	**9.633E-11**	**10.13**
S.D.	8.092E-11	0.37
COV (%)	84	3.60

Table B.6: 56 Day OPI for slag plain Portland cement concrete

100% PC		
Disk Number	**k (m/s)**	**OPI**
1	7.110E-11	10.15
2	5.392E-11	10.27
3	1.483E-10	9.83
4	9.467E-11	10.02
Mean	**9.200E-11**	**10.07**
S.D.	4.109E-11	0.19
COV (%)	45	1.86

B.2.2 Water Sorptivity Index

Table B.7: 56 Day WSI for slag bended cement concrete

50/50 PC/SL		
Disk Number	**Sorptivity (mm/hr$^{0.5}$)**	**Porosity (%)**
1	10.21	7.94
2	12.32	7.21
3	7.93	7.77
4	7.34	7.03
Mean	**9.45**	**7.49**
S.D.	2.28	0.44
COV (%)	24.09	5.85

Table B.8: 56 Day WSI for fly ash bended cement concrete

70/30 PC FA		
Disk Number	**Sorptivity (mm/hr$^{0.5}$)**	**Porosity (%)**
1	8.69	10.19
2	7.46	9.94
3	7.84	9.82
4	7.96	11.23
Mean	**7.99**	**10.30**
S.D.	0.51	0.64
COV (%)	6.44	6.25

Table B.9: 56 Day WSII for plain Portland cement concrete

100% PC		
Disk Number	**Sorptivity (mm/hr$^{0.5}$)**	**Porosity (%)**
1	9.83	8.96
2	8.77	9.17
3	8.81	9.23
4	10.00	14.93
Mean	**9.35**	**10.57**
S.D.	0.65	2.91
COV (%)	6.98	27.51

B.2.3 Chloride Conductivity Index

Table B.10: 56 Day CCI for slag bended cement concrete

50/50 PC/SL		
Disk Number	**Conductivity (mS/cm)**	**Porosity (%)**
1	0.550	3.25
2	0.488	3.28
3	0.658	3.47
4	0.438	3.36
Mean	**0.534**	**3.34**
S.D.	0.095	0.09
COV (%)	17.790	2.91

Table B.11: 56 Day CCI for fly ash bended cement concrete

70/30 PC FA		
Disk Number	**Conductivity (mS/cm)**	**Porosity (%)**
1	2.06	4.60
2	1.85	4.20
3	2.55	4.42
4	1.75	4.22
Mean	**2.05**	**4.36**
S.D.	0.36	0.36
COV (%)	17.36	4.29

Table B.12: 56 Day CCI for plain Portland bended cement concrete

100% PC		
Disk Number	**Conductivity (mS/cm)**	**Porosity (%)**
1	0.76	3.85
2	0.54	3.55
3	1.02	3.81
4	0.67	3.94
Mean	**0.75**	3.79
S.D.	0.20	0.20
COV (%)	27.07	4.37

B.3 Aggregate Sieve Analysis

B.3.1 Fine Aggregate (Andesite) Analysis

Table B.13: Fine Aggregate (Andesite) Analysis

Diameter (mm)	Mass of Sieve & Soil (g)	Soil Retained (g)	Soil Retained (%)	Cumm. Soil Passing (%)
6.70	0.00	0.00	0.00	100.00
4.75	52.90	52.90	3.49	96.51
2.36	526.30	526.30	34.71	61.80
1.18	355.10	355.10	23.42	38.38
0.60	220.00	220.00	14.51	23.87
0.30	145.70	145.70	9.61	14.26
0.15	140.60	140.60	9.27	4.99
0.08	67.50	67.50	4.45	0.54
Pan	8.20	8.20	0.54	0.00
	TOTAL:	1516.30	100.00	

B.3.2 Coarse Aggregate (Andesite) Analysis

Table B.14: Coarse Aggregate (Andesite) Analysis

Diameter (mm)	Mass of Sieve & Soil (g)	Soil Retained (g)	Soil Retained (%)	Soil Passing (%)
26.50	0.00	0.00	0.00	100.00
13.20	195.50	195.50	14.57	85.43
9.50	990.00	990.00	73.76	11.67
Pan	156.70	156.70	11.67	0.00
	TOTAL:	1342.20	100.00	

APPENDIX C: ACCELERATED CORROSION RESULTS

C.1 Gravimetric mass loss results

Table C.1: SL Gravimetric mass loss results

50/50 PPC/SL -GRAVIMETRIC TEST RESULTS								
Bar Number	Cover	Initial Mass (g)	Final Mass (g)	Start date	End date	No. of days	Actual mass loss (g)	Degree of corrosion (%)
1	20	440.39	427.88	6-Jul	14-Aug	39	12.51	2.84
9	20	443.67	430.02	6-Jul	14-Aug	39	13.65	3.08
18	20	443.32	431.18	6-Jul	14-Aug	39	12.14	2.74
2	35	444.34	429.85	6-Jul	26-Jul	21	14.49	3.26
6	35	443.02	429.88	6-Jul	14-Aug	39	13.14	2.97
16	35	443.60	427.73	26-Jul	14-Aug	20	15.87	3.58
4	50	443.4	426.22	6-Jul	19-Sep	75	17.18	3.87
8	50	439.04	428.83	6-Jul	19-Sep	75	10.21	2.33
10	50	444.34	418.17	6-Jul	9-Sep	65	26.17	5.89

Table C.2: FA Gravimetric mass loss results

70/30 PPC/FA - GRAVIMETRIC TEST RESULTS								
Bar Number	cover	Initial Mass (g)	Final Mass (g)	Start date	End date	No. of days	Mass loss (g)	Degree of corrosion (%)
2	20	444.00	432.22	19-Sep	29-Sep	10	11.78	2.65
5	20	442.41	428.22	14-Aug	25-Aug	11	14.19	3.21
8	20	443.68	428.84	14-Aug	25-Aug	11	14.84	3.34
3	35	443.34	436.83	19-Sep	29-Sep	10	6.51	1.47
11	35	444.28	437.95	19-Sep	27-Sep	8	6.33	1.42
15	35	443.11	432.87	9-Sep	19-Sep	10	10.24	2.31
6	50	444.78	428.99	14-Aug	27-Sep	44	15.79	3.55
7	50	443.79	429.55	14-Aug	27-Sep	44	14.24	3.21
12	50	443.51	432.09	25-Aug	27-Sep	33	11.42	2.57

Table C.3: PC Gravimetric mass loss results

100% PC - GRAVIMETRIC TEST RESULTS								
Bar Number	Cover	Initial Mass (g)	Final Mass (g)	Start date	End date	No. of days	Actual mass loss (g)	Degree of corrosion (%)
9	20	443.9	438.37	29-Sep	3-Oct	4	5.53	1.25
13	20	444.84	439.13	27-Sep	3-Oct	6	5.71	1.28
14	20	445.86	439.41	27-Sep	3-Oct	6	6.45	1.45
12	35	444.26	440.97	29-Sep	3-Oct	4	3.29	0.74
15	35	445.84	441.21	3-Oct	8-Oct	5	4.63	1.04
17	35	443.67	439.29	3-Oct	8-Oct	5	4.38	0.99
3	50	444.96	436.15	27-Sep	8-Oct	11	8.81	1.98
8	50	444.59	442	27-Sep	8-Oct	11	2.59	0.58
10	50	442.77	440.07	27-Sep	8-Oct	11	2.7	0.61

C.2 Faradaic mass loss results

Figures C.1 and C.2 show the typical V-T time curves for the different beams.

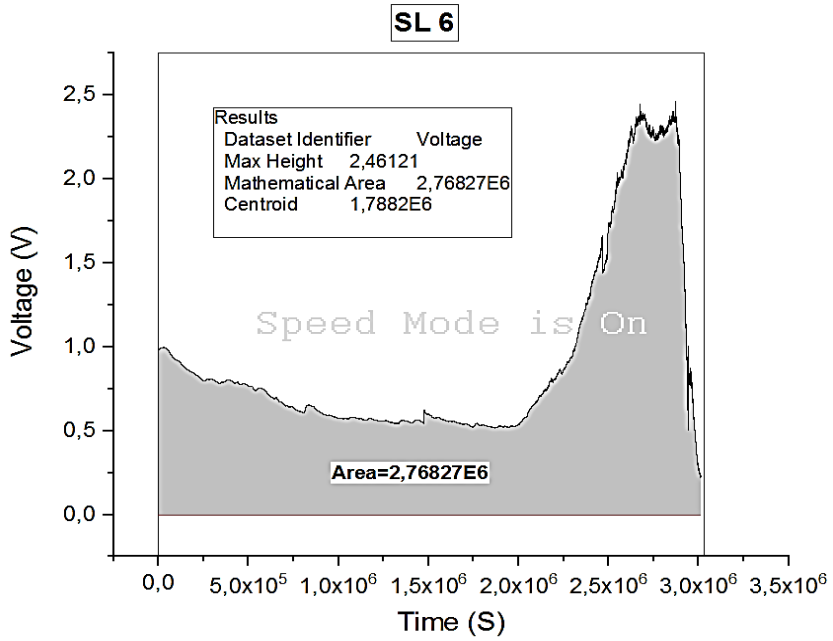

Figure C.1: Voltage – time graph for SL beam with cover depth of 35 mm

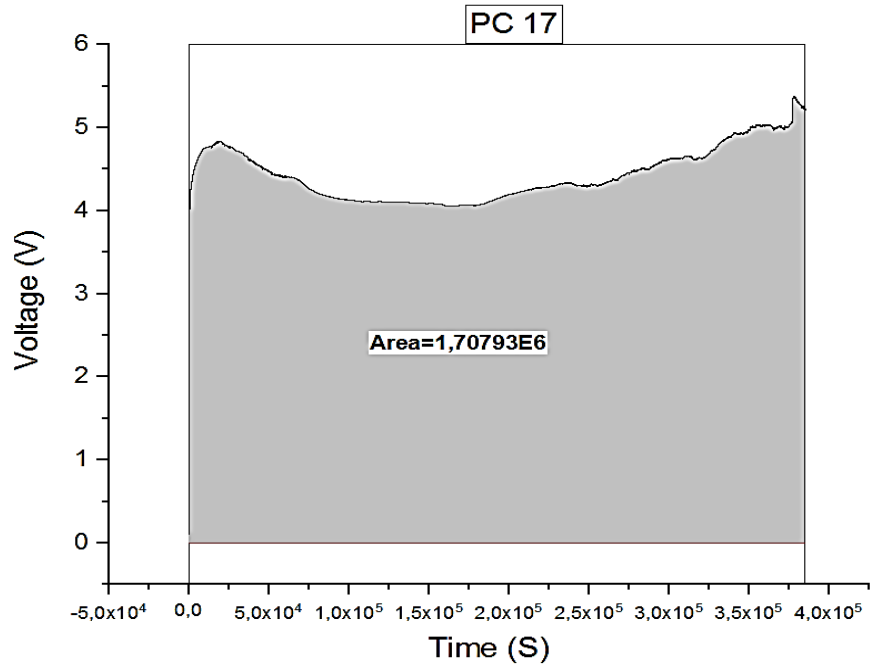

Figure C.2: Voltage – time current for FA beam with cover depth of 35 mm

C.3 Visual observations

Figure C.3.1: SL #2 prism with corrosion products

Figure C.3.1 shows the dark-green to black corrosion products protruding through the 1-2mm crack on to the surface of the SL #2 concrete beam. According to Vassie (1979) this green/black coloured oxide corrosion product suggests that the oxide was a type of iron chloride complex formed as an intermediate stage of chloride-induced corrosion.

Figure C.3.2: Progression of corrosion products in the direction of the chloride ingress

Upon retrieval of the bars a greenish black corrosion product paste with a reddish brown oxide on the periphery, around the aggregates was observed. Figure C.3.2 shows the progression of the corrosion products through the concrete in the direction of the salt solution ingress.

C.4 Accelerated corrosion set-up

Six power supply unts were used to impress current on 6 beams. The beams are shown at the bottom of the mgae.